

Thermal Spin Transfer Torque and Transverse Spin Relaxation in Spin Valves

THÈSE N° 5096 (2011)

PRÉSENTÉE LE 22 JUILLET 2011

À LA FACULTÉ SCIENCES DE BASE

LABORATOIRE DE PHYSIQUE DES MATÉRIAUX NANOSTRUCTURÉS

PROGRAMME DOCTORAL EN PHYSIQUE

ÉCOLE POLYTECHNIQUE FÉDÉRALE DE LAUSANNE

POUR L'OBTENTION DU GRADE DE DOCTEUR ÈS SCIENCES

PAR

Haiming YU

acceptée sur proposition du jury:

Prof. V. Savona, président du jury
Prof. J.-Ph. Ansermet, directeur de thèse
Dr A. M. Deac, rapporteur
Prof. D. Grundler, rapporteur
Prof. D. Yu, rapporteur



ÉCOLE POLYTECHNIQUE
FÉDÉRALE DE LAUSANNE

Suisse
2011

To My Parents

Acknowledgement

I would like to take this opportunity to thank all people who have helped me and who have taught me a lot during my PhD both in my academic study and in my everyday life in Switzerland. Without you all, I cannot finish my PhD so smoothly and cannot have so much fun living in Switzerland.

First of all, I feel very grateful to my thesis supervisor Prof. Jean-Philippe Ansermet. He helped me enormously during my PhD, from experimental advice to theoretical explanation of my data, from administrative issues to hospitality when I just arrived. It was very nice to meet his children Lydia and Julien. He treats me so well that sometimes I feel like being one of them. He is a special professor to me who can go down to reach and check some wire connections in the lab, who can grab a piece of paper and tell me in a few minutes how big the signal should roughly be by back-of-envelope calculation(just like magic!). I really appreciate his constant encouragement on my PhD study and his support for my future steps in the research academia. His true enthusiasm in physics amazes me and makes me want to become a physicist like him.

Secondly, I would like to thank my professor in China, Prof. Dapeng Yu. It is him who gave this opportunity to come to Switzerland, and be able to have such a wonderful experience. Not only is he an amazing physicist with broad and profound knowledge, but he is also a very nice, friendly, helpful and generous person for me. He always gives me encouragement and has great expectation on me even during my hard times. He is so helpful on my study that I remember once he did TEM for me himself. (Unfortunately, my sample was not so good that time) Moreover, being such a successful scientist, he is always very modest. Until he visited Switzerland last time, did I realize he speaks very good French. I learnt not only Physics from him, but also how to be a better person in general.

I would like to acknowledge all the other jury members who had to go through the following pages: Prof. Dirk Grundler, Dr Alina Deac, and the president of the jury Prof. Savona Vincenzo, especially Dr Alina Deac for her comments and suggestions on some corrections of the last chapter of my thesis with her expertise.

I must thank Dr. Simon Granville who helped me on every details of my experiments and papers. I feel very lucky to have him as my daily supervisor. I have to say he is an excellent teacher to me! I also learnt a lot English with him. "Neat!"

He is technically the first person I met in Switzerland who helped me settle down and get started in the lab. He also helped me going through my first international conference where I build my confidence on academic presentation. During the first year of my stay, Dr. Laurent Gravier also offered me great help on thermoelectric measurements. I loved the “brain-storming” we had together, usually Laurent, Simon and I, in the Physics Cafeteria. I thank Dr. Nicolas Bizi re for his help on teaching me mathematics which I used quite often for my PhD work. I thank Dr. Mohamed Abid, who shared office with me during my last stay for having a lot of interesting academic and non-academic discussions(the latter one is more interesting) and also for helping me with my French Abstract.

Special thanks to my two beautiful office-mates during my first stay, Aurore and Elena. I was so lucky to share a office with them when I just arrived from a far-away country with totally different culture. They are just like my sisters. I learnt a lot from them. I love the phalaenopsis, I love playing badminton with Aurore, I love the pizza and cake made by Elena, I love the m venpick icecream we had together.....

Furthermore,I want to thank Tatjana for telling me more about Switzerland. I love the Ragusa she first recommend to me, which becomes my favorite Swiss chocolate. I thank also Julie for fruitful discussion on V^{2f} and for sharing her brilliant calculation. I would like to thank also Elisa and Francesco who let me feel like being an Italian at the end of my PhD.(Although I still cannot pronounce well the Italian “r”). I thank Maria-Eleni for her kindness and her help on my learning Latex and so on. I thank Sylvain for offering me his Latex template and inviting me for dinner with his family around Christmas. I thank He Li for making my life colorful and beautiful during the last few months of my PhD. I thank Fiodar, Sami, and Arnaud for making me feel one of them.

Many thanks to Chantal and Florence, who helped me with my accommodation and other personal issues which are fundamental to me, especially as a foreigner. They are always very kind and smile to me. I like the moment that Chantal speaks English and I speaks very poor French. It was not easy, but interesting and friendly.

I would also like to thank Gilles, Claude, Philippe, Martial and all the technicians in the institute, who helped me enormously with my experiments and office problems. I feel lucky to have them around when I need help and they are all very professional and efficient.

Many thanks to all my colleagues in China, who helped me unselfishly with SEM, TEM and EBL, and spending great time together inside and outside the lab.

At the end, I would like to thank the most my parents for their infinite love and support to me. I love you!

Abstract

Spin caloritronics, i.e., the addition of thermal effects to the electrical and magnetic properties of nanostructures, has recently seen a rapid development. It has been predicted that a heat current can exert a spin torque on the magnetization in a nanostructure, analogous to the well-known spin-transfer torque induced by an electrical current. In this thesis, I provide the experimental evidence for this effect in spin valves, showing the switching field change with heat current.

I present measurements of the second harmonic voltage response of Co-Cu-Co pseudo-spin-valves deposited in the middle of Cu nanowires. I exploit the quasi-1D nature of the nanostructures to generate a heat current by way of asymmetric Joule heating in the Co layers. Both the magnitude of the second harmonic response of the spin valve and the field value of the maximum response are found to be dependent on the heat current. Both effects show that the magnetization dynamics of the pseudo-spin-valves is influenced by the heat current. Thus, the data provide a quantitative estimate of the thermal spin torque exerted on the magnetization of the Co layers.

In the last chapter, I measured the second harmonic response to an oscillating current crossing an exchange-biased spin valve as a function of the angle between the magnetization vectors of the fixed and free layers. This signal characterizes the linear response of the magnetization to a torque. A diffusive model is shown to predict that this angular dependence is quite sensitive to the value of the transverse spin diffusion length λ_J , i.e. the decay length of the spin polarization which is perpendicular to the magnetization. Our observations imply a value of about 6 nm for CoFe.

Keywords: spintronics, spin-transfer torque, spin caloritronics, nanowires, electrochemistry, spin diffusion

Résumé

Spin caloritronics, i.e., l'addition des effets thermiques aux propriétés électriques et magnétiques des nanostructures, a récemment vu un développement rapide. Il a été prévu théoriquement qu'un courant de la chaleur peut exercer un retournement (torque) de l'aimantation de la couche libre dans une nanostructure. Ce même phénomène de retournement de l'aimantation a été déjà fortement étudié par l'utilisation d'un stimuli électrique. Dans une première partie de cette thèse, je fournis l'évidence expérimentale qu'un courant de chaleur modifie le champ magnétique de retournement de l'aimantation.

Dans une seconde partie, je présente les mesures sur la seconde harmonique de la différence de potentiel électrique sur des pseudo-spin-valves Co-Cu-Co. En exploitant la nature quasi-monodimensionnelles des nanostructures afin de produire un courant de chaleur par effet joule. Ce courant chaleur est fortement dépendent de l'asymétrie de la nanostructure. Les résultats obtenus montrent clairement que les valeurs de champs de retournement d'aimantation et la valeur de la seconde harmonique dépendent fortement du courant de chaleur. Ainsi, les résultats obtenues nous permettent d'évaluer de façon quantitative le couple de rotation lié au courant de chaleur exercé sur l'aimantation des couches de Co.

Dans le dernier chapitre, je présente les résultats de la deuxième harmonique sur une nanopilliers lié à un courant oscillatoire en fonction de l'angle d'aimantation entre la couche libre et la couche fixe. Ce signal caractérise la réponse linéaire de l'aimantation au couple. Nous avons utilisé un modèle diffusive prévoyant que la dépendance angulaire sur ce genre de nanostructures est sensible à la valeur de diffusion du spin transverse λ_J . D'après nos résultats expérimentaux nous obtenons

une valeur de 6 nm dans le cas d'une couche de CoFe.

Keywords: Spintronics, spin-transfer torque, spin caloritronics, nanofils, electrochimie, diffusion de spin transverse

Content

Acknowledgements	v
Abstract	ix
Version résumée	xi
1 Introduction	1
2 Experimental method	5
2.1 Nanowire fabrication	5
2.2 Nanowire characterization	7
2.3 Electrical contacts	7
2.3.1 Electrochemical growth contact	7
2.3.2 Mechanical contact	11
2.4 Measurement setup	14
2.4.1 Lock-in detection	14
2.4.2 Laser heating	14
2.4.3 Joule heating and second harmonics detection	15
2.5 Probe of rotation	16
2.5.1 Labview control of rotating motor	16
2.5.2 Chip carrier and connection	17
2.5.3 Exchanged-bias spin valve sample	18
3 Transport measurements	21
3.1 MR on spin valve	21
3.2 MTGV on spin valve	23

3.3	V^{2f}	27
3.3.1	V^{2f} — Current susceptibility on spin valve	28
3.3.2	V^{2f} with I_{dc} — V^{2f} vs TGV on spin valve	36
3.4	V^{2f} and TGV on miscellaneous samples	39
3.4.1	Nanowire containing 5 spin valve	39
3.4.2	Co/Cu multilayer nanowires	40
4	Thermal spin transfer torque	49
4.1	Current-induced STT	49
4.2	Theoretical prediction on Thermal Spin transfer torque	50
4.3	Heat current—asymmetric spin valve	51
4.4	V^{2f} — a sensitive probe for switching field	53
4.5	Heat-current induced STT	53
4.5.1	Switching field shift	54
4.6	Supporting experiments	55
4.6.1	Symmetric spin valve	55
4.6.2	Isothermal measurement	55
4.6.3	Amplitude change of V^{2f}	58
4.7	Modeling for thermal spin torque	61
4.7.1	Onsager matrix combined with Pauli matrices	61
4.7.2	Fitting data on Switching field shift	63
4.7.3	Fitting data on the amplitude of V^{2f} peak height	64
4.8	Summary	67
5	Transverse spin relaxation in spin-valve	69
5.1	Concept of transverse spin diffusion length and the controversy . . .	69
5.2	Simulation on V^{2f} vs transverse spin diffusion length	70
5.3	Results on V^{2f} vs angle measurement	73
5.3.1	V^{2f} vs field	73

5.3.2	V^{2f} vs angle measurement	74
5.3.3	V^{2f} vs angle with different AC current	76
5.3.4	V^{2f} vs angle with a DC current	79
5.3.5	V^{2f} vs angle with different external field	81
5.4	Fitting data on V^{2f} vs angle	82
5.4.1	Estimation of the transverse spin diffusion length	82
5.4.2	Fitting data on V^{2f} vs angle with different external field using estimated λ_J	84
6	Conclusion and Perspectives	89
	Appendix A	91
	Bibliography	101
	CV	105

Chapter 1

Introduction

Spintronics has been studied intensively thanks to its fast application in the magnetic memories. The celebrated GMR (Giant Magnetoresistance) [1] [2] effect has been successfully applied in the industry and earned itself a Nobel prize in Physics in 2007. This effect was initially discovered in a spin valve sample, i.e. a normal metal sandwiched between two ferromagnetic layers. It has been established for some years now that an electrical current can be used to induce magnetization reversal in nanostructures such as spin valves. This current-induced magnetization switching (CIMS) operates by way of a current-induced spin-transfer torque (STT) that is exerted on the magnetization of the switching layer. The critical current density needs to make the switch is about $10^7 A/cm^2$ [4] [5].

Recently there appears increasing interest and rapid development in the field “spin caloritronics” [3], i.e. the addition of thermal effects to the electrical and magnetic properties of nanostructures. For instance, a recent study has observed and demonstrated the novel spin-Seebeck effect , in which the temperature gradient along an extended metallic ferromagnetic metal generates a spin current. Relevant theories on this effect are discussed concerning transport of heat by motions of conduction electrons in the ferromagnetic metal. In multilayered nanowires, the magnetothermoelectric power and Peltier effect has been measured and described

in terms of spin-dependent and spin-flip processes in the bulk layers by Gravier et al [6]. Hatami et al. [29] had earlier theoretical prediction on a substantial thermally driven spin transfer torque effect in all-metallic spin valves. We found evidence for the thermal spin transfer torque in a Co/Cu/Co spin valve by observing the heat-current-induced influence on the switching field. [7]

In this experiment, we use a unique measurement technique called V^{2f} measurement. In this technique, we apply an AC current and a DC current at the same time and we lock-in at AC current-induced Joule heating frequency which is at $2f$ (Joule heating). Significantly, we find this measurement is highly sensitive to the switching field. Therefore, we can precisely probe the switching field change induced by the heat current. Interestingly, when we remove the DC current in this measurement protocol, we can still observe a response in V^{2f} signal, which we interpreted as a result of the current susceptibility on spin valve. [8] When we use the AC current to alternate the heat current induced by Joule heating, we observed a clear change in the switching field position, which is a strong evidence for the thermal spin torque effect. The amplitude of the V^{2f} peak offers us supporting information on this effect by means of transport properties. We are able to rule out spurious effects by repeating the same measurements in samples with no heat current and isothermal measurements. The theoretical explanation is given by a thermodynamic model in which heat, charge and spin currents are linked by Onsager reciprocity relations.

Meanwhile, the V^{2f} peak shape, i.e. peak position and full-width at half-maximum is strongly dependent on the transverse spin relaxation length (λ_J) in magnetic layer. [40] The value of λ_J is very important for fundamental understanding on spin dynamics, but has yet been determined via experiments. There are basically two schools of thoughts. Based on the band structure arguments, Slonczewski [38] estimates this length to be about 0.1 nm; however, according to diffusive models of

spin dependent transport, Fert and Levy [39] estimate it to be of a few nanometers. Since these viewpoints differ by more than one order of magnitude, it is possible to clarify this controversy with the measurements we have planned. We design an experiment of measuring the V^{2f} on an exchanged-bias spin valve as a function of the angle between the two layers magnetization, so as to calculate the value of λ_J relying on published models of V^{2f} versus angle. [40]

Chapter 2

Experimental method

2.1 Nanowire fabrication

We grow nanowires in porous polycarbonate membrane template by electrodeposition. This fabrication technique was developed by this group and has been used to prepare magnetic nanowire samples for spin dependent transport measurement. [9] We use a conventional 3-electrode deposition system, consisting of working electrode, counter electrode, and reference electrode. The reference electrode we use is a Ag/AgCl electrode filled with saturated KCl so as to ensure a constant potential at the working electrode. We use potentiostatic control by monitoring the current flow and applying a constant potential.

The typical dimension of the nanowires fabricated with this method is about $6\mu\text{m}$ long and 50nm in diameter. The diameter of the nanowires can vary from 10nm to 200nm according to different template pore size. With specific recipe for the electrolyte (or solution bath), we are able to grow nanowires containing multilayers or spin valves(Fig 2.1) of Cobalt and Copper.

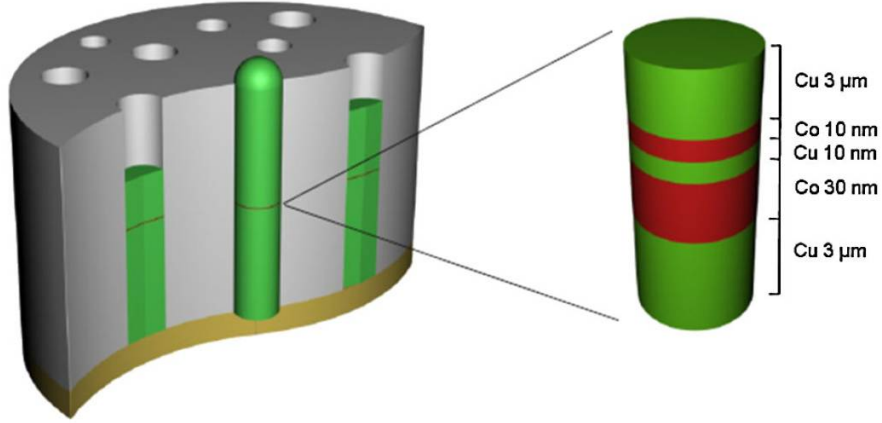


Figure 2.1: *electrodeposited nanowires containing spin-valve structure in porous polycarbonate membrane*

The solution bath composite for Co/Cu is as follow,

Co-Cu double bath

120g/L $CoSO_4 \cdot 7H_2O$

3g/L $CuSO_4 \cdot 5H_2O$

45g/L H_3BO_3

The typical deposition voltages for Cobalt and Copper are -1.0V and -0.3V, respectively. Nevertheless, we might need to conduct a cyclic voltammetry so as to precisely decide the best deposition condition, especially for a newly prepared electrolyte. Since the deposition voltages of Cobalt and Copper are quite far from each other, we mainly deposit one particular kind of material at its own voltage. However, based on the test of former member of the group, Co layers contain approximately 15 % of Cu and Cu layers contain about 1 % of Co. The solution is kept in a thermal bath of 40°C during deposition in order to keep the deposition temperature stable. As for the deposition speed, we normally do a calibration for

each solution before actually grow the samples we need. For the Co-Cu double bath, we first deposit only Co from bottom to top and record the deposition time for the nanowire to fill the $6\mu\text{m}$ pore, so we can calculate the growth rate of Cobalt. Then, from the same work for copper, we also know its growth rate. Now, if we want to deposit, for example, 10nm Cobalt, we can calculate how much time we need to deposit. With this technique, we can grow spin valve or multilayers of Co-Cu with different thickness.

2.2 Nanowire characterization

I did some microscopic characterization of the Co-Cu multilayer in the microscopy lab in Peking University. In these pictures we can see the multilayer is very well structured. The thickness of each bilayer is Co 20nm/Cu 20nm. The dark wire in the SEM photos or white wire in TEM photos is Platinum wire, which we grow together for other measurement purposes.

2.3 Electrical contacts

2.3.1 Electrochemical growth contact

In order to conduct transport measurement, we need to make contacts to the two ends of the nanowire. There are basically two different methods we use in our experiments. The first one is an electrochemical contact. [10] In this method, we sputter a thin gold layer on the top of the membrane. This layer is thin enough that it does not cover all the pores. Therefore, when the nanowire grow to the top of the membrane, it will automatically touch the thin gold layer.(Fig 2.3a)

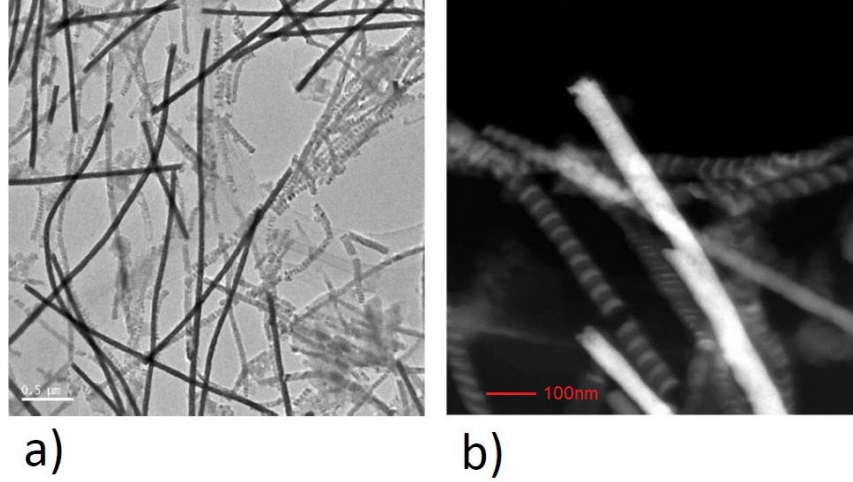


Figure 2.2: *microscopic characterization of multilayers: (a) Scanning Electron Microscopy of Co-Cu multilayers. (b) Transmission Electron Microscopy image of Co-Cu multilayers*

Then, along with the thin gold layer at the bottom of the membrane, we now have contacts on both ends of the nanowire.

Here in Fig 2.4 we show a typical electrodeposition curve of Cu nanowire containing a single spin valve with this contact method.

where we can see that the deposition current for Cu is at about $-3\mu\text{A}$, at around 50s deposition time, we deposit a spin valve structure of Co 10nm/Cu 10nm/Co 10nm. The deposition current for Co is much higher than Cu, and the deposition speed of Co is about 10 times faster than that of Cu. In addition, this particular process of spin valve deposition is accomplished within 0.5 second. Therefore, we only see a spike out of the Cu deposition curve at 50s. At about 310s, the deposition current suddenly drops from $-3\mu\text{A}$ to at s the deposition current suddenly drops to more than $-40\mu\text{A}$, and then relax towards the level of $-10\mu\text{A}$. This sudden drop indicates that the first nanowire has grown to the top of the membrane and contacts the

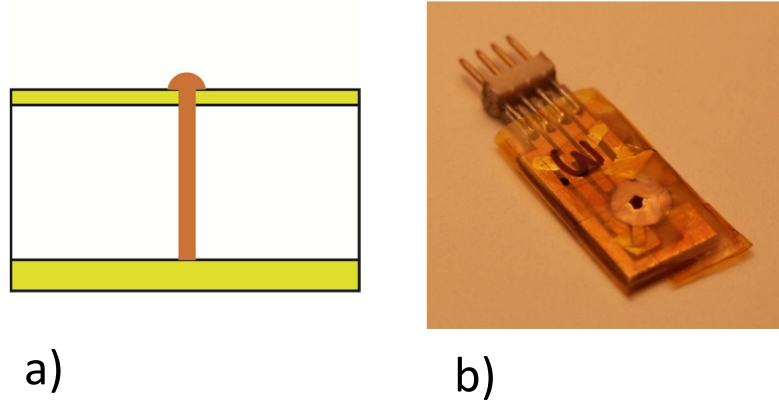


Figure 2.3: *Electrochemical growth contact: (a)cartoon schematic of electrochemical growth contact of nanowire inside the membrane. (b)photo of 4-pin plug sample holder, “plaquette”*

thin gold layer on the top. From the deposition time, we can tell that the spin valve structure was grown at the position of $1\mu\text{m}$ from the bottom of the $6\mu\text{m}$ long nanowire. This is simply because 300s for deposition of $6\mu\text{m}$ gives us 50s for the deposition of $1\mu\text{m}$. By this way, we can easily fabricate spin valve in any position inside the Cu nanowire.

We use a piece of 4-pin plug sample holder, which we call a “plaquette” in our group(Fig 2.3b). The advantage of this sample holder is that after we have done the electrodeposition in membrane, we can directly take the entire sample holder out, dry it and plug it into our measurement set-up for spin-dependent transport measurement. This can completely avoid the potentially destructive post-

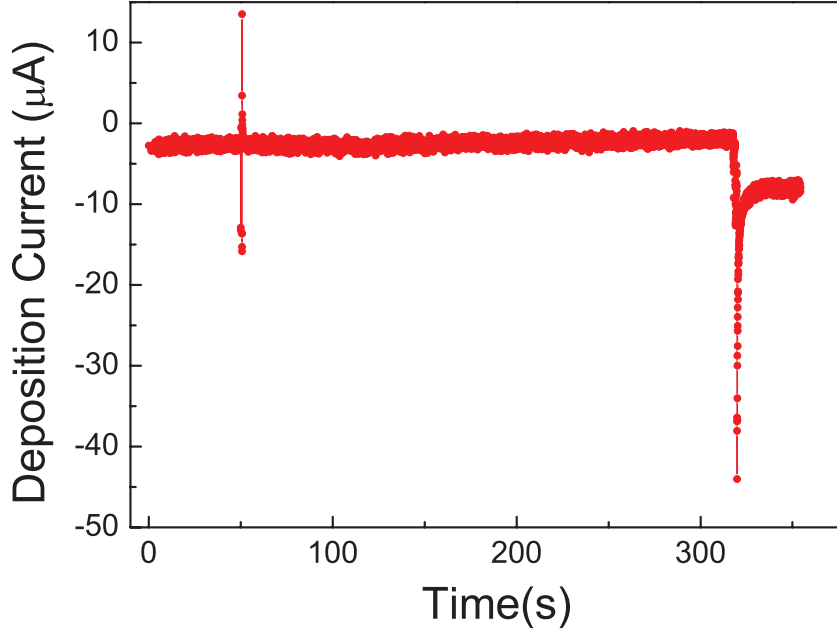


Figure 2.4: *Electrodeposition curve for fabrication of Cu nanowire containing single spin valve on a “plaquette” sample holder. Deposition potential is -0.3V for Cu, and -1.0V for Co*

processing.

Another advantage of this contact method compared to the mechanical contact in the next section is that “plaquette” sample holder is particularly designed for a laser heating measurement, because we can see in Fig 2.3b that the top of the membrane is exposed and we can shine a laser on this spot so that we can generate a heating on the nanowires. With this design, we can conduct the laser heating “TGV” measurement, which will be introduced in the next chapter.

Last but not the least, this sample holder can be plugged into a “cold finger” probe, with which we can conduct low-temperature measurement down to 4.2K.

2.3.2 Mechanical contact

The second method is a mechanical contact. In this method, instead of using thin gold layer on top, we use a gold wire to touch the small overgrowth of the nanowire. This method was developed by my colleagues, Nicolas Biziere and Elena Murè [11] and very well elaborated in the thesis of Dr. Elena Muré. [12] When the nanowires grow to the top of the membrane, they will start to form a little overgrowth, which we call “mushrooms” in our lab. We control the electrodeposition time to let the mushroom grow to a reasonable size(not too big to touch each other and cover the membrane and not too small to be able to contact the gold wire). We then use a gold wire to scan on the surface to contact the “mushroom”. Meanwhile, we monitor the resistance signal. If it changes from a open-circuit signal to a reasonable resistance of a single nanowire, we can stop and start transport measurement. The advantage of this method is that if the nanowire we are measuring is broken, we can simply move the gold wire to touch another “mushroom”, so we can immediately measure another nanowire in the membrane which is assumably the same structure as the formal one. Thus, this method is highly efficient experimentally.

Fig 2.6 shows a typical electrodeposition curve of a single spin valve grown in the middle of a Cu nanowire with this mechanical contact connector.

where we can see that the deposition current for Cu is at about $-5\mu\text{A}$, at around 50s deposition time, we deposited a spin valve structure of Co 10nm/Cu 10nm/Co 10nm. We observe a sharp spike when we deposit the spin valve at 150s. This is similar to the spike observed in Fig 2.4. The key difference between this deposition curve and that of Fig 2.4 in “plaquette” sample holder is that we don’t see a sharp drop at the end of the deposition, but a gradual change from $-5\mu\text{A}$ to around $-12\mu\text{A}$. This is because we don’t have a thin gold layer on the top of the membrane in this case. Nevertheless, the gradual change also indicates that

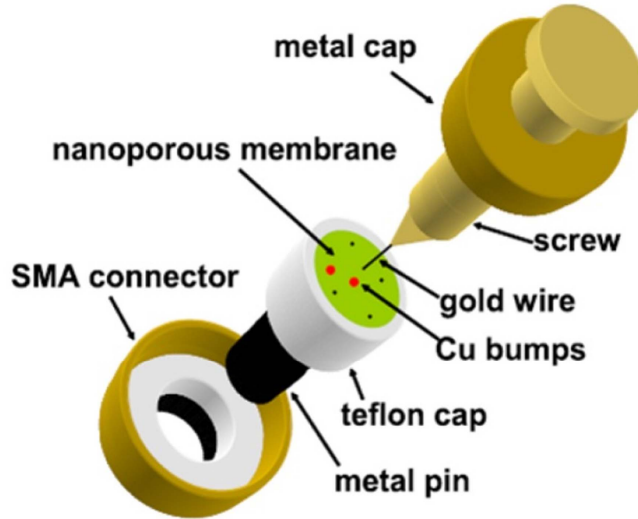


Figure 2.5: Sample holder for mechanical contact [11]: the filled membrane is situated in an SMA connector. A micro-size gold wire is used to scan on the surface and contact the “mushroom”. The contact procedure is monitored by the signal of resistance measurement.

the nanowire has reached the top of the membrane, and also start to form “mushrooms” on the top of the membrane. We then stop this process at a reasonable time when the mushrooms have grown to a proper size that we can easily make contacts with a gold wire; however, we should not wait too long time, because then the big “mushrooms” may start to contact to each others. As a result, we will measure several nanowires in parallel rather than a single nanowire. This process and techniques are very well studied in ref [12]. We notice that at the beginning of this curve, there appears a quick change of deposition current from $-40\mu\text{A}$ towards a stabilized current of around $-5\mu\text{A}$. This phenomenon is commonly observed in deposition in porous membrane. The cause of this effect is as follow: when the deposition starts, the metallic ions near the working electrode surface (gold layer

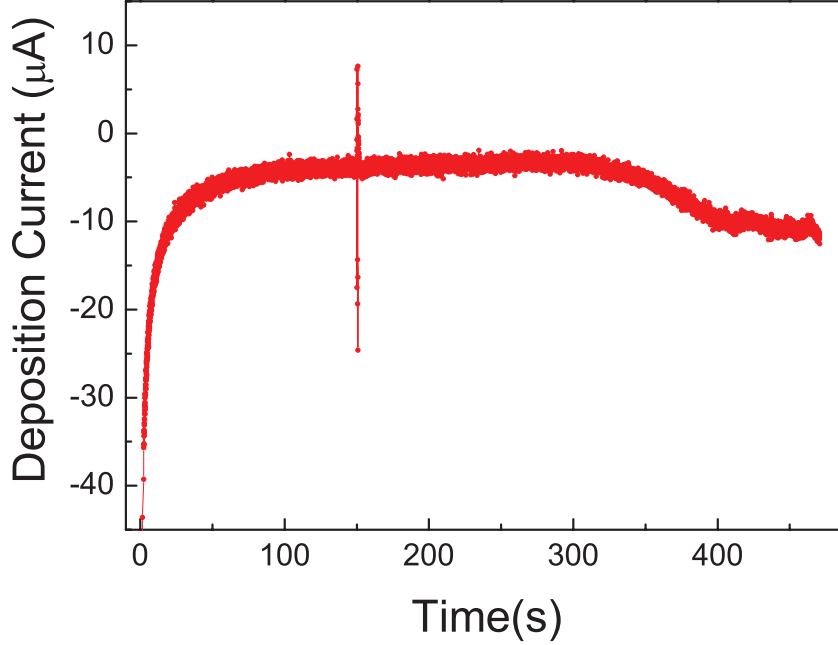


Figure 2.6: *Electrodeposition curve for fabrication single spin valve in the middle of a Cu nanowire on an SMA connector sample holder. Deposition potential is $-0.3V$ for Cu, and $-1.0V$ for Co*

in our case) quickly deposits on the electrode. This results in a lack of this metallic ions in the neighborhood of the working electrode surface. Consequently, the metallic ions from other part of the solution will diffuse quickly towards this area. As we observed, this effect normally can last several seconds before reaching an equilibrium state where we have a stabilized deposition current. Nevertheless, in some case this effect happens so fast that we do not see it in the deposition curve, such as in Fig 2.4

In addition, this SMA connector system is designed for high frequency measurement. Therefore this method can be used to study FMR on spin valve nanowire, whereas the electrochemical growth contact method cannot.

With this sample holder, we also designed a small “tunnel” where we can plug in a

laser fibre, so that we can also carry out the laser heating thermal galvanic voltage measurement which will be introduced in the next chapter; however, due to the precision of the laser shooting on the mushroom, we usually find this method less efficient than the “plaquette” as in conducting the laser related measurement.

2.4 Measurement setup

The measurement setup is designed for spin-dependent transport measurement on nanowires inside of the membrane. This setup can apply a magnetic field up to 1 tesla, and go down with temperature to 4.2K.

2.4.1 Lock-in detection

In order to enhance the signal-to-noise ratio (SNR), we utilize lock-in detection. We apply an AC current at a typical frequency of 400Hz), and we lock-in at this current frequency to measure the voltage signal, which can be converted to the resistance of the sample. In addition, in our V^{2f} measurement, we simply lock-in at twice the current frequency to measure the voltage which we will discuss elaborately in latter chapter. In another measurement, instead of lock-in at the current frequency, we lock-in at the laser frequency to measure the thermal galvanic voltage.

2.4.2 Laser heating

Thermal Galvanic Voltage(TGV) measurement set-up is that we shine a laser on the nanowire oscillating at certain frequency, while at the same time, we apply a DC current, then we lock-in at the laser frequency to measure the TGV signal(Fig 2.7a). The typical laser frequency we use in our experiment is around 22Hz. With this

measurement set-up, we can also measure the thermoelectric power (TEP) of the nanowire, when we don't induce any DC current. We use laser as the heat source in the magnetic thermal galvanic voltage measurement (MTGV) [27]. The laser diode is connected to a function generator, which can control the laser shining at a given frequency. In the experiment for thermal spin torque we replace the laser heating by joule heating induced by an AC current.

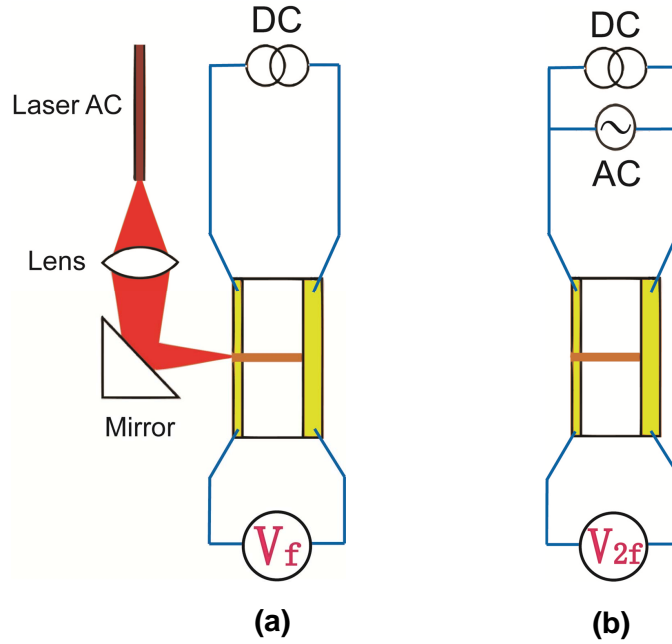


Figure 2.7: cartoon schematic of TGV(a) and V^{2f} (b) measurement setup

2.4.3 Joule heating and second harmonics detection

In this V^{2f} measurement set-up, we simply replace the laser heating by Joule heating. We keep the DC current, and then apply an additional AC current. Now the AC current will generate a Joule heating oscillating at twice the frequency ($2f$). We

lock-in at this double frequency to measure the so-called V^{2f} signal.(Fig 2.7b) This signal is found to be very sensitive to the switching field of the spin valve.

In the V^{2f} measurement we apply an AC current and DC current at the same time. The AC current is applied by the Lock-in amplifier and the DC current is generated by a separated DC current source. Typically, we set the AC current at the frequency of 400Hz at the amplitude from $50\mu A$ up to 1mA. The DC current we apply is in the order of magnitude of $100\mu A$.

We also carried out V^{2f} measurement in the absence of the DC current, and then we are measuring the current susceptibility of the spin valve, which will be explained in the next chapter.

2.5 Probe of rotation

In order to measure the angular dependent V^{2f} and magnetoresistance, we designed a probe of rotation that can be controlled by computer. With a labview programme , we are able to tell the motor to turn a certain angle and measure the V^{2f} and magnetoresistance at the same time. The probe goes into the cryostat, so we can also conduct low temperature measurement.

2.5.1 Labview control of rotating motor

We developed a labview programme which is compatible to the rotating motor. With this programme, we can remote control the probe to rotate to a certain angle, stop and we measure the signal from the lock-in amplifier, and rotate again. Fig 2.8 is an example of the front panel of the Labview programme controlling the rotation.

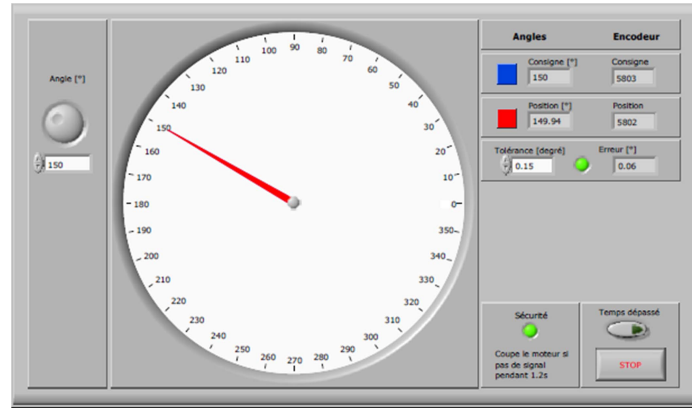


Figure 2.8: an example of Labview front panel of controlling the rotating probe.

2.5.2 Chip carrier and connection

At the bottom of the probe, we have designed a chip carrier socket where we can fit in our sample. The contacts on the chip carrier will eventually connect to a 19-plug box. With this design we can do four point measurement on nanostructures. In addition, this probe sample holder is also compatible to “plaquette” sample holder, because we connect a 4-pin female plug at the edge of the socket which connect to the plugs of N°13 to 16 in the box.

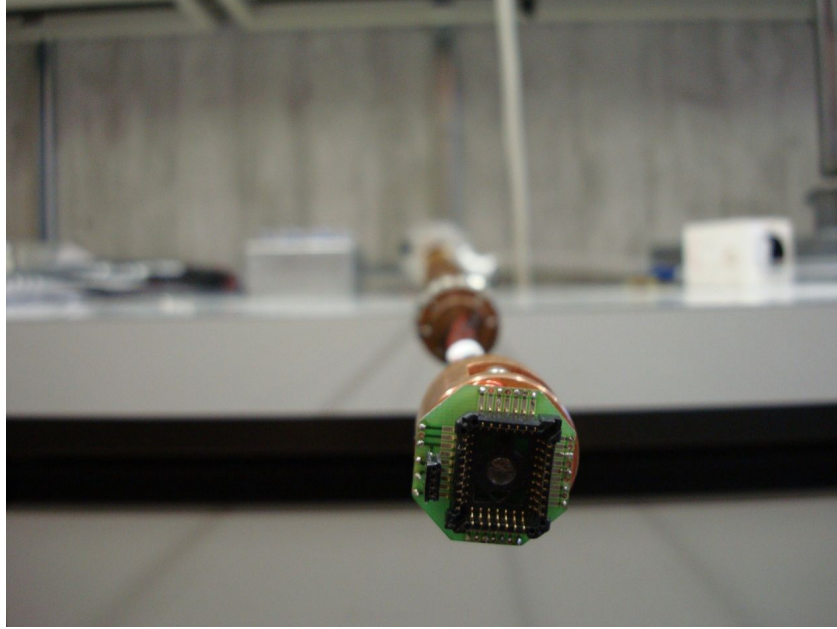


Figure 2.9: a close-up of the chip carrier socket and plaquette connection at the end of the rotating probe

2.5.3 Exchanged-bias spin valve sample

The exchanged-bias spin-valve sample was provided by our colleague and collaborator Mohamed Abid who fabricated it in Ireland. The detailed structure of the spin-valve sample is Si/SiO₂/buffer/IrMn 6/CoFe 3.5/Cu 2.8/CoFe 2.5/Cu 2.8/CoFe 2.5/IrMn 10/Ta 5 (thickness in nm). The buffer layer is Ta 5/CoFe 3/Cu 3. The free layer is 2.5nm CoFe. The stack composition is shown in Fig 2.10a.

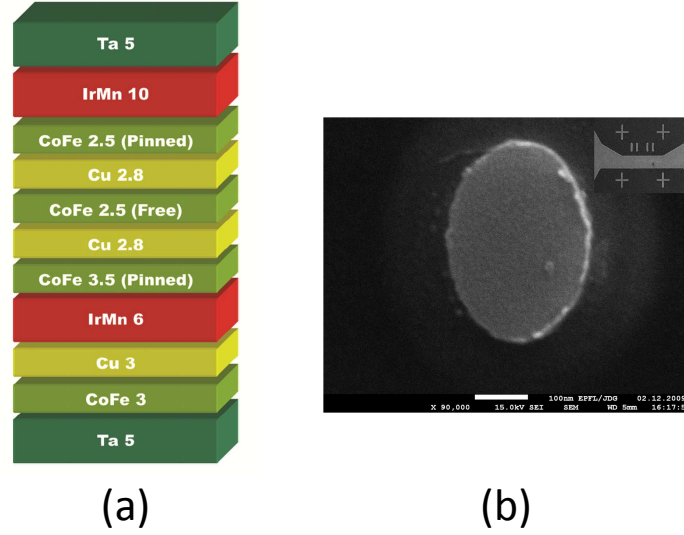


Figure 2.10: Dual spin valve nanopillar: (a) detailed structure of the dual spin-valve stack. thickness in nm. (b) Top-view SEM picture of spin valve nano-pillar.

The easy axis of both the free and pinned layers is aligned along same direction by applying a field of 10mT while deposition. After that, the sample was annealed at 250°C under an external field of 800mT for 2 hours.

The bottom has two contact pads, whereas the top each one has one extended contact. We took a top-view SEM picture of the nano-pillar(Fig 2.10b). As we can see, the dimension of the pillar cross-section is $250\text{nm} \times 400\text{nm}$.

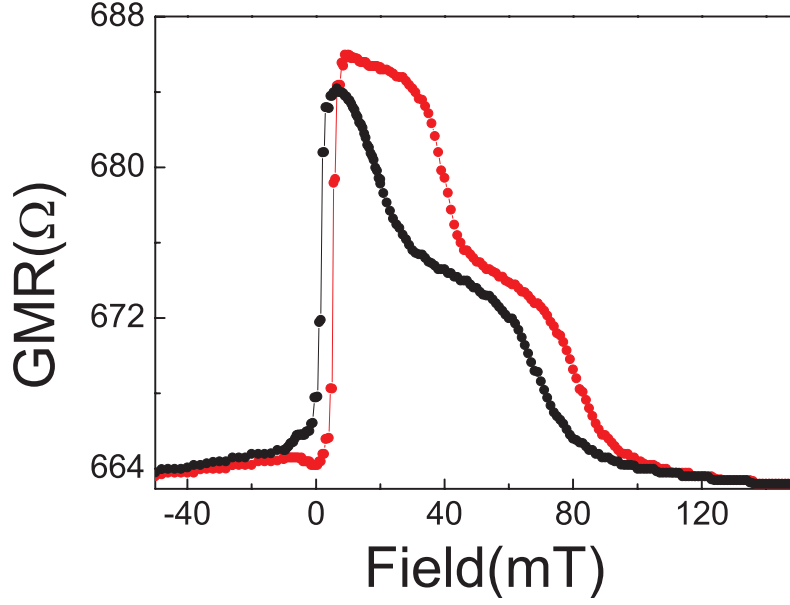


Figure 2.11: *GMR of double-pinned exchanged-bias spin valve. Red curve is measured when the field is swept from negative to positive, and black curve stands for positive to negative. The applied AC current is $500\mu A$.*

We measured the GMR of the sample(Fig 2.11) when we apply an external field along its easy axis, and as expected we observed two steps in the GMR curve where the sharp jump is when the free layer switches. The current is applied perpendicular to the plane(CPP).

Chapter 3

Transport measurements

3.1 MR on spin valve

The Magnetoresistance is measured by conventional detection of the AC voltage subject to an applied AC current using a lock-in amplifier (AMETEC 7270) while sweeping the field from negative to positive saturation. The typical AC current we applied to the sample is $1\mu\text{A}$ at the frequency 400Hz , which is far from the frequency of the resonance. In all measurements, if not specified, we measure at room temperature, we take time constant to be 500ms , and we do auto-phase before all the measurement. The geometry of the nanowire ensures that the AC current is applied perpendicular to the plane(CPP). The voltage measured is of about $100\mu\text{V}$. The Lock-in detection can filter the noise, therefore enhance the signal-to-noise ratio(SNR).

We measured a nanowire sample containing single spin valve structure in the middle. (Fig 3.1) The spin valve sample was fabricated by electrodeposition described in Chapter 2. The spin valve we are measuring here is actually a "pseudo spin valve", because the magnetization of the hard layer is not deliberately pinned as exchanged-bias spin valve. Nevertheless, our asymmetric deposition ensures that the magnetization of each layer switches at different values of the applied field,

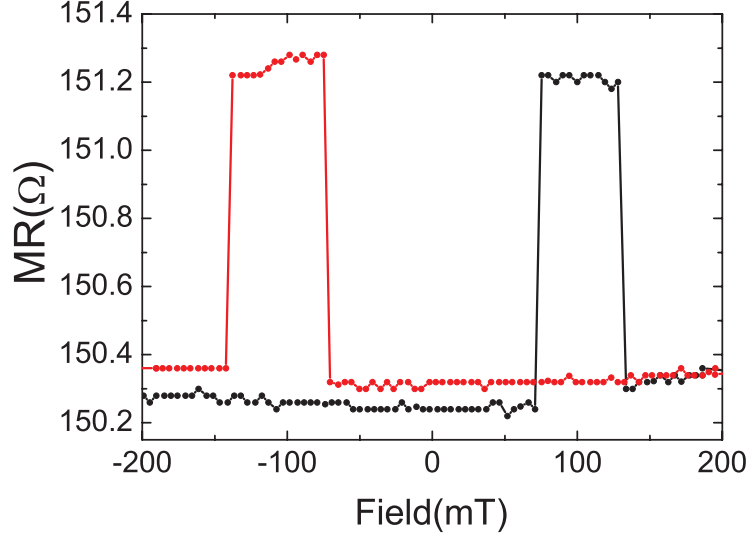


Figure 3.1: *MR measured on a nanowire containing a spin valve of Co 10nm/Cu 10nm/Co 30nm. The applied AC current is $100\mu\text{A}$ perpendicular to the plane and the field is applied parallel to the nanowire, which is perpendicular the layer. The black curve is the field sweeping from negative to positive, whereas the red one is from positive to negative.*

which can be clearly observed in Fig 3.1. All the spin valve samples we refer to in Chapter 3 and 4 are like this unless specified. The MR ratio reaches 0.5 percent in this sample. Although this percentage looks fairly small, this MR change comes only from the tiny spin valve in the middle of the entire nanowire, when the total resistance is mainly attributed to the copper lead. If only consider the spin valve structure, we have about 1 Ohm MR change coming out of the spin valve with an estimated resistance of 2.4 Ohm. Thus, the MR ratio of the spin valve is over 40 percent. This indicates that the electrode deposited spin valve in nanowire has very high quality for spin-dependant transport study.

3.2 MTGV on spin valve

We conduct this so called Magneto thermal galvanic voltage(MTGV) on spin valve sample, just as former group member had done on Co/Cu multilayer nanowires [14] and magnetic cluster samples [15]. This measurement protocol as introduced in Chapter 2, consists of an oscillating laser heating and an applied DC current. By locking-in at the laser frequency of 22Hz, we detected a voltage signal. The magnetic field dependence of this signal is usually larger than the GMR on the same sample.

In Fig 3.2, we measured MTGV and MR on the same sample. In this sample, we deposited a single spin valve structure of 10nmCo/10nmCu/30nmCo in the middle of the nanowire. The TGV signal does not differ at parallel(P) and anti-parallel(AP) state; however, at the transition region, we can observe a very sharp peak. These peaks are very sensitive to the magnetic field, with a typical full-width at half-maximum(FWHM) of about 3 mT.

In Fig 3.3, we measured the MR and MTGV on another spin valve sample. In this sample, we have deposited two spin valve structure in series isolated by more than $1\mu\text{m}$ copper lead. The MR shows 4 switches in a single field sweep: two reversible and gradual transitions as well as two irreversible and sharp transitions. We can observe from the TGV response that the sharp peaks are detected in MTGV curve exclusively when the GMR of the spin valve sample undergoes a gradual and reversible transition. This suggests that the MTGV peaks are provoked by the non-collinear configuration of the two cobalt layer in a spin valve. The magnetic dependent change of signal is about 5 percent, much higher than the GMR ratio of 0.2 percent. Similar observation are found in penta-layer($5\times\text{Co/Cu}$) structures. [9]

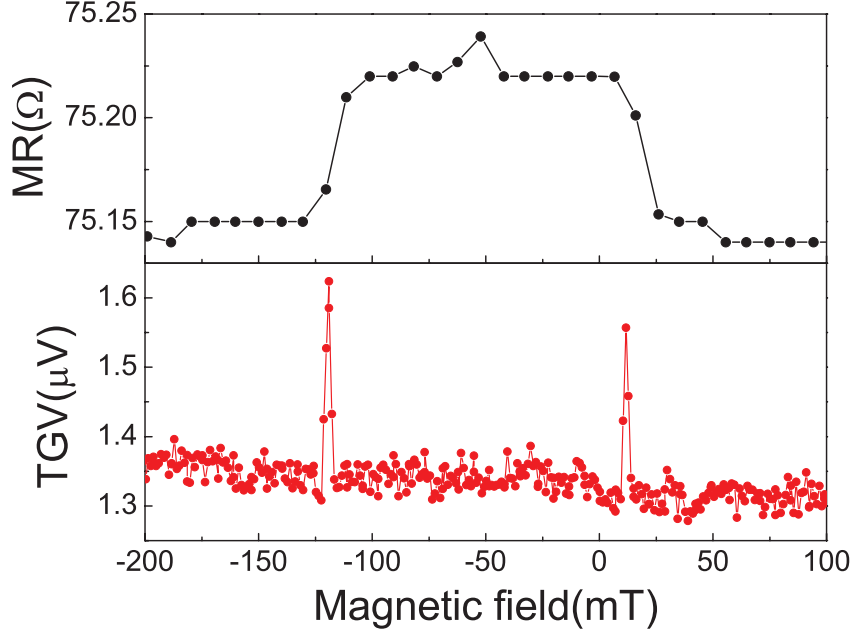


Figure 3.2: *MTGV and MR on nanowire containing a single spin valves in series. The spin valve structure is 10nmCo/10nmCu/30nmCo. The applied AC current is 100μA perpendicular to the plane. The magnetic field is applied perpendicular to the nanowire.*

We also measured the TGV signal as a function of the applied DC current (Fig 3.4), and we find the signal behave linearly. In fact, we can write:

$$TGV = \frac{dR}{dT} \Delta T_{AC} I_{DC} \quad (3.1)$$

where ΔT_{AC} is the temperature variation induced by the oscillating laser heating.

Here, we can see that TGV signal is proportional to I_{DC} , and the slope of the line is the $\frac{dR}{dT} \Delta T_{AC}$. At saturation and at zero fields, the isothermal resistance has the same temperature dependence. When there is no I_{DC} and we only have an oscillating laser and measure the voltage at the same frequency, the data point is actually measuring the thermoelectric power $S \Delta T_{AC}$.

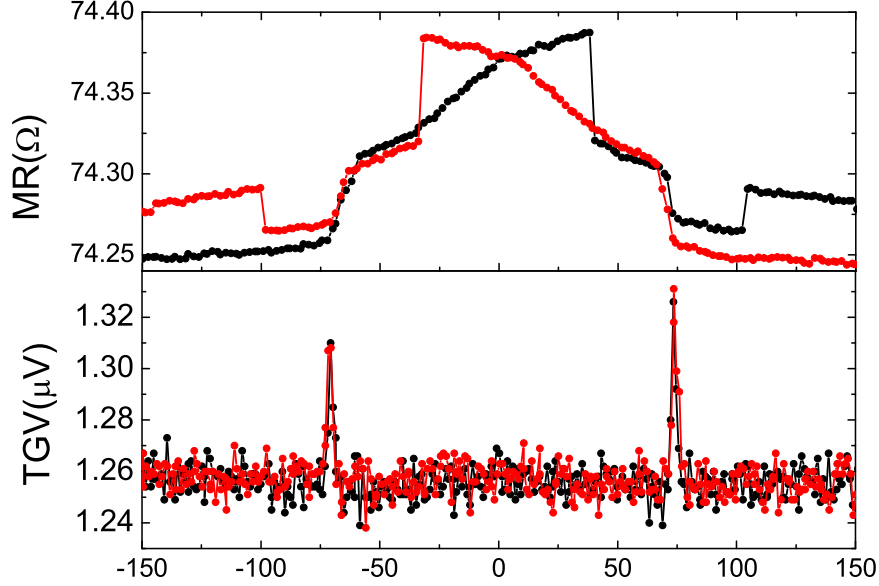


Figure 3.3: MTGV and MR on nanowire containing 2 spin valves in series.

The spin valve structure is 10nmCo/10nmCu/30nmCo. The applied AC current is $100\mu A$ perpendicular to the plane, at the frequency of 814Hz. The magnetic field is applied parallel to the nanowire ramping up (black) and down (red). Time constant is set to be 1 second.

Now how do we explain the sharp peaks which appear in the magnetic dependent measurement of TGV on spin valve? We account for the existence of TGV signal in non-collinear configurations of the magnetization of spin valves by using Eq 3.1 and a commonly used model of angular dependent GMR(Eq 3.2) found in the literature:

$$\frac{R(\theta) - R(0)}{R(\pi) - R(0)} = \frac{1 - \cos^2(\theta/2)}{1 + \chi \cos^2(\theta/2)} \quad (3.2)$$

where χ was initially introduced as a phenomenological parameter. Eq 3.2 was sup-

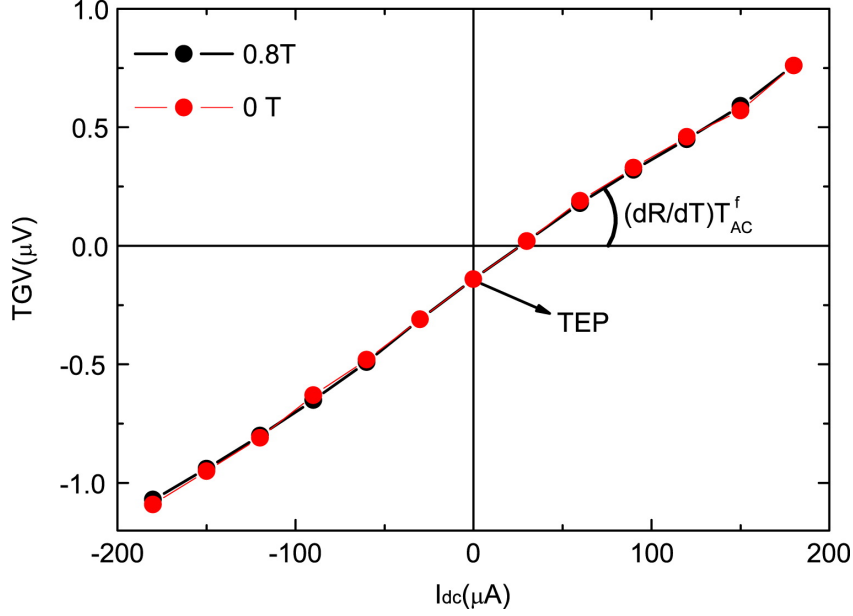


Figure 3.4: *TGV as a function of the DC current applied. This characteristic is about the same in the magnetic configurations at low and high fields. The $I_{DC} = 0$ intercept is the thermoelectric power due to the small temperature gradient across the nanowire.*

ported by magnetoelectric circuit theory [16] or by using the diffusion equations for the spin accumulation in non-collinear configuration. [43] Using our data which measures dR/dT , we can characterize the temperature dependence of this parameter χ . Indeed, taking the temperature derivative of Eq 3.2, we find [17]:

$$\frac{1}{\chi} \frac{d\chi}{dT} = \frac{MTGV}{GMR} \left(\frac{1}{\rho} \frac{d\rho}{dT} \right) \left(\chi \frac{dR_n(\theta_{max})}{d\chi} \right)^{-1} \quad (3.3)$$

where ρ is the effective resistivity of the spin valve, θ_{max} is the angle at which the magnetoresistance is maximum, GMR is the amplitude of the step normalized to the saturation value and $MTGV$ is the peak height normalized to its baseline value. R_n is the normalized resistance. Using the values for $MTGV$ and GMR from our experimental data, we find values that lead approximately to:

$$\frac{1}{\chi} \frac{d\chi}{dT} \approx 0.4 \frac{1}{\rho} \frac{d\rho}{dT} \quad (3.4)$$

For Shpiro et al. [43], the parameter χ is a function of λ_J , the transverse spin diffusion length, which is proportional to \sqrt{T} . In chapter 5, we will measure this parameter using angular dependant transport measurement. In diffusive model of Shpiro *et al.*, we have: $\frac{1}{\chi} \frac{d\chi}{dT} \approx 0.5 \frac{1}{\rho} \frac{d\rho}{dT}$. For Brataas *et al.* [16], χ is directly proportional to the spin mixing conductance $g_{\uparrow\downarrow}$, which is proportional to T , so that $\frac{1}{\chi} \frac{d\chi}{dT} \approx 1.0 \frac{1}{\rho} \frac{d\rho}{dT}$. We can see here that our data, as expected, are better described with a diffusive model.

3.3 V^{2f}

In V^{2f} measurement, we simply lock in at twice the frequency of the applied AC current to detect the V^{2f} voltage response. We conduct all of our V^{2f} measurement at room temperature unless specified otherwise. The frequency we use is between 200Hz and 1kHz, which is far from resonance. The current density is of the order of magnitude of 1×10^6 A cm⁻², which is much smaller than the threshold current needed for the excitation of the magnetic layer. We detect pronounced peaks at the same field position when and only when the MR curve experiences a gradual and reversible transition. This is found in the measurement on samples with different structures.

V^{2f} measurements present very high signal-to-noise ratio, which can be higher than that of the GMR in the same sample. (Fig 3.5)

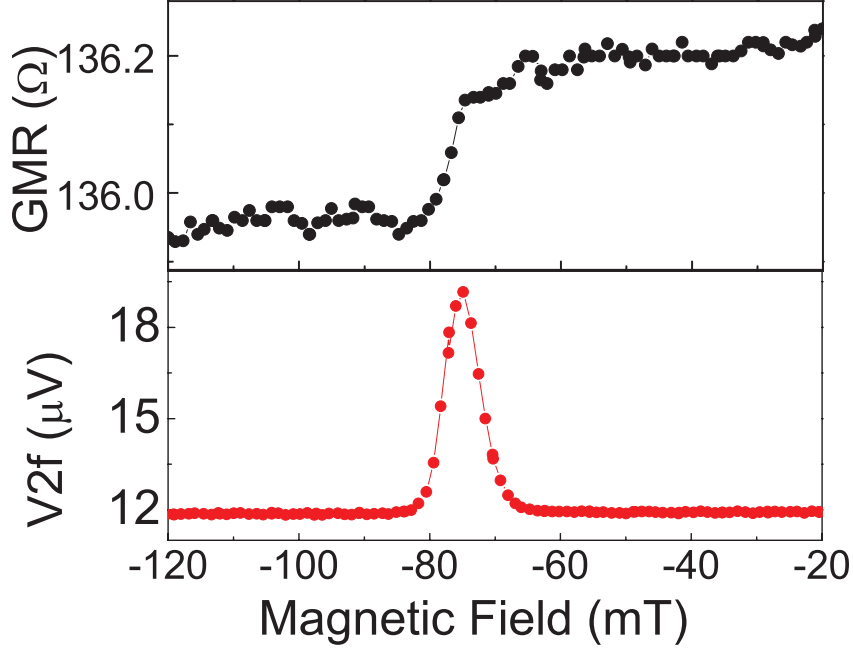


Figure 3.5: *Magnetoresistance(MR) and voltage response at frequency $2f$ to an oscillating current at frequency f while a DC current of 0.1mA is applied to the nanowire containing a single spin valve. The field was swept from negative to positive values. V^{2f} on spin valve as a function of the DC current I_{dc} while the nanowire is subjected to an AC current of $100\mu A$ at frequency f . The zero-current intercept is due to the current susceptibility of the spin valve, which is described in the previous section.*

3.3.1 V^{2f} — Current susceptibility on spin valve

We measure the V^{2f} and MR (Fig 3.6) on a Cu nanowire containing two spin valves in series, separated by several micrometers within the nanowire. The field is applied parallel to the axis of the wire. The presence of the sharp V^{2f} peaks shows that the second harmonic voltage signal is just as sensitive to the applied field as the magnetoresistance of the same sample. A significant feature of the data is that the V^{2f} peaks only appear when the layer magnetization switches over a finite

field range (around $\pm 70\text{mT}$), but not at all at a sudden switch ($\pm 40\text{mT}$). Since the external field is applied parallel to the wire, it is perpendicular to the plane of the layers, and typically the magnetization rotates over a finite field range, though it may be small. It is worth noting that, due to the very weak baseline, the relative magnitude of the peaks in the second harmonics signal is fairly large compared with the sharp MR transitions. We can see in Fig 3.6, V^{2f} changes by up to $0.5\mu\text{V}$ on a baseline of $0.75\mu\text{V}$, which is a change of 67%, whereas the maximum GMR ratio of the same sample at a sharp transition is $\sim 0.05\Omega/74.25\Omega = 0.06\%$. V^{2f} changes of over 100% are commonly found in many spin valve samples investigated as a part of this study.

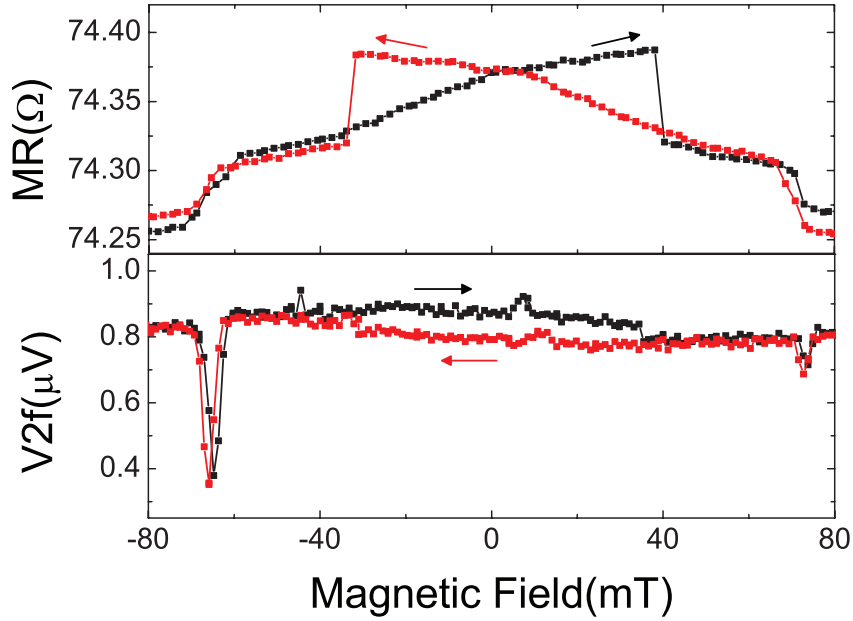


Figure 3.6: MR and V^{2f} of a Cu nanowire containing two spin valves $\text{Co}(10\text{nm})/\text{Cu}(10\text{nm})/\text{Co}(30\text{nm})$ in series, with the magnetic field applied parallel to the nanowire ramping up(black) and down(red).

Now we discuss the origin of the magnetic dependence of V^{2f} based on considerations of how the resistance of a spin valve depends on the quasi-static perturbation

of the configuration of the two magnetic layers. The second harmonic of the voltage generated in response to an applied ac current has also been calculated by my former colleague Julie Dubois from a theoretical description based on a diffusive model of spin transport in spin valves. [40] In that work, the magnitude of the calculated voltage response closely agrees with the size of the peaks in the V^{2f} signal in experiments. Non-linearity in the voltage response V versus current I is expected whenever the resistance depends on the magnetization, which depends on current. This idea was exploited by Juretschke [18] to obtain a dc voltage when electromagnetic irradiation is at resonance with the fundamental ferromagnetic resonance mode [19] or spin wave modes [20] in homogeneous thin films. Since we are at very low frequency compared with the resonance modes to probe the non-linear voltage response, we refer to the work of Kovalev et al [26], who calculated the voltage response of spin valves to an applied ac current and take the limit $\omega \rightarrow 0$. In this work, they start with a generalized Landau-Lifshitz-Gilbert (LLG) equation

$$\frac{d\mathbf{M}}{dt} = -\gamma \mathbf{M} \times \mathbf{H}_{eff} + \frac{\alpha}{M_s} \mathbf{M} \times \left(\frac{d\mathbf{M}}{dt} \right) + \gamma \frac{\hbar}{2e} \frac{I(t)}{V_m} \eta_1 \mathbf{m} \times (\mathbf{m}_{fixed} \times \mathbf{m}), \quad (3.5)$$

where M is the magnetization of the free layer and m and m_{fixed} are the unit vectors of magnetization for the free and fixed magnetic layers, respectively. $I(t)$ is the applied AC current, η_1 denotes the strength of the spin-transfer torque and the other constants take their usual definitions. Here we have omitted the effective-field-like term given rise by a ‘spin-transfer exchange field’, as this term is thought to be relevant in tunnel junctions, but negligible in metallic structures [21], such as spin valve. H_{eff} contains terms including the externally applied field, anisotropy, demagnetization and dipolar fields.

With reference to the diagram of Fig 3.7, the total resistance of the spin valve is

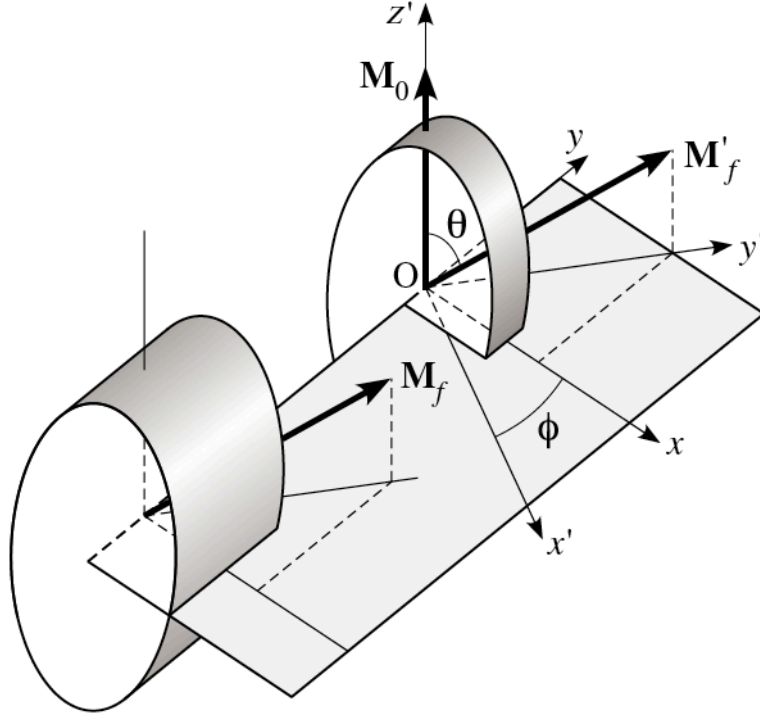


Figure 3.7: Fixed layer M_f and free layer M_0 magnetization vectors. M'_f is M_f shifted to O . Ox' is defined as the normal to the plane containing M'_f and M_0 . θ is the angle between M'_f and M_0 . ϕ defines a rotation of M_f which keeps θ fixed. The shaded plane containing $Ox'y'$ is a guide to the eye.

given as

$$R = R(\cos \theta) - \frac{\partial R(\cos \theta)}{\partial (\cos \theta)} \sin \theta \delta \theta, \quad (3.6)$$

where angle between two magnetization is dependent on the applied magnetic field. Here the AC current induces a small perturbation of the relative magnetization angle $\delta\theta$, which to first order is equal to the oscillatory component of magnetization $m_{y'}$. The total voltage resulting from the influence of the AC current on the

resistance is equal to a dc term plus a term proportional to I^2 at twice the frequency ω of the current

$$V^{2f} = I_0 \frac{dR}{d\theta} \delta\theta, \quad (3.7)$$

where I_0 is the magnitude of the AC current.

According to ref [26], we have

$$\delta\theta = \frac{M_{y'}}{M_s} = \frac{M_{y'}/I_0}{M_s} I_0 = \frac{\chi_{y'I}}{M_s} I_0, \quad (3.8)$$

Here we define $\chi_{y'I} = M_{y'}/I_0$ and $M_{y'}$ is defined in the expansion of the free energy close to equilibrium,

$$F(\mathbf{M}) = F(\mathbf{M}_0) + N_{x'} M_{x'}^2/2 + N_{y'} M_{y'}^2/2 + N_{x'y'} M_{x'} M_{y'} \quad (3.9)$$

Combining eq. 3.7 and eq. 3.8, we have

$$V^{2f} = \frac{I_0^2 \sin \theta}{2M_s} \frac{\partial R(\cos \theta)}{\partial (\cos \theta)} | \chi_{y'I} |, \quad (3.10)$$

where

$$\chi_{y'I} = \frac{-\hbar\gamma \sin \theta}{2eV_m} \frac{\eta_1 (N_{x'y'} + \alpha N_{x'})}{\gamma M_s (N_{x'} N_{y'} - N_{x'y'}^2)}, \quad (3.11)$$

In Eq ?? we have taken the linear response function $\chi_{y'I}(\omega)$ of [26] with $\alpha \ll 1$, $\eta_2 = 0$, in the limit $\omega \rightarrow 0$ as appropriate for the low frequency of our applied AC current. Here we use the relations of their notations, $\Gamma_{y'} = \eta_1 (N_{x'y'} + N_{x'} \alpha)$ and $N_x^d N_y^d = N_{x'} N_{y'} - N_{x'y'}^2$, so that we transform eq 16 in ref [26] into our eq 3.11.

Thus, the signal at $2f$ involves the current susceptibility of magnetization at low frequency.

We transform Eq 3.10 and Eq 3.11 using the system of coordinates of fig. 3.7 in order to demonstrate more explicitly the sensitivity of V^{2f} to specific switching processes. The form of V^{2f} with damping then becomes

$$V^{2f} = \frac{1}{2}\eta_1 I_0 \frac{\partial R(\nu)}{\partial \nu} \frac{I_0/e}{\gamma M_s} \frac{\gamma \hbar/2}{V_m M_s} \sin^2 \theta \frac{N_x^d}{N_y^d} \times \left[\left(\frac{N_y^d}{N_x^d} - 1 \right) \cos \phi \sin \phi - \alpha \left(\frac{N_y^d}{N_x^d} \sin^2 \phi + \cos^2 \phi \right) \right], \quad (3.12)$$

where N_x^d and N_y^d are the diagonal components of the demagnetization tensor. Typically, $(N_x^d/N_y^d) < 1$. As indicated in ref [26], $N_{x'} = N_x^d \cos^2 \phi + N_y^d \sin^2 \phi$, $N_{y'} = N_y^d \cos^2 \phi + N_x^d \sin^2 \phi$ and $N_{x'y'} = (N_x^d - N_y^d) \cos \phi \sin \phi$. Using Eq 3.12 and Fig 3.7, we can understand a switching process that gives rise to a sharp peak in V^{2f} where the change in MR is gradual, such as experimentally seen around $\pm 70mT$ in the measurements of Fig 3.6. From Eq 3.6, R is determined entirely by the angle θ between the layer magnetization, which is in the $Oy'z'$ plane in Fig 5.2. However, V^{2f} is also dependent on angle ϕ , besides θ , which is in the $Ox'y'$ plane. We will have a more extensive discussion of Eq 3.12 in Chapter 5, where we investigate the angular dependence of the V^{2f} signal.

A systematic observation representative of the many samples measured is that the V^{2f} is almost insensitive to the situations of parallel and anti-parallel configuration of the Co Layers. At the fields where MR shows a sharp transition, the V^{2f} changes from the baseline is very small at best, whereas a pronounced peak is observed when the MR presents a progressive transition. The case of small “steps” between magnetization orientations is best illustrated in Fig 3.8, showing the V^{2f} and the MR of a Cu nanowire containing a single spin valve. Here, only a small change

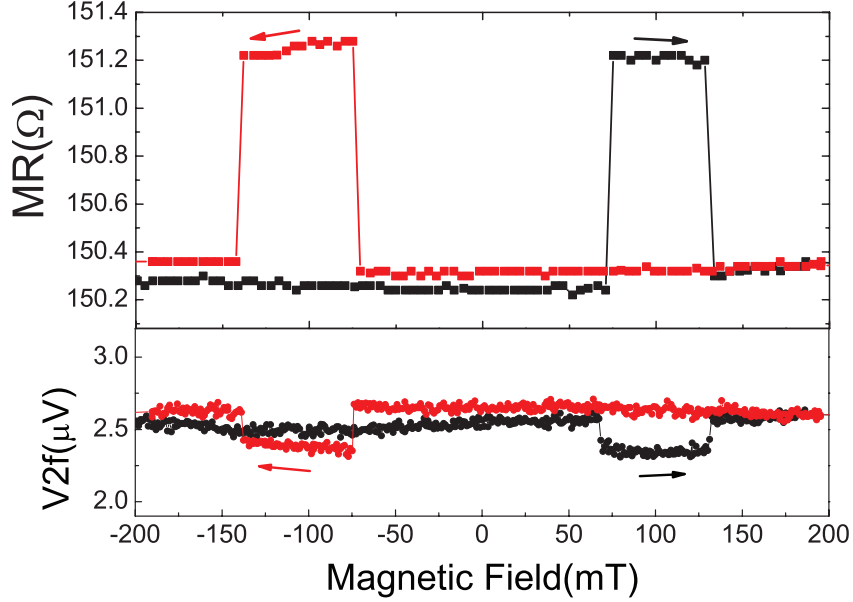


Figure 3.8: V^{2f} and MR of a nanowire containing a single spin valve. The applied AC current is $100\mu\text{A}$. The magnetic field is applied parallel to the wire, ramped up(black) and down (red).

in V^{2f} appears when the spin valve changes to the anti-parallel state. This type of V^{2f} response can also be observed in Fig 3.6, at the field position where sharp MR transition occurs. According to the model of spin-transfer torque response, pronounced peaks in V^{2f} are expected only in the cases where the Co layers switch gradually, so that non-collinear orientations of the two layers occur in the quasi-static regime.

In the cases where the MR has sharp switches, as seen in Fig 3.8 and Fig 3.6, θ apparently rotates by approximately 180° within a field range less than that of successive field values applied in the experiment ($<2\text{mT}$). In these cases there is no peak, instead a small step in the V^{2f} signal. This step may be understood as evidence for oscillations of θ on a local scale, being due to distortions of the magnetization given rise by the Oersted field H_{ind} induced by the applied current

along the nanowire. Owing to the cylindrical geometry of our spin valves, H_{ind} is poloidal. The induction expected from the current loop formed by the overall contacting circuitry is calculated to be of the order of about 0.01mT, small compared with the value of $\mu_0 H_{ind}$ at the surface of a nanowire., which reaches 0.5mT. As pointed out by Devolder *et al* [22], when the spin valve is in the parallel branch of the hysteresis loop H_{ind} tends to keep the magnetization of the layers collinear at each point of the cross section, whereas H_{ind} opens up the angle θ between adjacent magnetizations on the anti-parallel branch. As a result, a deformation of the magnetizations due to H_{ind} will necessarily emerge in the V^{2f} signal by way of a small change in the resistance; however, it is small compared with the current susceptibility of the magnetization due to spin transfer torque. Below we provide a rough and brief estimation of the contribution of this effect in our V^{2f} signal. The perturbation of θ is calculated by $\delta\theta \simeq H_{ind}/H_{sw}$ where we take the experimentally measured spin valve switching field H_{sw} to be around 100mT as seen in fig. 3.8. We use a simplified V^{2f} expression $V^{2f} = I_0 \frac{dR}{d\theta} \delta\theta$. Here we can calculate $\frac{dR}{d\theta}$ using eq. 3.2 and taking the value of $R(\pi) - R(0)$ and $R(0)$ from our experimental results in fig. 3.8. I_0 is 100 μ A in this measurement. We thus estimate that a uniform field of the order of magnitude of the poloidal field would produce a rotation of the magnetization that yields a voltage response of about 0.1 μ V, which is close to the size of the small steps observed in Fig 3.8 and Fig 3.6.

In summary, in this section I have shown the measurements of the voltage at twice the frequency of a $< 2kHz$ ac current in individual PSVs at low current densities are extremely sensitive to an externally applied magnetic field. Sharp peaks or small shifts appear in the V^{2f} signal during field sweeps at room temperature. Owing to the low baseline of the V^{2f} signal, the sharp peaks are more sensitive than the MR response of the same samples. The current density applied in the experiments is below the threshold needed to excite the ferromagnetic modes of

the magnetic layers. The frequencies are low enough that it is appropriate to consider the quasi-static regime, which gives a key distinction of these results from similar experiments previously performed on other systems such as thin magnetic films. This means that the measured V^{2f} is a probe of the linear response of the layer magnetizations to an applied current. Additionally, the V^{2f} signal has been demonstrated to be sensitive to particular types of layer switching processes that go unseen in the MR measurement.

3.3.2 V^{2f} with I_{dc} — V^{2f} vs TGV on spin valve

However, if we apply an additional DC current in the spin valve while doing the V_{2f} measurement described in the previous section, we find the signal being enhanced dramatically. We measure the V^{2f} signal as a function of the applied DC current, and we observed a linear behavior. (Fig 3.9)

This results can not simply be explained by the linear response of AC spin-transfer torque; Nevertheless, we can find a close similarity between this measurement Fig 3.9 and that of Fig 3.4, where we measured the TGV signal as a function of I_{dc} . [27]

This similarity of I_{dc} dependence can be understood as follow. In TGV measurement, we generate an oscillating temperature ΔT_f with a chopped laser heating and at the same time we apply a DC current, and then we lock-in at this laser frequency to measure Voltage V_f , which is the TGV signal(Eq 3.13). Whereas in the V^{2f} with I_{dc} measurement, the AC current generate a Joule heating oscillating at twice the frequency, and we lock-in at the Joule heating frequency to measure the V^{2f} signal.(Eq 3.14) Here, we denote by ΔT_{2f} the amplitude of the temperature oscillation at frequency $2f$.

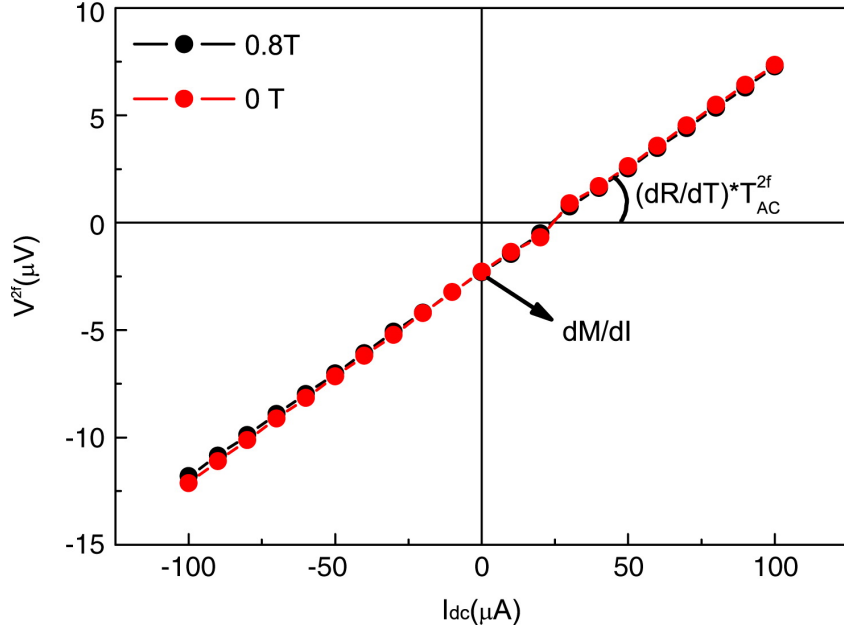


Figure 3.9: V^{2f} on spin valve as a function of the DC current I_{dc} while the nanowire is subjected to an AC current of $100\mu A$ at frequency f . The zero-current intercept is due to the current susceptibility of the spin valve, which is described in the previous section.

$$V_f(TGV) = \left(\frac{dR}{dT} \Delta T_f \right) \cdot Idc, \quad (3.13)$$

$$V_{2f} = \left(\frac{dR}{dT} \Delta T_{2f} \right) \cdot Idc, \quad (3.14)$$

In other word, V^{2f} is an alternative measurement to TGV, but much simpler experimentally, because we can avoid the complex and delicate laser system. In Fig 3.9, we find a residual value at $I_{dc} = 0$, which is exactly what we measured and discussed in the previous section. Hence, together we can write:

$$V_{2f} = \left(\frac{dR}{dT} \Delta T_{2f} \right) \cdot Idc + \frac{dR}{dM} \frac{dM}{dI} I_{AC}^2, \quad (3.15)$$

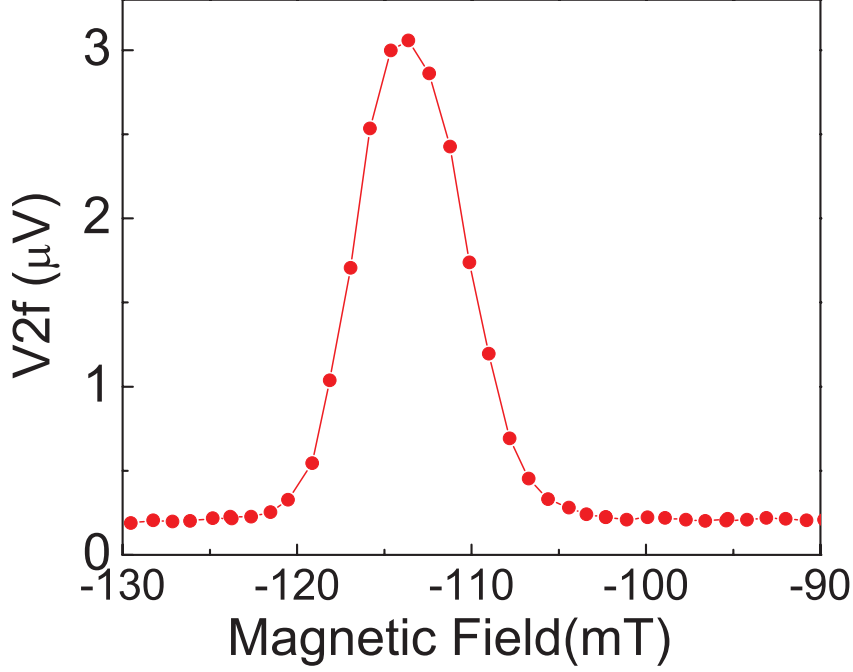


Figure 3.10: V^{2f} signal detected in a nanowire containing a spin valve (10nm Co/10nm Cu/ 10nm Co) under an alternating current of $100\mu A$ and zero direct current. The field was swept from negative to positive values.

In particular, the data are the same in Fig 3.9 at low and high fields. However, when the measurement is carried out at a set DC current, as a function of applied magnetic field, there appear sharp peaks near the fields at which the GMR data indicate switching of one layer. (Fig 3.5) We have collected numerous data on similar samples. Depending on the magnetic anisotropy of a sample and the direction of the applied field, we can find such sharp peaks away from the edge of the GMR data. These observations show that these sharp peaks are not spurious effects of our detection scheme that happen because the resistance changes sharply (Ref. [23])

The V^{2f} measurement has the added advantage over GMR of having a much larger signal-to-noise ratio(SNR) (Fig 3.5). The GMR presents a change of only 0.1%, whereas the V^{2f} changes by more than 60%. We also find that the baseline of the V^{2f} response can be strongly modulated by an applied dc current. [27] The peak height of V^{2f} can reach up to 1000% relative to the baseline in some samples (Fig 3.10)

3.4 V^{2f} and TGV on miscellaneous samples

3.4.1 Nanowire containing 5 spin valve

In a nanowire containing 5 spin valves in series with about $1\mu\text{m}$ between each other, we observed several MR steps, and we can clearly see that the V^{2f} peaks and TGV peaks are not exactly the same but correspond to each other. (Fig 3.11)

Here we can see that the V^{2f} peaks and TGV peaks are fairly common in spin valve structures; however, both of them only show strong response when the GMR presents a progressive transition.

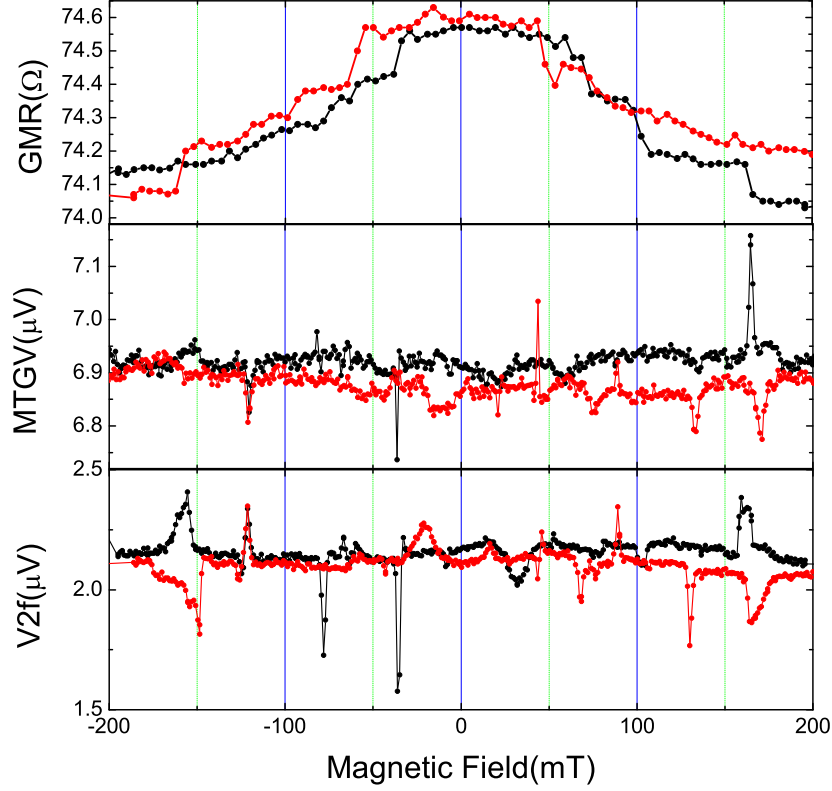


Figure 3.11: 5 spin valves of 10nm Co/10 nm Cu/30nm Co in series with about $1\mu\text{m}$ Cu lead between each other. The external field is applied parallel to the nanowire, ramped up (black) and down (red). The GMR was measured under an AC current of $100\mu\text{A}$ at the frequency of 400Hz. TGV was measured with a laser heating oscillate at 22 Hz with a DC current of $200\mu\text{A}$. V^{2f} was measured with an AC current of $100\mu\text{A}$ at the frequency of 400Hz. All measurements were carried out at room temperature.

3.4.2 Co/Cu multilayer nanowires

We also measured both the TGV and V^{2f} on Co-Cu multilayers, where we have about 300 repeated times of Co 10nm/ Cu 10nm from bottom to the top of the

nanowire. This structure is quite easy to fabricate by electroplating, because we only need to create a loop of the deposition potential in labview programme. The TGV measurement has been extensively studied and explicitly discussed in the thesis of a former member of the group Santiago SERRANO GUIBAN [9], thus here I will focus on the V^{2f} on Co-Cu multilayers. First I measured the GMR of the sample (Fig 3.12), then on the same sample, I did the MTGV measurement (Fig 3.13)

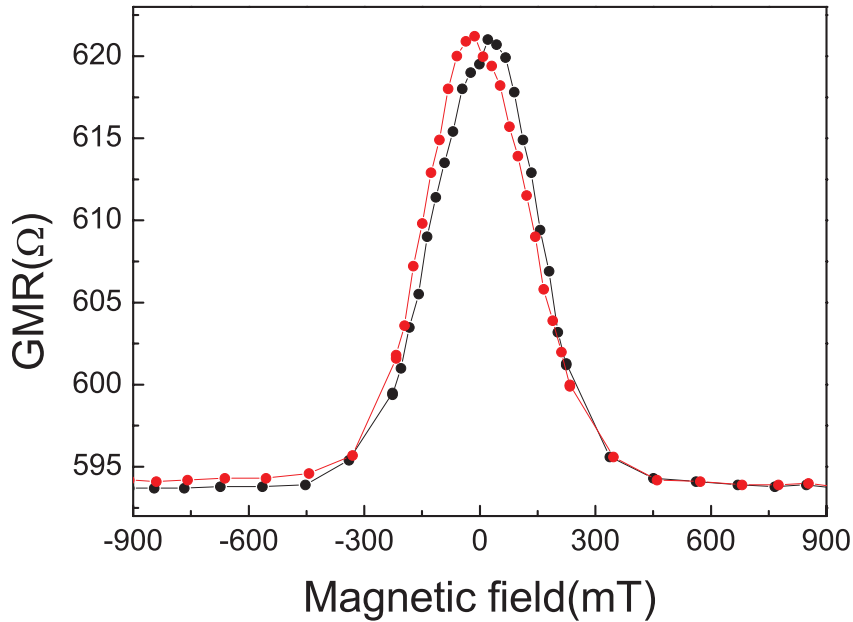


Figure 3.12: GMR of Co/Cu multilayer nanowire sample. An AC current of $1\mu\text{A}$ was applied. The external field is applied parallel to the nanowire, ramped up (black) and down (red).

In the TGV measurements, we find two characters of the curve. One is the GMR-like shape, where we have minimum at 0 field and maximum at saturating field. The other is the little "spikes" along the curve. They are not very strong, but definitely out of the noise level. This observation is analogous with what was discussed in Chapter 6 of ref [9].

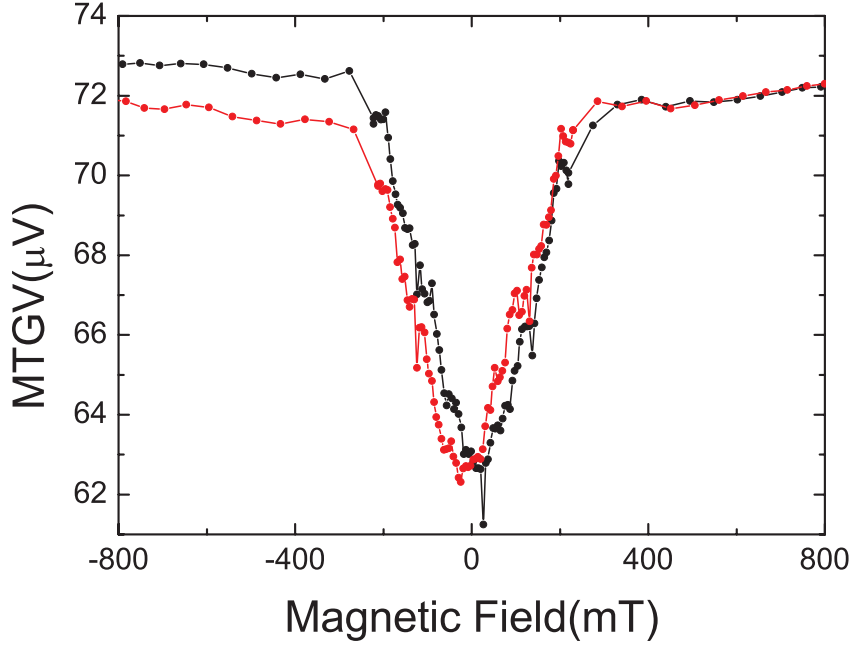


Figure 3.13: *MTGV measured on a Co/Cu multilayer nanowire sample with a laser heating oscillating at 22 Hz and a DC current of 100 μ A. The external field is applied parallel to the nanowire, ramped up (black) and down (red).*

Then we carried out the V^{2f} as a function of the applied field measurement on this sample.(Fig 3.14) Here, we can observe also the GMR-like shape, where we have maximum at 0 field and minimum at saturating field. V^{2f} vs field shows strongly enhanced “spikes”, and they appear some a characterization of symmetry versus the 0 field position.

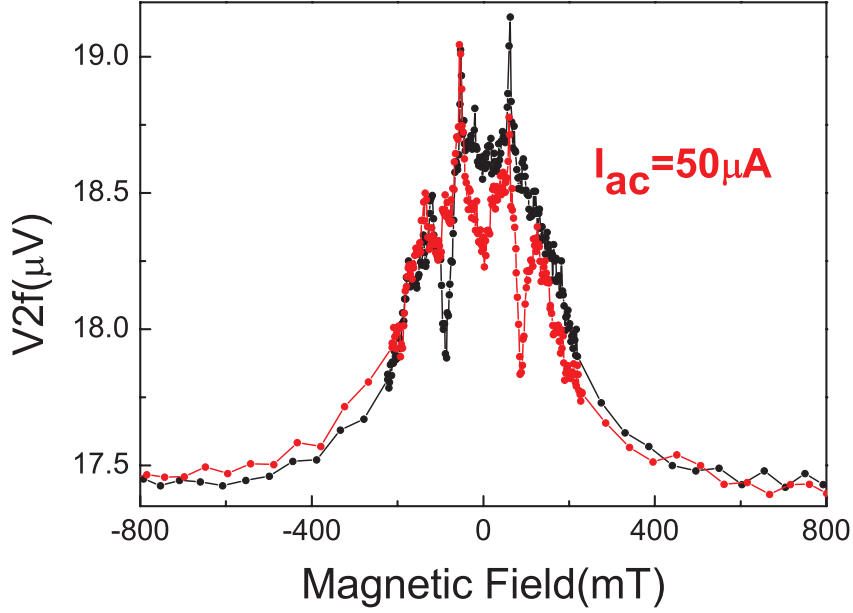


Figure 3.14: V^{2f} of the multilayer Co/Cu nanowire of which MTGV is shown in Fig 3.13 with $I_0 = 50\mu A$ applied at 406 Hz and magnetic field applied parallel to the nanowire, field ramped up (black) and down (red)

The nature of these spikes is not yet fully understood. This effect points to a strongly interaction between the magnetic layers and spin polarized current, that occurs for specific magnetic configurations when Co layer magnetization is forced to turn out of alignment with one another. It could involve precession phenomena of the cobalt layer magnetization induced by a spin transfer mechanism which can occur because the magnetic field is approaching the switching field value [24]. In other word, this observation can possibly be accounted for by the collective behavior of the effect of current susceptibility of spin valve discussed in the former part of this chapter. The difference is that in all these Co layer, the magnetization is strongly affected by that of the other layers, particularly the adjacent ones. Therefore, it is not very possible that one layer magnetization rotates while all the other stay still and then the next one rotates. It is more likely to be a collective

behavior. If so, this collective switching process of magnetization can be potentially applied in a so-called "3-dimensional spintronics" proposed by others [25] for data storage and processing applications.

On the same sample we did a series of measurements on V^{2f} vs field with different AC current. (Fig 3.15, Fig 3.16, Fig 3.17)

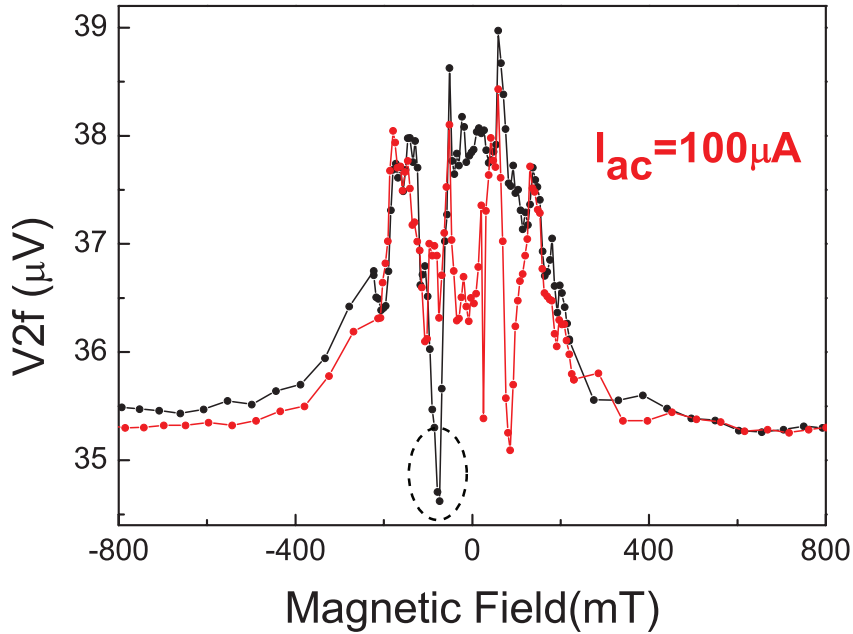


Figure 3.15: V^{2f} of a multilayer Co/Cu nanowire with $I_{ac} = 100\mu A$ applied at 406 Hz and magnetic field applied parallel to the nanowire, field ramped up (black) and down (red)

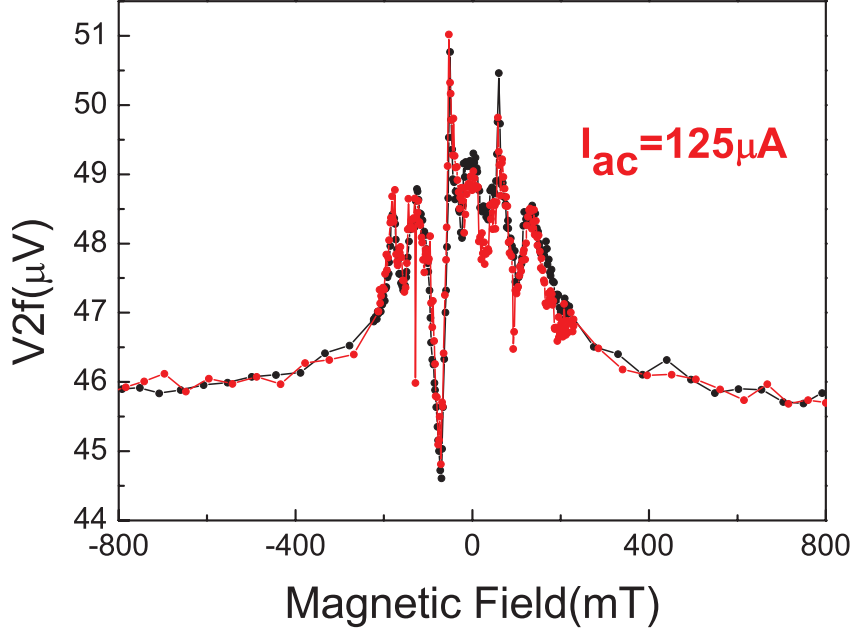


Figure 3.16: V^{2f} of a multilayer Co/Cu nanowire with $I_{ac} = 125\mu A$ applied at 406 Hz and magnetic field applied parallel to the nanowire, field ramped up (black) and down (red)

As the AC current increases, we find that the spikes become more and more significant, whereas the GMR-like shape does not change. The magnitudes of these spikes scale as I_{ac}^2 , which is in agreement with Eq 3.12. This observation demonstrates that these sharp spikes are induced by the linear response of resistance to the AC current, just as the current susceptibility of the spin valve.

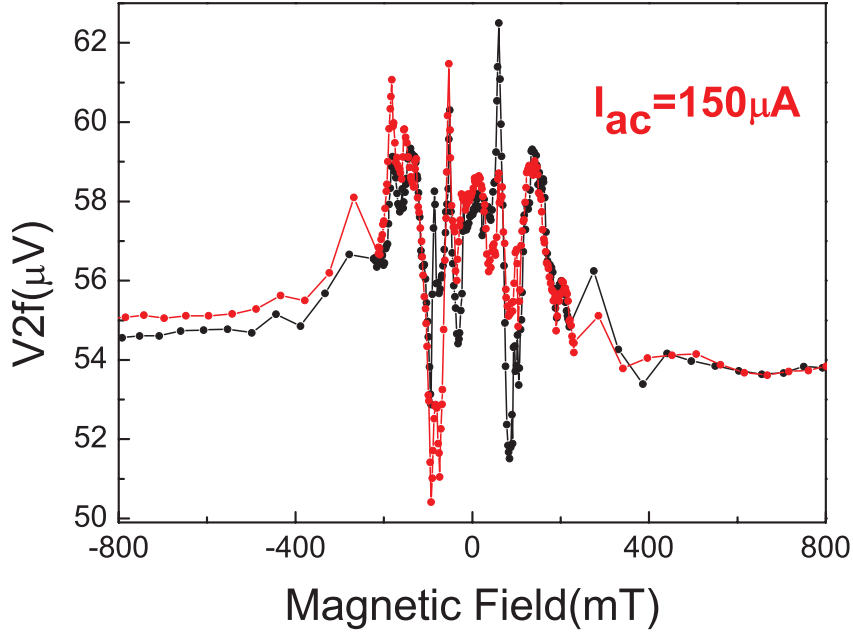


Figure 3.17: V^{2f} of a multilayer Co/Cu nanowire with $I_{ac} = 150\mu A$ applied at 406 Hz and magnetic field applied parallel to the nanowire, field ramped up (black) and down (red)

We also notice that in some measurements such as Fig 3.16 the spikes are mostly reversible when we scan from negative saturation field to positive one and sweep back. However, in Fig 3.15, for example, the spike in the grey circle is apparently not reversible when we do a full-loop scan. In Fig 3.18, we measured the same spike, but swept the field in a local loop (from -900mT to -45mT and ramp down directly from -45mT back to -900mT), and then we find this time the spike becomes completely reversible.

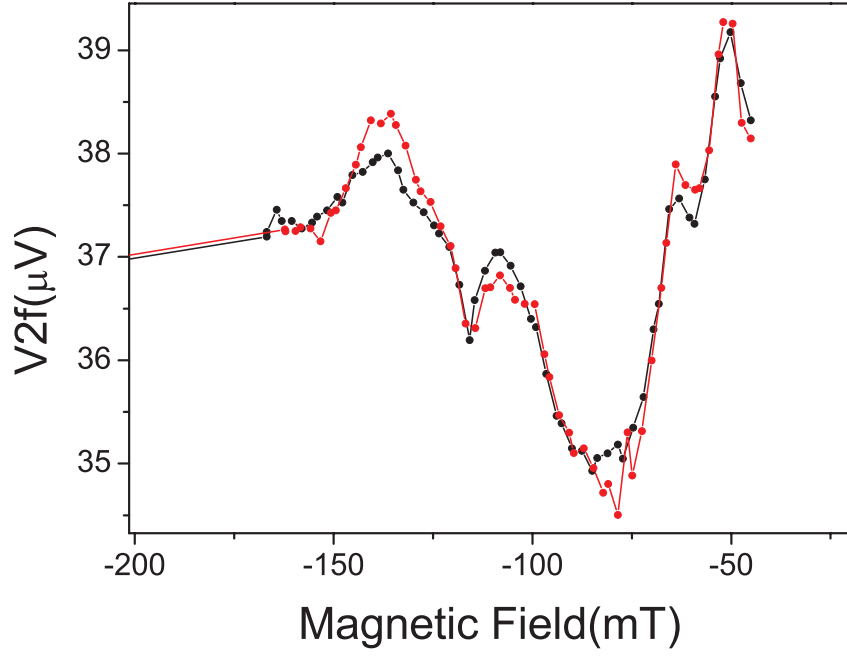


Figure 3.18: V^{2f} of a multilayer Co/Cu nanowire with $I_{ac} = 100\mu A$ applied at 406 Hz and magnetic field applied parallel to the nanowire, field ramped up (black) from -900mT to -45mT and ramp down from -45mT back to -900mT (red)

This indicates that this single switching process through non-collinear configuration is reversible in a local field range before other layers switching occurs to affect this particular layer magnetization switching.

Chapter 4

Thermal spin transfer torque

4.1 Current-induced STT

It has been proved that a spin polarized electrical current can exert a spin transfer torque(STT) on the local magnetization. Let us take spin valve for example, if the current density reaches a critical value, it can flip the magnetization of the free layer, therefore we can switch the configuration of the spin valve between parallel and anti-parallel. One of the strong evidence of the spin transfer torque effect is the observation of a shift in switching field shift experiment. [28] In our spin valve samples, I did the similar set of measurements in order to prove that there is indeed a spin-transfer torque effect in our sample. We can see in Fig. 4.1 that the switching field of the GMR moves when we apply different DC current. In addition, we also find that the V^{2f} peak position moves along with the GMR switching. Since V^{2f} has higher signal to noise ratio and very sensitive to the switching field, we are going to use it as a probe of the switching field position in our thermal spin torque experiment. We will find further advantage in the V^{2f} measurement, in that the amplitude of the V^{2f} signal at switching depends on the magnitude of the thermal spin torque, introduced below.

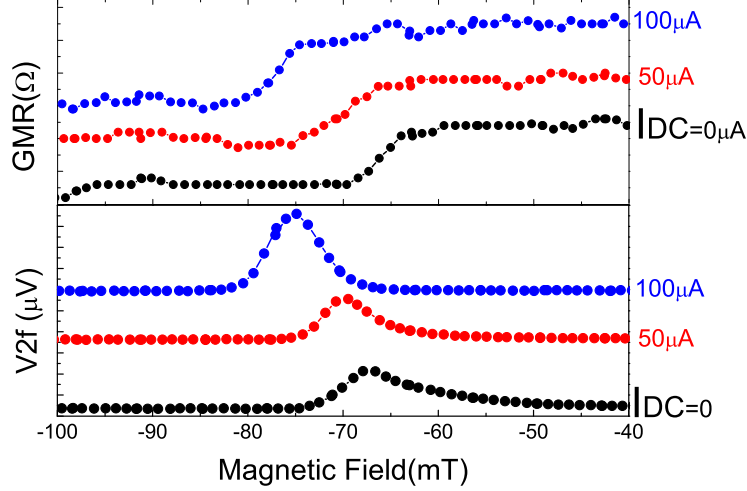


Figure 4.1: *GMR and V2f vs field with different applied DC current.*

4.2 Theoretical prediction on Thermal Spin transfer torque

It was first predicted by theoreticians in Leiden [29] that a heat current can exert a spin-transfer torque just as charge current does. In this work, they provide a torque expression with two contributions(Eq 4.1).

$$\tau_{STT} \sim P\Delta V + P'S\Delta T \quad (4.1)$$

The first term is the conventional spin-transfer torque(STT) term, and the second term is the thermal spin torque(TST) term, where $P = (G^\uparrow - G^\downarrow)/G$ is the polarization of the conductance, and $P' = \partial_\epsilon(G^\uparrow - G^\downarrow) |_{\epsilon_F} / \partial_\epsilon G |_{\epsilon_F}$ is its energy derivative at the Fermi level. Apparently, here the value of P has to be smaller than 1; P' , on the other hand, does not have this limit. Thus, according to this model $P'S$ can reach a considerably large value in some circumstances, such as when a

van Hove singularity is close to Fermi level in one spin direction. At the end, the authors provide a comparison between the STT and TST in magnetization reversal. According to Slonczewski [30], the threshold electrical current needed to yield magnetization switching is around $10^7 Acm^{-2}$. Here, the authors replace $P\Delta V$ with $P'\Delta T$, and estimated that we demand $S\delta T \sim 100\mu V$ so as to exert a thermal spin torque to switch the magnetization, just as the charge current does. This value is not unrealistic because we can possibly obtain a laser heating induced temperature rise up to 100K. In addition, as analyzed, the P' might be large. In conclusion, the authors predicted that pure thermal spin torque can be large enough to reverse magnetization. As far as we know, a year after our publications confirming this effect, nobody else has tried this experiment.

4.3 Heat current—*asymmetric spin valve*

Here is how we tried to use the experiment to observe this thermal spin torque effect. The key issue in this experiment is to generate a large temperature gradient in our nanostructures. We use Joule heating to generate a temperature gradient, then a heat current. We design our spin valve with one cobalt layer much thicker than the other (Fig. 2.1). Since the resistivity of Cobalt is much higher than Copper, we consider the cobalt layer as the heat source here. Then, the thicker cobalt layer will produce more heating than the thinner one. Therefore, there will be a heat flow from the thick layer to thin one. Here we have an assumption that the heat will only dissipate along the nanowire. This is reasonable because the heat dissipation from metal to polycarbonate membrane is considerably harder than that from metal to metal.

The temperature profile (Fig 4.2) in the nanowire is obtained by integration of the

Fourier equation(Eq 4.2) in the stationary regime, having the massive electrodes at both ends of the nanowire as a heat bath remaining at a set temperature.

$$\rho j_e^2 + \kappa \nabla^2 T = C_v \frac{\partial T}{\partial t} \quad (4.2)$$

where ρ is the resistivity, j_e is the electrical current density, κ is the heat conductivity, T temperature, t time, C_v heat capacity. Since we consider a stationary regime, $\frac{\partial T}{\partial t} = 0$. Taking account the all the continuity of j_e and j_q (heat current)at the interfaces of Co-Cu as along with boundary conditions at both ends of the nanowire, we come to the result of temperature profile plotted in Fig 4.2. Here we use transport parameters published earlier by former members of the group [31] [40]. At room temperature(300K), we take $\rho_{Co} = 3.49 \times 10^{-7}$, $\rho_{Cu} = 8.73 \times 10^{-8}$ (Ωm). From Fig 4.2, we can read the temperature gradient at the thin Cobalt layer is around 2000K/cm.

The result of this calculation is actually close to that of a simple argument as follow: The heat is assumed to flow equally towards both ends of the nanowire. Considering this, we have,

$$\frac{1}{2} \rho \frac{d}{\pi r^2} I^2 = j_q \pi r^2 \quad (4.3)$$

where ρ is the resistivity of electrodeposited cobalt taken from previous work [31], d the thickness of the thick Cobalt layer, and πr^2 the cross-sectional area of the nanowire. Notably, we can generate a large $j_Q \propto 1/r^4$ when we decrease the radius r of the nanowire. In other word, the nanowire with small diameter, with which the group is familiar with is actually an ideal sample to generate a large heat current. Considering $j_Q = -\kappa \nabla T$ and taking κ to be a typical value of 10 W/mK. Then after a simple calculation we can obtain a temperature gradient as large as 1000K/cm for an applied AC current of 100 μA .

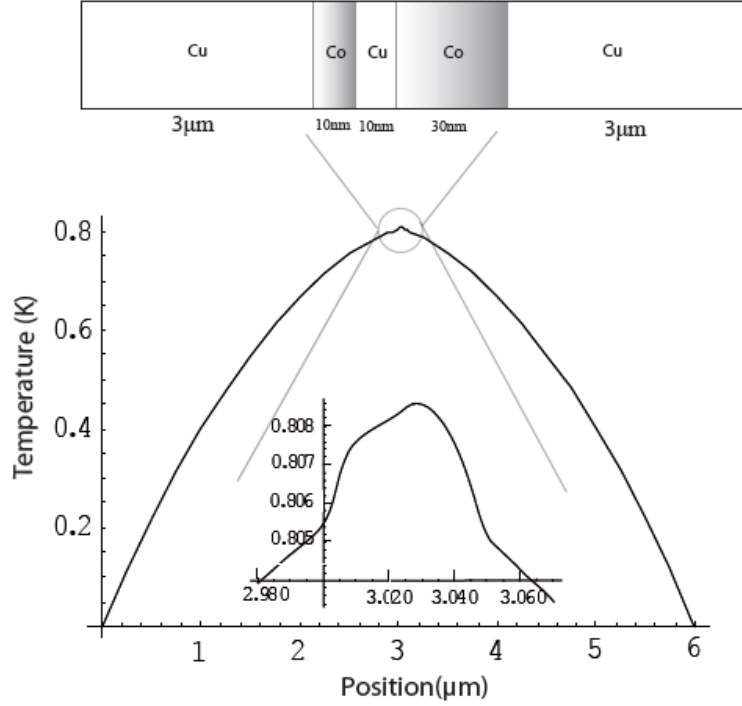


Figure 4.2: GMR and V_{2f} vs field with different applied DC current.

4.4 V_{2f} — a sensitive probe for switching field

4.5 Heat-current induced STT

Now that we know that Joule heating in an asymmetric spin valve can induce a large temperature gradient, hence a large heat current, we try to see what happens when we add joule-heating to STT-type measurements.

4.5.1 Switching field shift

As introduced in Chapter 3, V^{2f} peaks are highly sensitive to the switching field H_{sw} . Additionally, in Fig 4.1, we find V^{2f} is an ideal probe for the H_{sw} due to its high signal-to-noise ratio. Unlike the measurement in Fig 4.1, this time we keep the I_{dc} constant and change the ac current, and we observe a clear dependence of H_{sw} on the applied ac current,(Fig 4.3) which we attribute to the effect of heat current on the magnetization of the thin Co layer. It will be demonstrated in the next section that it is not the AC current-induced conventional spin-transfer torque that gives rise to this observation,.

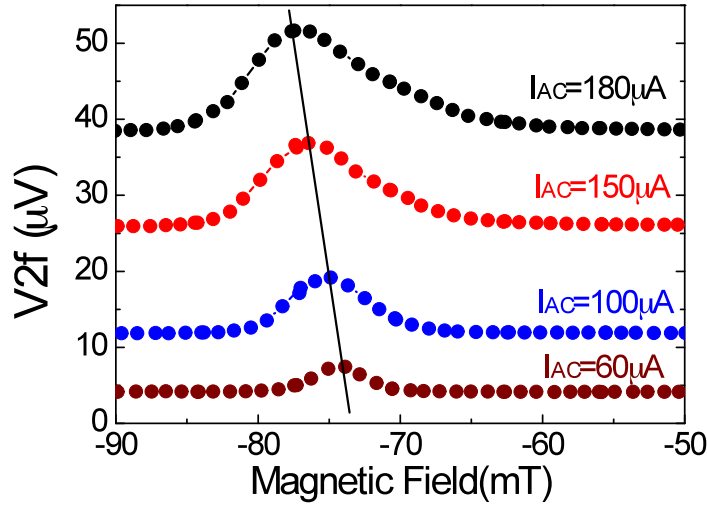


Figure 4.3: V^{2f} vs field measured on a nanowire containing an asymmetric spin valve(10 nm Co/10 nm Cu/30 nmCo) at a set dc current of -100μ A for different values of ac current as indicated in the graph. The field is swept from negative to positive values. The line is a guide for the eye

4.6 Supporting experiments

Indeed, there could be other factors that can possibly lead to the observation of the switching field shift in the experiment. Therefore, we designed several supporting experiments to rule out potential spurious effects.

4.6.1 Symmetric spin valve

First of all, we design another sample, a nanowire containing a symmetric spin valve (Co10nm/Cu10nm/Co10nm). In this sample, we have joule heating equally from both Co layers, therefore, no heat current in any direction. Then we did exactly the same series of V^{2f} vs field measurements, but this time we observed no change in the switching field when we increase the AC current.(Fig 4.4)

This result implies that it is not the AC current-induced spin torque that gives rise to the switching field shift observed in Fig 4.3, because otherwise we should be able to observe the same behavior also in Fig 4.4. In addition, there might be a possibility that the overall temperature rise due to joule heating might play a role in the observation in Fig 4.3; however, if so, we should also detect the same influence in Fig 4.4, since the overall heating is about the same in both experiments. Apparently, we did not observe the same switching field change in symmetric spin valve, thus we can rule out the overall heating effect.

4.6.2 Isothermal measurement

In order to have a stronger evidence to rule-out the overall heating effect, we did also isothermal measurements. First of all, we need to estimate how much do we heat up the sample in our measurements. We place the sample in a sealed

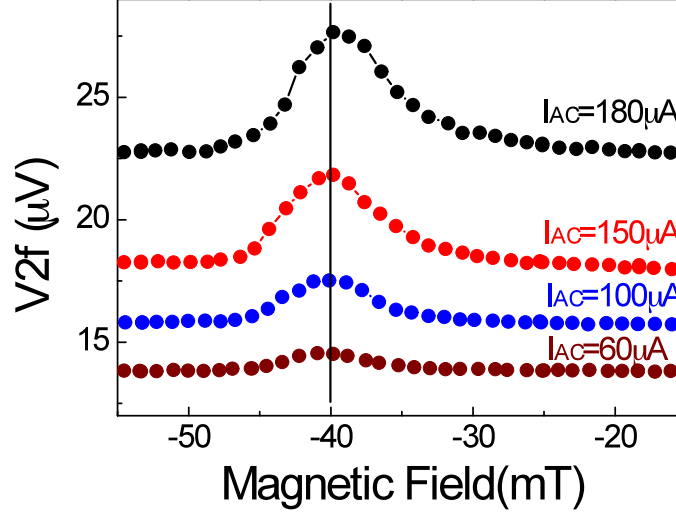


Figure 4.4: V_{2f} vs field measured on a nanowire containing a symmetric spin valve (10 nm Co/10 nm Cu/10 nm Co) at a set dc current of $-100 \mu A$ for different values of ac current as indicated in the graph. The field is swept from negative to positive values. The line is a guide for the eye

chamber and we heat it up from room temperature to $50^\circ C$, and we measure the resistance as a function of the temperature. (Fig 4.5) We find a linear behavior. The slope $\frac{dR}{dT} = 0.13 \Omega/K$. Then we measure the resistance vs I_{ac} (Fig 4.6), we find a quadratic curve because of the joule heating. Now, we can estimate how much $100 \mu A$, for instance, can heat up the sample. With an AC current we have $\Delta R = 0.06 \Omega$. Accounting for the temperature dependence of the resistance, we can calculate to derive: $\Delta T = 0.5 K$ with $100 \mu A$ ac current. This value is actually consistent with the temperature profile calculation. In Fig 4.2, we can see that the average temperature rise in the entire nanowire is approximately $0.4 K$. Therefore, both methods imply with $I_{ac} = 100 \mu A$, we are heating up the sample by less than $1 K$.

Then we carried out measurements of H_{sw} using an external heat source to heat

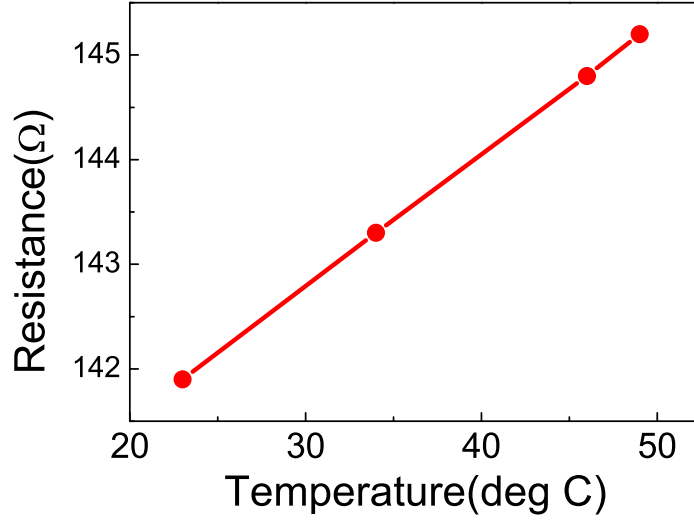


Figure 4.5: Resistance measured at different temperature.

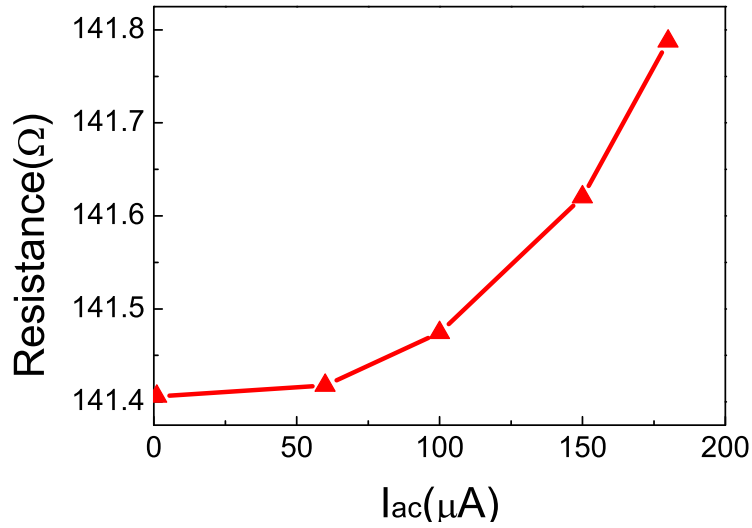


Figure 4.6: Resistance measured with different ac current applied at room temperature.

the nanowires (Fig 4.7), where we see that a 30K temperature increase changes the H_{sw} of only 1.2mT. Hence, with 1K temperature rise during the V_{2f} measurements

we expect an H_{sw} shift of 0.03mT. Apparently, this effect is insufficient to account for the actual H_{sw} shift observed during the measurement of Fig 4.3, which is 2 orders of magnitude larger.

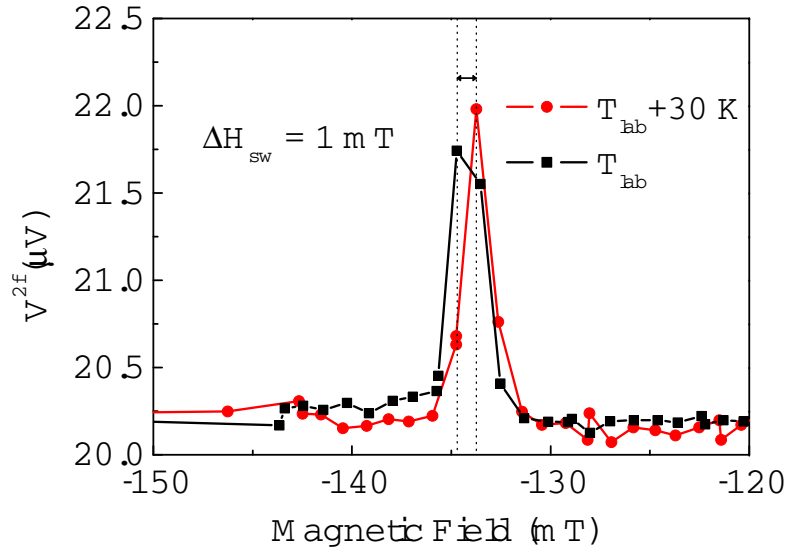


Figure 4.7: Isothermal measurement of H_{sw} . black curve was measured at room temperature, and red curve was measured after heating up by 30K with external heat source.

4.6.3 Amplitude change of V^{2f}

Apart from observing thermal spin torque in switching field experiment, we also find its evidence in V^{2f} peak height change with respect to the applied DC current. Here we apply a fixed AC current and vary the DC current, and then we measure the V^{2f} peak height as a function of applied field on an asymmetric spin

valve(Fig 4.8). The data shows that the V^{2f} peak height changes clearly when we vary the applied DC current.

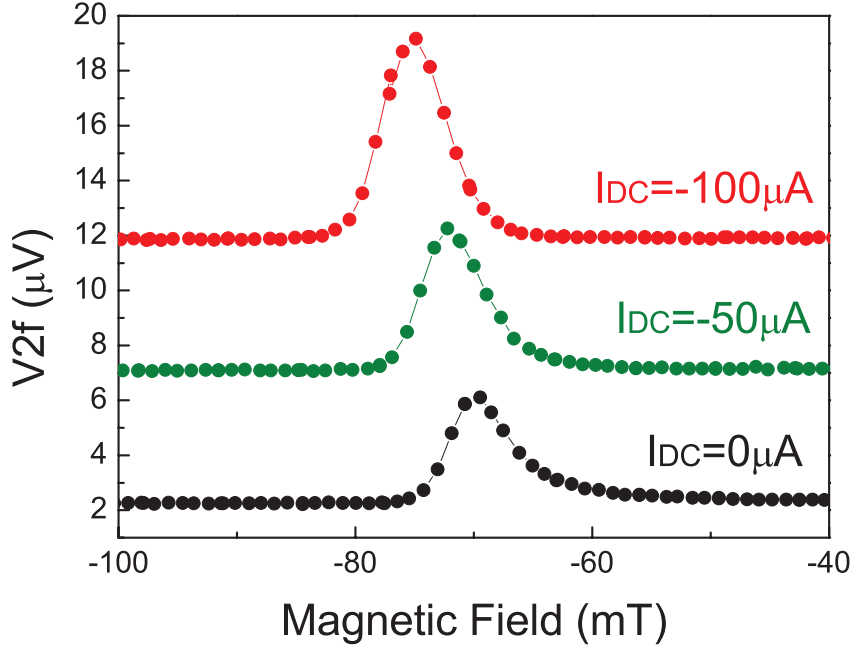


Figure 4.8: V^{2f} measured as a function of field with different DC current as indicated in the plot, for a fixed $I_{ac} = 100 \mu A$ an asymmetric spin valve(Co 10nm/ Cu 10nm/ Co 30nm). The field was swept from negative to positive values.

To the contrary, in the check experiment of Fig 4.9, we did the same set of measurements on a symmetric spin valve sample, and we find that the peak height of the V^{2f} signal barely changes when we vary the value of DC current.

This phenomenon can be accounted for by assuming that there is a thermal spin torque(TST) effect induced by a heat current produced by the Joule heating, as shown now. By considering the various contributions to V^{2f} , we can determine the origin of this effect. We can write:

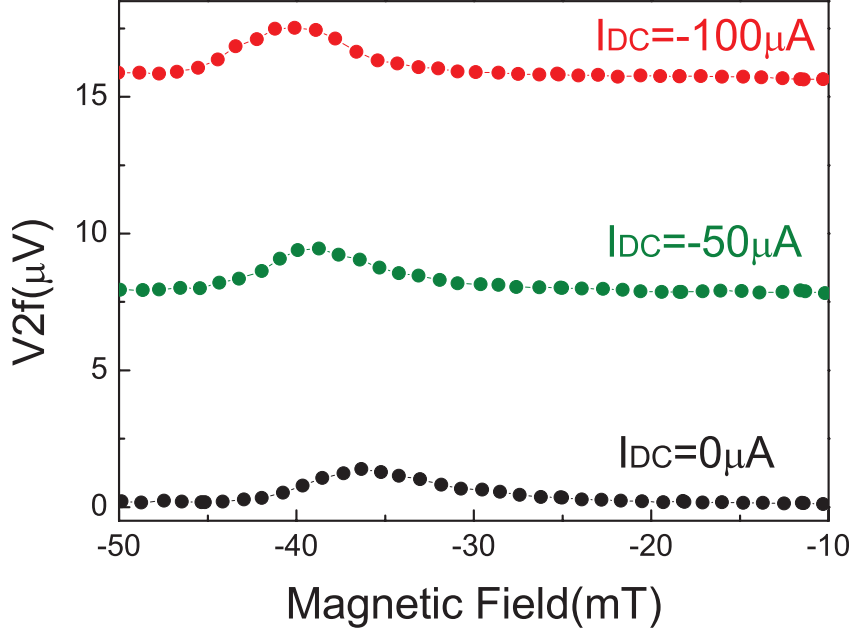


Figure 4.9: V^{2f} measured as a function of field with different DC current as indicated in the plot, for a fixed $I_{ac} = 100\mu A$ a symmetric spin valve (Co 10nm/ Cu 10nm/ Co 10nm). The field was swept from negative to positive values.

$$V^{2f} = \frac{dR}{d\tau} (I_{ac}\tau_{STT}^f + I_{dc}\tau_{TST}^{2f}) + I_{dc}\frac{dR}{dT}\Delta T^{2f} \quad (4.4)$$

The first term is the conventional AC spin transfer torque $\tau_{STT}^f = \frac{d\tau}{dI}I_{ac}$. This term is independent of I_{dc} . [23] The second torque term contains a thermal spin torque $\tau_{TST}^{2f} = \frac{d\tau}{dj_q^{2f}}$ that oscillates at frequency $2f$, because the heat current has a component j_q^{2f} that oscillates at frequency $2f$. This term is proportional to I_{dc} . The last term is simply the contribution of the temperature dependence of R , which is equivalent to the TGV signal discussed in the previous chapter. Based on Eq 4.4, we know that the STT term is independent of I_{dc} . According to our extensive measurements of TGV in spin valves, we expect a TGV contribution of no more than $0.6\mu V$ with a DC current of $100\mu A$. We can expect a fixed temperature rise,

but this has no effect on the peak height of V^{2f} response. Therefore, the main contribution of this change in peak height must arise from the second term, which is the heat-current-induced thermal spin torque. In a symmetric spin valve, the symmetric heating of the Co layers determines that the heat current is close to zero and as a result, we do not expect a dependence of peak height on the DC current, just as what we observed in Fig 4.9. The dc-driven STT was found to be effective in symmetric spin valves, as shown by switching field move indicated by the V^{2f} peak position.

4.7 Modeling for thermal spin torque

We can understand the coupling of heat current and magnetization in the framework of a thermodynamic approach. The relevance of such method has been discussed before, starting with the seminal work of Johnson and Silsbee [32] [33] [34]. Due to the thickness of the layers in the range of 10nm or above, and due to the defects that one can expect in electrochemical growth metals, it is clear that electronic transport is in the diffusive regime in which the thermodynamic approach is relevant.

4.7.1 Onsager matrix combined with Pauli matrices

Thermodynamics of irreversible processes implies that the heat current and electrical current have linear relations with their respective generalized forces, which are the Onsager reciprocity relations. Now we consider the charge carriers are of two different types, up spins and down spins, with notation of a subscript \uparrow and \downarrow , respectively. Then we obtain a three current model involving a heat current density as well as two charge current densities as introduced in ref [6]. A similar

three-current model was also applied recently by ref [35]. The Onsager reciprocal relations considering 3 current model yields:

$$\begin{pmatrix} j_q \\ j_\uparrow \\ j_\downarrow \end{pmatrix} = - \begin{pmatrix} \mathcal{L}_{qq} & \mathcal{L}_{q\uparrow} & \mathcal{L}_{q\downarrow} \\ \mathcal{L}_{\uparrow q} & \mathcal{L}_{\uparrow\uparrow} & \mathcal{L}_{\uparrow\downarrow} \\ \mathcal{L}_{\downarrow q} & \mathcal{L}_{\downarrow\uparrow} & \mathcal{L}_{\downarrow\downarrow} \end{pmatrix} \begin{pmatrix} \nabla T \\ \nabla \mu_\uparrow \\ \nabla \mu_\downarrow \end{pmatrix} \quad (4.5)$$

where j_q is the heat current density or entropy current density and j_\uparrow and j_\downarrow are the electric current densities of the spin up and spin down carriers, respectively. For convenience, here we use the notation of Valet and Fret [36] $\mu_\uparrow = \mu_0 + \Delta\mu$ and $\mu_\downarrow = \mu_0 - \Delta\mu$. The Onsager coefficients $\mathcal{L}_{\uparrow\downarrow}$ and $\mathcal{L}_{\downarrow\uparrow}$ are the spin mixing terms. These terms are important for describing the magnetic dependence of the thermoelectric power. [37] At this point, we convert j_\uparrow and j_\downarrow into total charge current density $j_e = j_\uparrow + j_\downarrow$ and spin current density $j_p = j_\uparrow - j_\downarrow$. Then we can convert Eq 4.5 into Eq 4.6, whose detailed mathematical calculation was elaborated in ref [40]

$$\begin{pmatrix} j_q \\ j_e \\ \mathbf{j}_m \end{pmatrix} = 2 \begin{pmatrix} -l_0 & Tk_0 & T \frac{k_e}{e} \mathbf{M} \\ -k_0 & c_0 & \frac{c_e}{e} \mathbf{M} \\ -k \mathbf{M} & c \mathbf{M} & \frac{c_0}{e} \end{pmatrix} \begin{pmatrix} \nabla T \\ \nabla V \\ \frac{d\mathbf{m}}{dx} \end{pmatrix} \quad (4.6)$$

where j_q is the heat current, j_e is the charge current, \mathbf{j}_m is the spin current. \mathbf{M} is the unit vector representing the direction of local magnetization of one layer and \mathbf{m} has the dimensions of a chemical potential. c_0 and c are defined by $\hat{C} = c_0 \hat{I} + c \mathbf{M} \cdot \sigma$ where \hat{C} is a 2×2 matrix representing the electrical conductivity. l_0 represents the heat conductivity. According to ref [40], $k_0 = \varepsilon_0 c_0 (1 + \beta\eta)$, $k = \varepsilon_0 c_0 (\beta + \eta)$, where ε_0 is the Seebeck coefficient, and the dimensionless coefficients β and η define the asymmetry of the spin-dependent conductivity and Seebeck coefficients.

In this linear regime we may expect the torque to be proportional to the spin current \mathbf{j}_m , which has two main contributions, one from the gradient of the elec-

trostatic potential ∇V , the other from the gradient of temperature ∇T . In our experiment, both gradients are imposed on a thermodynamic system. Taking the notation of ref [40][Eq. (18)], we have:

$$\mathbf{j}_m = 2c(\nabla V - S_{eff}\nabla T) \quad (4.7)$$

with $S_{eff} = \varepsilon_0(1 + \eta/\beta)$, which has the same units as a Seebeck coefficient.

A torque τ was calculated for a spin valve by Hatami *etat.* [29], considering spin-dependent heat and charge transport at the interface between a ferromagnetic metal and a normal metal. Two contributions are found in Eq 4.1 where P and P' characterize, respectively, the spin asymmetry of the conductivity and of the Seebeck coefficient S , with similarity to Eq 4.7. However, as the authors of Ref [29] pointed out in their conclusion, their calculation concerns interface spin effects. Thus, it is a temperature difference ΔT which is relevant in this case. In the diffusive transport regime, it is the temperature gradient ∇T that plays a role: at 1000K/cm this is quite large, whereas the temperature difference between the two layers is of the order of only 1 mK. If we account for our data based on Eq 4.1, we need to assume for S a value 1000 times larger than typical values for the Seebeck coefficient in metals. Therefore we choose to analyze our experimental results in a diffusive regime using Eq 4.7, rather than an interface effect.

4.7.2 Fitting data on Switching field shift

With Eq 4.7, we try to model our data on switching field shift experiment as we observed in Fig 4.3. The change of switching field due to the thermal spin-transfer torque(TST) τ_{TST}^0 induced by the dc heat current relative to that due to the conventional spin transfer torque(STT) τ_{STT}^0 associated with dc charge currents

estimated by:

$$\frac{\Delta H_{sw}^{TST}}{\Delta H_{sw}^{STT}} = \frac{\tau_{TST}^0}{\tau_{STT}^0} = \frac{j_{m,TST}^0}{j_{m,STT}^0} = \frac{S_{eff} \nabla T}{\nabla V}. \quad (4.8)$$

As demonstrated in the section of symmetric spin valve, ΔH_{sw}^{STT} is independent of I_{ac} , and the value was determined experimentally with $I_{dc} = -100\mu A$ as we can see in Fig 4.8 for example. Therefore, for a fixed DC current, we expect a dependence of ΔH_{sw}^{TST} which is quadratic in I_{ac} , because $\nabla T = A_1 I^2$ with $A_1 = \frac{\rho d}{2\kappa\pi^2 r^4}$ calculated from Eq 4.3. Taking the resistivity and Seebeck coefficients for the electrodeposited Co and Cu layers from L. Gravier *etal.* [31], we can calculate the ΔH_{sw}^{TST} with respect to different I_{ac} and fit our data (Fig 4.10) assuming that the actual diameter of the nanowire is 37nm, instead of the 50nm average pore size of the polycarbonate membrane. This estimated value is realistic, because we are measuring one single nanowire individually contacted among a large number of them grown simultaneously. This fitting may also potentially indicate that in our sample fabrication process, the pore with comparably smaller size can be filled faster, which is also reasonable by intuition.

4.7.3 Fitting data on the amplitude of V^{2f} peak height

In order to fit the data on V^{2f} amplitude change, we need to analyze what the V^{2f} peak consists of. We take the resistance as function of the torque and the temperature $R(\tau, T)$. Considering the torque as a function of j_m , we can write the voltage equation:

$$\Delta V = I \left[\left(\frac{\partial R}{\partial \tau} \frac{\partial \tau}{\partial j_m} j_m \right) + \frac{\partial R}{\partial T} \Delta T \right]. \quad (4.9)$$

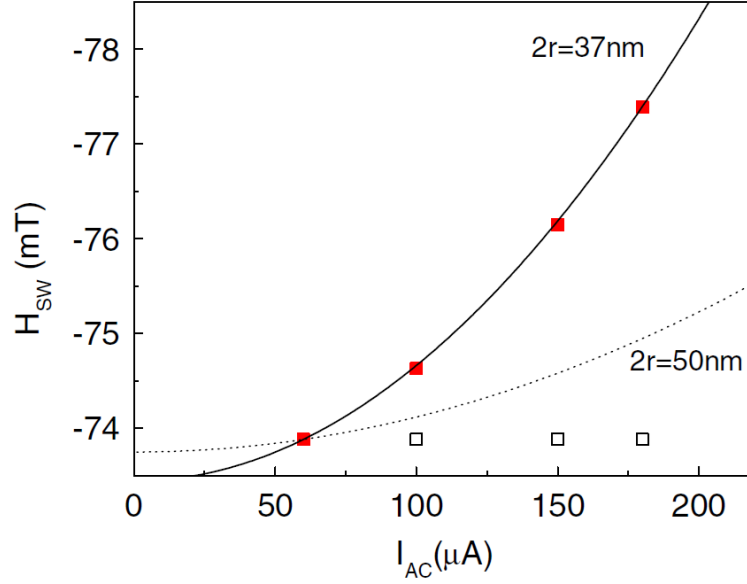


Figure 4.10: Switching field measured as a function of I_{ac} , for fixed $I_{dc} = -100\mu A$. Square dots(red) are the experimental data for an asymmetric spin valve. The open boxes(black) are the data for a symmetric spin valve. The lines(black) are the result of result of calculations with different values of nanowire diameters indicated near the curve.

where τ is the torque, j_m is the spin current. Now we take the spin current expression(Eq 4.7) obtained from the onsager matrix(Eq 4.6). Since the temperature gradient is due to the asymmetric Joule heating, when we have $\nabla T = A_1 I^2$. Then we introduce both the DC and AC component of the current. We combine all these together and find:

$$\Delta V = (I_{AC} + I_{DC}) \left[-\frac{\partial R}{\partial \tau} \frac{\partial \tau}{\partial j_m} 2c \left(\rho \frac{(I_{AC} + I_{DC})}{\pi r^2} S_{eff} A_1 (I_{AC} + I_{DC})^2 \right) + \frac{\partial R}{\partial T} \Delta T^{2f} \right]. \quad (4.10)$$

With a little algebra, we select the second harmonics term in the voltage expression

and obtain:

$$V_{peak}^{2f} = \frac{dR}{d\tau} \frac{d\tau}{dj_m} 2c \left(\frac{\rho}{\pi r^2} + 3S_{eff} A_1 I_{DC} \right) I_{AC}^2 + I_{DC} \frac{dR}{dT} \Delta T^{2f}. \quad (4.11)$$

Now we can seek the origin of this V^{2f} peak height change versus I_{DC} in this formula. We notice that the first term is not I_{DC} dependent. This term is actually the cause of the current susceptibility of the spin valve when we only apply an AC current. The last term is what we have been studying in this group for a long time, the thermogalvanic voltage(TGV) signal [9], which is discussed extensively in Chapter 2. Based on our massive data on TGV on spin valve, we know this term is about a fraction of $1\mu V$ when I_{dc} is $100\mu A$. But evidently the V^{2f} peak height change we observed in Fig 4.8 is considerably larger than this value. Therefore, the main contribution of this effect is given rise by the second term, which is the thermal spin torque term.

In Fig 4.11, we show the calculation of Eq 4.11 using the same values for all parameters as in the calculation of Fig 4.10, including the estimated radius of the nanowire. The small difference between the measured data and the calculation are attributed to the contribution of the 3rd term, which is V^{2f} of the temperature dependence of the resistance. Based our previous data on TGV, we find in Fig 4.11 a difference between the data and the prediction of Eq 4.11 which is about the right size for a TGV contribution.

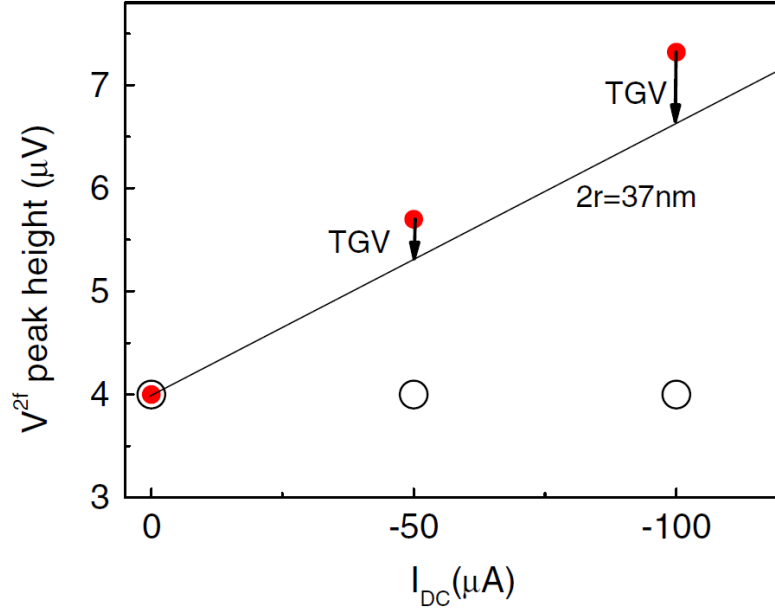


Figure 4.11: V^{2f} peak height as a function of I_{dc} , for fixed $I_{ac} = \mu A$. The red dots are the experimental data for an asymmetric spin valve. The open black circles are the experimental data for a symmetric spin valve. The arrows indicate a linear correction to the data of the asymmetric spin valve by subtraction of an estimated value for the TGV signal. The black line is a calculation using the nanowire diameter of 37nm as indicated in the text.

4.8 Summary

We took advantage of Joule heating in a spin valve embedded in a nanowire to produce a large local temperature gradient. We find two independent effects of the heat current produced this way: a change in switching field as a function of the applied AC current, and a change of the amplitude of the peak in the second harmonic voltage as a function of the DC current. We rule out the spurious effects

such as a fixed temperature rise in the spin valve and an AC spin-transfer torque by verifying that a symmetric spin valve is insensitive to a change in applied ac current. Also we used isothermal measurements on the asymmetric spin valve to calibrate the resistance versus heating and the change of switching field versus heating. Our results provide evidence for a thermal spin transfer torque associated with heat current. The effect of the heat current on magnetization is interpreted as the coupling of heat, charge, spin currents, as described by the thermodynamics of transport given by the Onsager reciprocal relations. This method simultaneously models both observations concerning switching field and V^{2f} peak height respectively with the same values of all parameters. Fits are obtained for reasonable values of all parameters. Thus the model provides a reasonable estimation from the observed heat-current-driven thermal spin torque relative to the spin-transfer torque.

Chapter 5

Transverse spin relaxation in spin-valve

5.1 Concept of transverse spin diffusion length and the controversy

When a spin polarized current enters a magnetic layer, the spin of conduction electrons relaxes over a certain distance. Here we take a spin valve structure for example. (Fig 5.1) In this illustration, the electrons go from right down to left. We suppose the magnetization of the two layers are perpendicular to each other. When the electrons enter the second magnetic layer, the spin angular momentum rotates from almost vertical to horizontal direction. This occurs over a certain distance, called the transverse spin diffusion length. Following some authors, we denote it λ_J .

In fact, there is a controversy about how big λ_J might be. Slonczewski estimated it to be about 1 Å based on band structure argument [38]. Zhang, Levy and Fert believe that it is on the order of a few nanometers calculated from spin dependant transport. [39] We carried out angular dependence measurements of the spin trans-

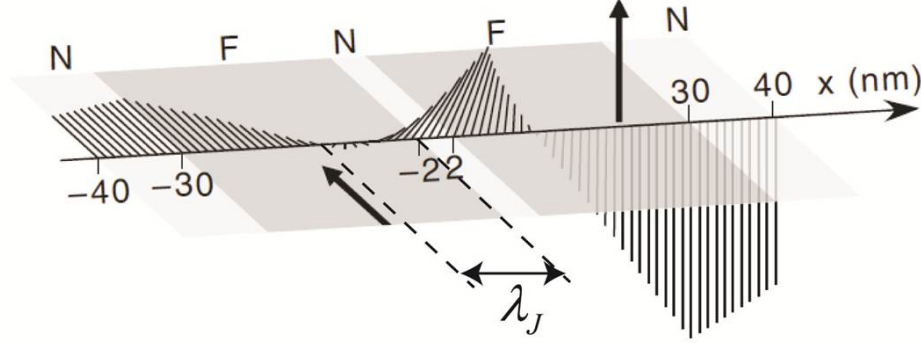


Figure 5.1: *spin relaxation in spin valve. The grey zones are two ferromagnetic layers in spin valve. The black bars stand for the local spin accumulation. [42]*

fer torque. Analyzing the data with the model demonstrated in the next section, we can tell that in our samples λ_J is close to the value estimated by Zhang, Levy and Fert.

5.2 Simulation on V^{2f} vs transverse spin diffusion length

This idea to estimate λ_J through experiment comes from the simulation of V^{2f} vs angle carried out in our group by Julie Dubois [40]. However, here we choose to refer to analytical models published by others, rather than the numerical results of Julie Dubois. From Kovalev's paper [26], we have a V^{2f} expression, which is proportional to the spin transfer torque (Eq 5.1).

$$U_{2\omega} = \frac{1}{2} \eta_1 I_0 \frac{\partial R(\nu)}{\partial \nu} \frac{I_0/e}{\gamma M_s} \frac{\gamma \hbar/2}{V_m M_s} \sin^2 \theta \frac{N_x^d}{N_y^d} \times \left[\left(\frac{N_y^d}{N_x^d} - 1 \right) \cos \phi \sin \phi - \alpha \left(\frac{N_y^d}{N_x^d} \sin^2 \phi + \cos^2 \phi \right) \right], \quad (5.1)$$

where N_x^d and N_y^d are the diagonal components of the demagnetization tensor. Typically, $N_x^d/N_y^d < 1$. The parameter $\nu = \cos \theta$. I_0 is the applied current amplitude. $\eta_1 I_0$ is actually the spin-transfer torque τ_{STT} . α is the Gilbert damping constant, γ is the gyromagnetic ratio. M_s is the constant saturation magnetization of the free layer. V_m is the volume of the free layer. θ and φ are defined in Fig 5.2

We consider the magnetization of both layers are mostly in plane, i.e. ϕ is close to $\pi/2$. We introduce the angular dependent torque expression (Eq 5.2) from reference [41]

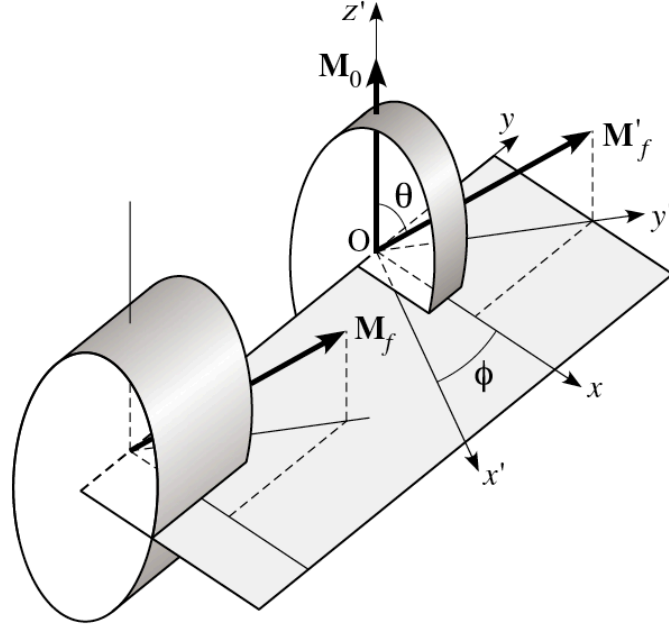


Figure 5.2: Fixed layer M_f and free layer M_0 magnetization vectors. M'_f is M_f shifted to O . Ox' is defined as the normal to the plane containing M'_f and M_0 . θ is the angle between M'_f and M_0 . ϕ defines a rotation of M_f which keeps θ fixed.

$$\tau_{STT} = \frac{p(\chi + 1)|\sin \theta|}{\chi(\cos \theta + 1) + 2} I_0 \quad (5.2)$$

where $p = (g_{\uparrow} - g_{\downarrow})/(g_{\uparrow} + g_{\downarrow})$. the parameter χ here is dependant on λ_J [43].

$$\chi = \frac{\sqrt{2}l_{sf}}{\lambda_J} - 1 \quad (5.3)$$

Here, l_{sf} is the longitudinal spin diffusion length due to spin-flipping process, and λ_J is the transverse spin diffusion length due to precession. In most case, λ_J is much smaller than l_{sf} , so the transverse component decay much faster than the longitudinal one. In our simulation, we take l_{sf} of CoFe to be 12nm according to reference [44].

We can find the parameter χ also in the angular dependent magnetoresistance equation from Slonczewski [38],

$$R(\theta) = R_P + \Delta R \frac{1 - \cos^2(\theta/2)}{1 + \chi \cos^2(\theta/2)} \quad (5.4)$$

where R_P is the resistance of spin valve at parallel configuration, and $\Delta R = R_{AP} - R_P$, R_{AP} stands for the resistance of spin valve at anti-parallel configuration.

Now with the equations above, I first did a simulation of the GMR vs angle with different value of λ_J (Fig 5.3).

Then when we combine the spin transfer torque(Eq 5.2) with the angular dependence of GMR(Eq 5.4), we can estimate of V^{2f} vs angle(Fig 5.4) based on Kovalev's V2f equation(Eq 5.2).

Here we can see clearly that the peak shape of V^{2f} vs angle is highly dependent on the value of λ_J . When we change λ_J from 0.8nm to 10nm, we observe that the peak position moves towards 180 degree, and the peak shape becomes sharper. Apparently, the behavior of the V^{2f} vs angle is much more sensitive to λ_J than the

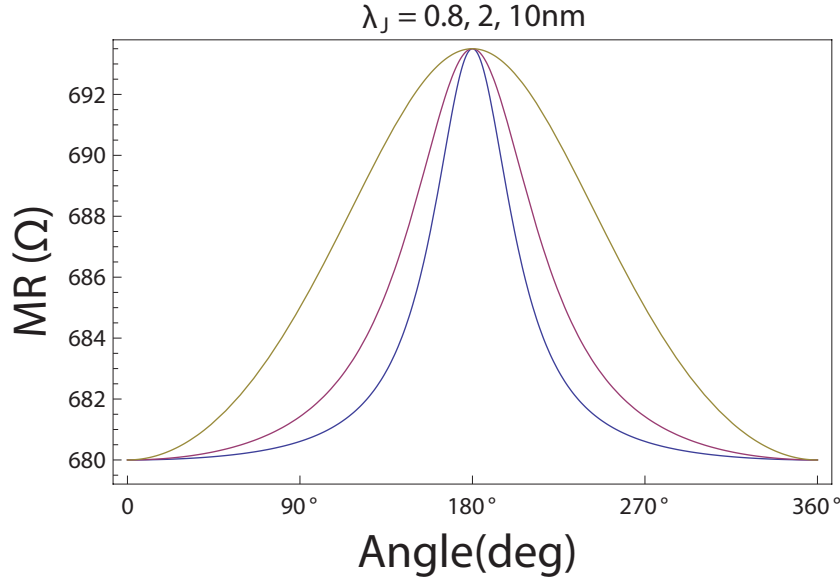


Figure 5.3: angular dependant GMR simulation, the yellow curve is calculated when we assume the λ_J is 10nm, and red for 1nm, blue for 0.1nm. We find the angular dependance of GMR becomes "thinner" when we decrease the value of λ_J from 10nm to 0.1nm.

angular dependent GMR. Hence we will mainly use the V^{2f} vs angle experimental data to estimate the value of λ_J , meanwhile we can also take advantage of the GMR vs angle to confirm the estimation.

5.3 Results on V^{2f} vs angle measurement

5.3.1 V^{2f} vs field

As I introduced in the sample preparation section, the GMR of the double-pinned spin valve has a sudden change near the zero field, where the free layer switched. We also measured the V^{2f} at the same time when we measure the GMR on this sample (Fig 5.5). We find the V^{2f} peaks appear only around this transition where the

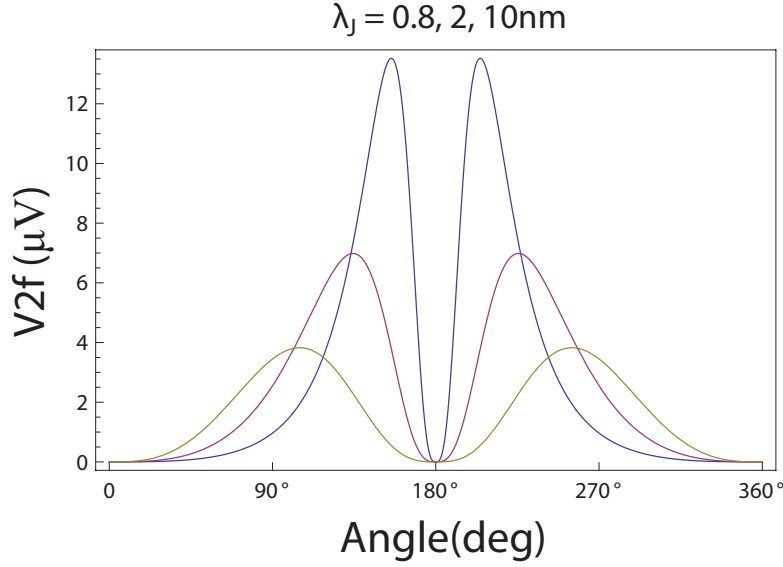


Figure 5.4: V^{2f} vs angle simulation with respect to different value of λ_J .

The yellow curve stands for the simulation when we take the value λ_J to be 0.8nm whereas red is for 2nm and blue is for 10nm.

free layer switched, not around the step where one of the hard layer switched.

We can see that this transition happens at the field between 0 and 10mT. Therefore an external field of 10mT will be definitely enough to rotate the magnetization of the free layer, but obviously far from the value at which we can rotate one of the hard layers.

5.3.2 V^{2f} vs angle measurement

Now we apply an external field in plane. First, we saturate the field up to 800mT, so all the layers' magnetization line up to this direction. Then we change the field amplitude to 10mT, and rotate the sample from 0 to 360 degree. In this process, the hard layer magnetization is pinned and will rotate with the entire sample, but the free layer will stay along the applied field direction. In this V^{2f} vs angle

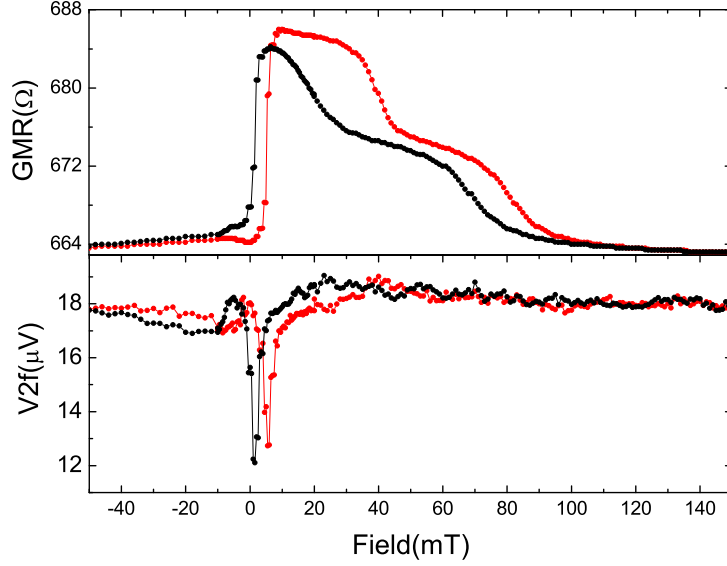


Figure 5.5: GMR and V^{2f} of an exchanged bias double-pinned spin valve, magnetic field applied in plane, measured with field ramped up(red) and down (black). The current applied is $500\mu A$ at $400Hz$, perpendicular to the layer.

measurement, we rotate the probe and let it stabilize by 2 seconds and measure GMR and V^{2f} at the same time.

We can see from the measurement that the GMR reaches the maximum at 180° degree, and minimum at 0° or 360° degree. On the other hand, V^{2f} has almost the same signal at 0° and 180° degree; however, it shows two “valleys” or peaks around 130° and 230° degree. (Fig 5.6) The asymmetry should be considered as a drift during the measurement.

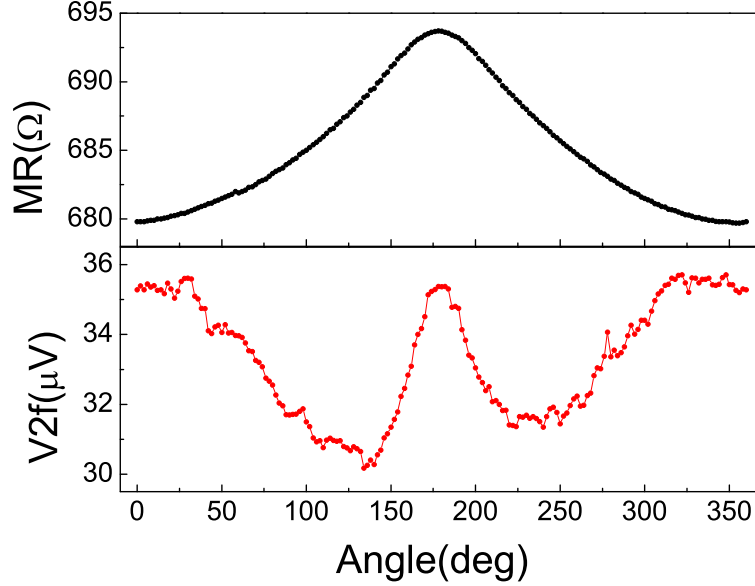


Figure 5.6: *GMR and V^{2f} measured as a function of angle between free layer and hard layer magnetization. Field applied in plane. The AC current applied is 1mA at 400Hz, perpendicular to the layer. Rotating field is 10mT*

5.3.3 V^{2f} vs angle with different AC current

We also did a series of measurements on V^{2f} vs angle when we apply different AC currents. Here we also applied a saturation field at the beginning of each measurement, and then apply an external field of 1mT to rotate the free layer.

We can see from these six measurements that when we increase the AC current value, the peak position and the peak shape barely change; however, the difference between 0 degree and 180 degree appear and was enlarged by the applied AC current. We can understand it as an effect of the poloidal field in the nanopillar, since we have a fairly “large” cross-section of the nanopillar which is 250nm \times 400nm. So when we apply a large current, at the edge of the nanopillar will

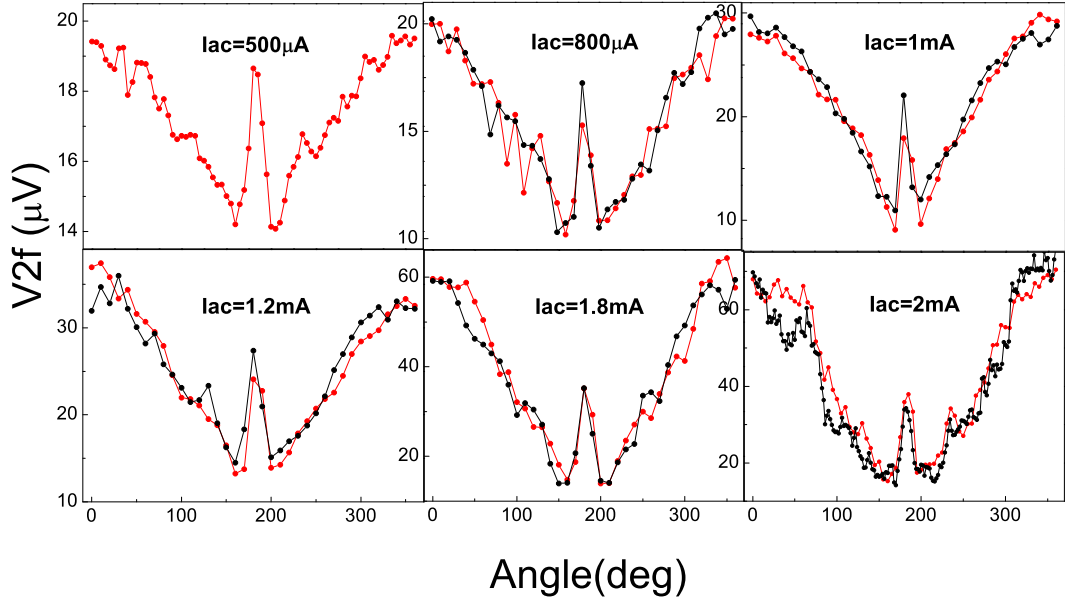


Figure 5.7: V^{2f} vs angle measured at different applied AC current. An external field of 1mT is applied in plane. The AC current applied at 400Hz, perpendicular to the layer. Red curve were measured when we rotate clock wise; black for counter clock wise.

appear an electrical current induced poloidal field, which oscillate also at the same frequency and affects the magnetization, hence the magnetoresistance at this frequency. Now, if we multiply this ΔR_{AC} with I_{ac} , we have a $2f$ signal. This signal is positive when the magnetic configuration is parallel, and becomes negative at antiparallel orientation. Here we can estimate briefly the influence of this effect with Eq 5.5

$$\frac{B}{\mu_0} \cdot 2\pi r = j\pi r^2 \quad (5.5)$$

where the B is the poloidal field at the edge, r is the radius, j is the current density.

Then we can calculate that with 2mA AC current, we introduce a poloidal field at $r=400\text{nm}$, around 1mT. This value is already the same as the external field we apply to rotate the magnetization of the free layer. Therefore, it is not so surprising this effect shows up when we apply an AC current above 1mA.

Now if we continue to increase the AC current value, we suddenly reach a different regime where V^{2f} signal “exploded” from tens of μV to a few mV, almost enlarged by 100 times.(Fig 5.8) This is because the current has reached the critical value of the current-induced magnetization switching(CIMS), as a result, the magnetic configuration of the spin-valve jumps between parallel and anti-parallel due to the spin transfer torque induced by the oscillating AC current.

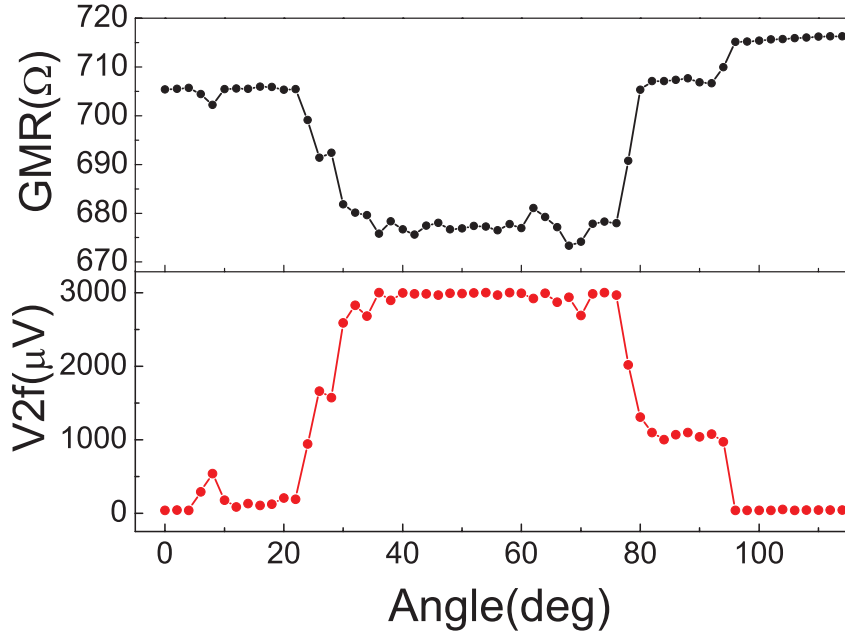


Figure 5.8: GMR and V^{2f} vs angle measured under a current of 2.5mA, over the threshold value for the CIMS. External field is 10mT.

This experimental data can be understood as follow. At 0 degree, there is no spin-transfer torque or very small; however when we rotate the sample to a certain angle, we reach the noncollinear configuration of the spin-valve and the spin transfer

torque becomes large enough that it can flip the magnetization back and forth. Then the average resistance over time becomes $R_{average} = (R_P + R_{AP})/2$, as a result we can see a step in the magnetoresistance. As for the V^{2f} , since the Resistance change periodically between P and AP state at the same frequency as the I_{ac} , we have $V = I_{AC} \times (R_{average} + \Delta R_{AC})$, and select the $2f$ term, then we have $V^{2f} = I_{AC} \times \Delta R_{AC}$, where the amplitude of the ΔR_{AC} is $(R_{AP} - R_P)/2$.

From this result, we can see the V^{2f} becomes extremely sensitive to the angle in the regime where we reach the threshold current for switching. At zero degree, it is about $40\mu V$, but between the angle of around 30 and 80 degree, the V^{2f} signal increases suddenly to 3mV. Thus, the signal changes up to 7500 percent. Consequently, this method has potential application on high-sensitivity detection on the non-collinear configuration of the spin-valve.

5.3.4 V^{2f} vs angle with a DC current

Then we applied an additional DC current, and then we did exactly the same measurement of V^{2f} vs angle.

Here we notice that the MR curve barely change; however the V^{2f} signal was enhanced significantly from $30\mu V$ to around $90\mu V$. This is not very surprising, because in the Eq 3.5 in Chapter.3, we know that with a DC current we have some additional terms in the V^{2f} signal expression. Two terms are related to the DC current, namely, the TGV term and the thermal spin-transfer torque term. Apparently both terms are caused by thermal effects. Now if we subtract the data on V^{2f} with I_{dc} by the data we measured without I_{dc} , we obtain the data in Fig 5.10. This shows the I_{dc} related terms are also angular dependent, i.e. influenced by the magnetic orientation of the free layer. Nevertheless, we cannot discern yet whether this effect is caused by TGV or thermal spin-transfer torque. All we can

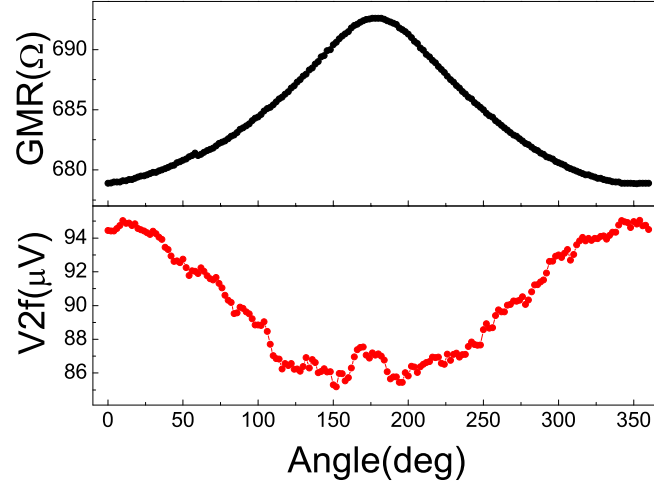


Figure 5.9: GMR and V^{2f} vs angle measured in the presence of a DC current of $500\mu A$. The AC current is $1mA$ at the frequency of $400Hz$. External field is $10mT$.

conclude for now is that this behavior is a result of magnetic thermal effect.

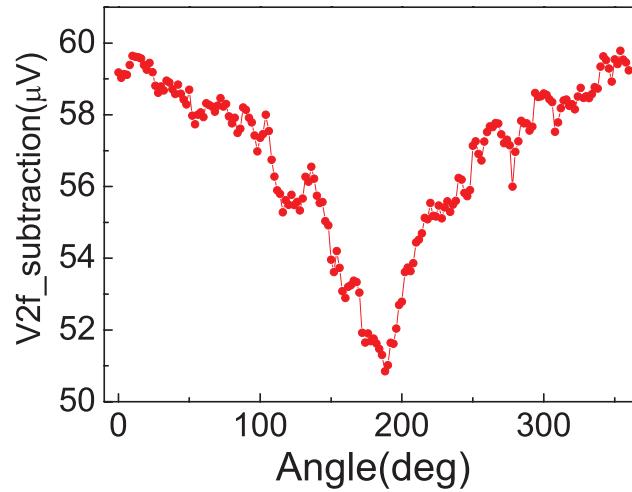


Figure 5.10: V^{2f} with $I_{dc}=500\mu A$ subtracted by V^{2f} with no I_{dc} , measured as a function of angle. External field is $10mT$

5.3.5 V^{2f} vs angle with different external field

We can see from GMR vs field measurement, the sudden jump of the magnetoresistance happens between 0 and 10mT. Then, we did a series of measurements on V^{2f} vs angle with different applied field.

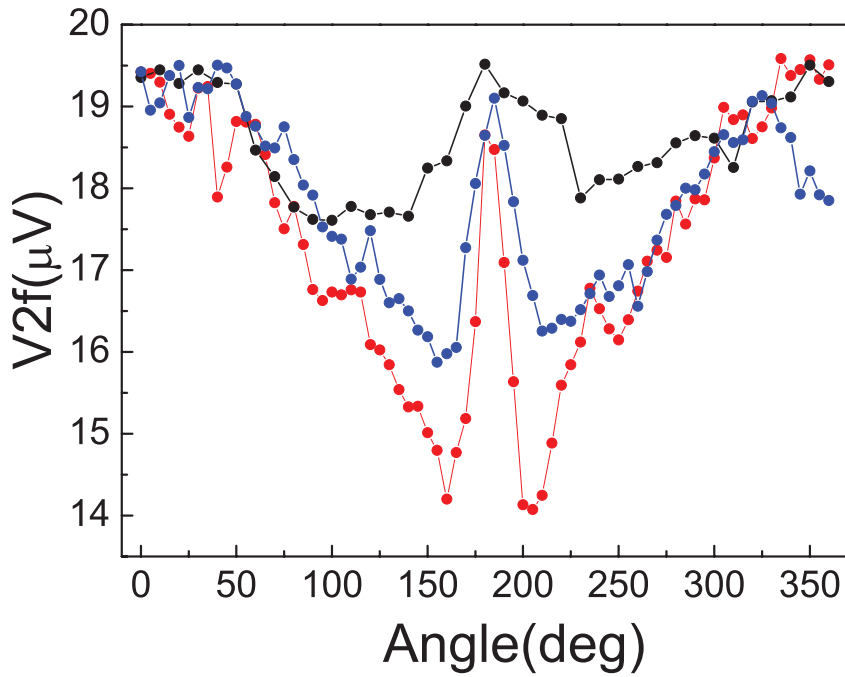


Figure 5.11: V^{2f} vs angle measured with different applied field.

$I_{ac}=500\mu A$. Red for 1.5mT, blue for 4.5mT, black for 10mT

At the same time, we also measured the angular dependent GMR with different applied field of 1,3,10mT.

The amplitude change of V_{2f} peak with respect to the external field can be understood as follow, the AC current induced spin-transfer torque is equivalent to an applied field H_{STT} perpendicular the magnetization, the oscillation angle of the free layer magnetization $\delta\theta$ is dependent on the ratio of H_{STT}/H_{eff} . When we decrease the external field applied, we decrease the amplitude of H_{eff} . This

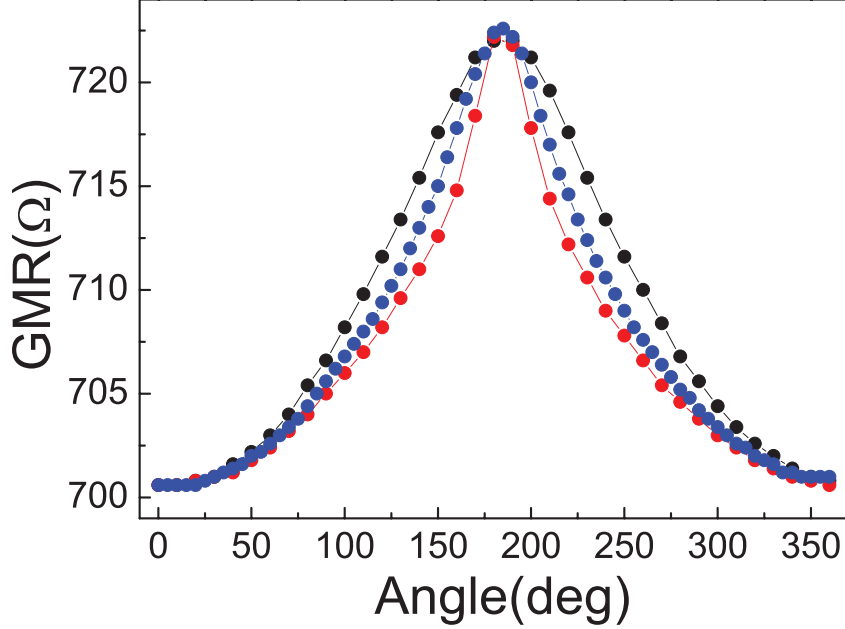


Figure 5.12: *GMR vs angle measured with different applied field.*

I_{ac}=500 μA. Red for 1.5 mT, blue for 4.5 mT, black for 10 mT

change gives rise to a change in the ratio of H_{STT}/H_{eff} , therefore, an increased perturbation of $\delta\theta$, which gives rise to the V_{2f} signal. Moreover, we also observed a change in the V_{2f} peak position. This can be accounted for the influence of H_{ani} . Both effects will also slightly affect the shape of angular dependence of GMR. The detailed simulation of these effects on experimental curves will be provided in the modeling work in the next section.

5.4 Fitting data on V^{2f} vs angle

5.4.1 Estimation of the transverse spin diffusion length

Now we try to fit our data using the simulation we introduced in the first section of this chapter. Here we take the experimental data of Fig 5.8 and find that we

can fit both the V^{2f} and GMR fairly well simultaneously if we take the value of λ_J as 6nm (Fig 5.13). Here in the V^{2f} fit, I shifted the baseline and changed the sign of the V^{2f} signal if we consider a 180 degree phase difference induced by the measurement setup.

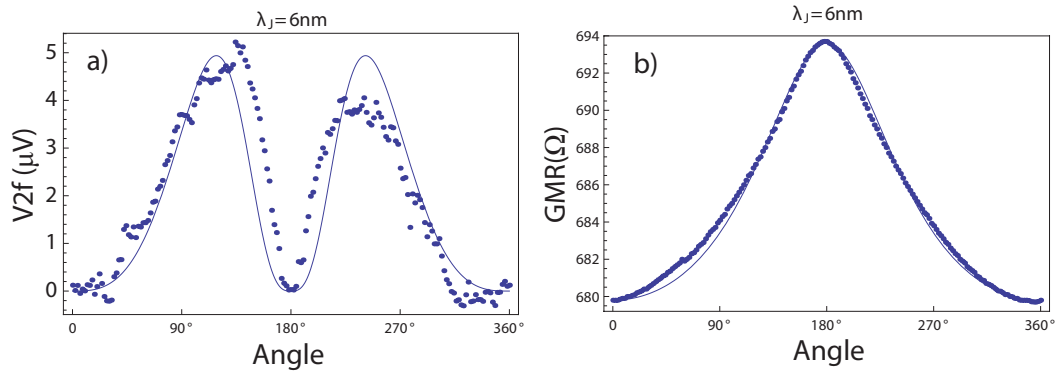


Figure 5.13: fit the V^{2f} (a) and GMR(b) vs angle data with the simulation when we assume the λ_J is 6nm. Dots are the actual experimental data, whereas, the solid line is the fit from the simulation. The phase has been adjusted. The baseline was shifted to overlap the fit.

From this data fit, we can estimate the transverse spin relaxation length λ_J is about 6nm in CoFe free layer. This estimation favors the argument of Zhang, Levy and Fert [39], where they provide an estimation of several nanometers. In order to show the sensitivity or accuracy of this method, we also tried to “fit” our data when we assume the λ_J is 2nm, and we find the fit curve is far from the experimental data both for GMR and V^{2f} (Fig 5.14).

In conclusion, we use the angular dependant measurement of V^{2f} and GMR vs angle to estimate the transverse spin relaxation length is around 6nm rather than 1Å.

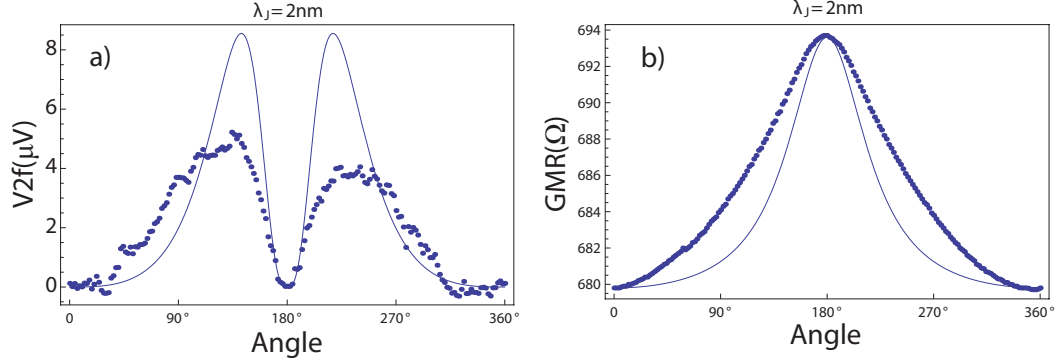


Figure 5.14: attempt to fit the V^{2f} (a) and GMR(b) vs angle data with the simulation when we assume the λ_J is 2nm. Dots are the actual experimental data, whereas, the solid line is the fit from the simulation.

5.4.2 Fitting data on V^{2f} vs angle with different external field using estimated λ_J

Now, we take the value of λ_J as 6nm, estimated in the last section, and try to fit our data in Fig 5.11 of V^{2f} vs angle with different applied field. We find in ref [26] that N_x^d and N_y^d are both dependent on external field \mathbf{H}_{ext} and the anisotropy field \mathbf{H}_{ani} . This dependence directly gives rise to the V^{2f} peak height variation with the external field applied according to Eq 5.1. In order to have an explicit understanding of the influence of applied field on the V^{2f} signal, I did a calculation step by step from LLG-Slonczewski equation in the limit of the frequency $\omega \rightarrow 0$, see Appendix A, and obtain,

$$V^{2f}(\theta) = I_{AC}^2 \frac{dR(\theta)}{d(\cos \theta)} \frac{\alpha \hbar}{2eV_m M_s} \frac{\eta_1(\theta)}{H_{\text{tot}}} \sin^2 \theta \quad (5.6)$$

where H_{tot} is the vectorial sum of anisotropy field H_{ani} and applied field H_{ext} .

This equation shows a clear dependence of V^{2f} peak height on H_{ext} .

Nonetheless, we also observed a change of V_{2f} peak position with respect to the applied field. This is resulted from the existence of anisotropy field H_{ani} . The angle between the magnetization of free layer and fixed layer is determined by H_{tot} . When H_{ani} is comparable to the H_{ext} , the deviation angle of H_{tot} from H_{ext} is no longer negligible, as indicated in Fig 5.15.

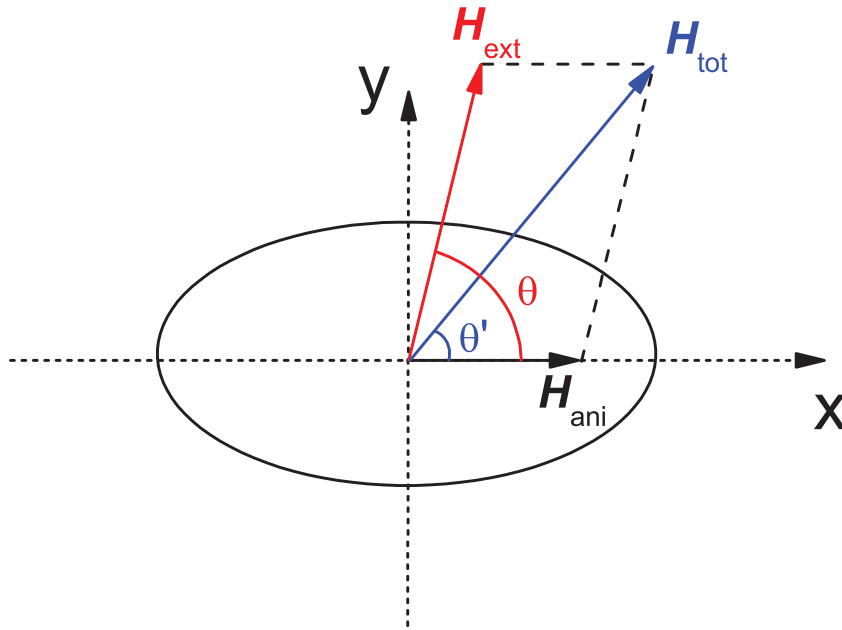


Figure 5.15: Simple illustration of angular relations of H_{ext} , H_{ani} and H_{tot} . Here θ is the angle we took to plot our experimental data, whereas θ' is in fact the angle between two magnetization in spin valve.

Since the angle we use to plot in our experimental data is the angle of the external field with respect to the fixed layer magnetization. When we decrease the external field applied from 10mT to 1mT, as we can see in Fig 5.15, the deviation between θ and θ' increases accordingly. This influence can explain why the V^{2f} peak position shift when we decrease the external field.

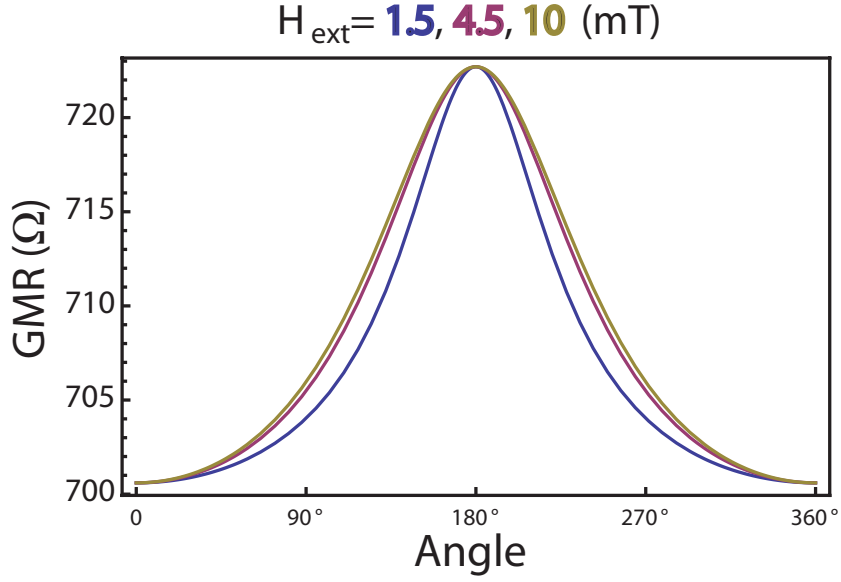


Figure 5.16: Simulation of GMR vs angle measurement with different applied field. $I_{ac}=500\mu A$. blue for 1.5mT, red for 4.5mT, yellow for 10mT

Then according to the V^{2f} signal amplitude dependence on H_{ext} as well as the simple argument of the V^{2f} position dependence on H_{ani} , we did modeling of V^{2f} vs angle with different external field in Fig 5.17, where we assume the anisotropy field is 0.7mT. At the same time, we use the same condition to simulate the GMR vs angle with different applied field in Fig 5.16.

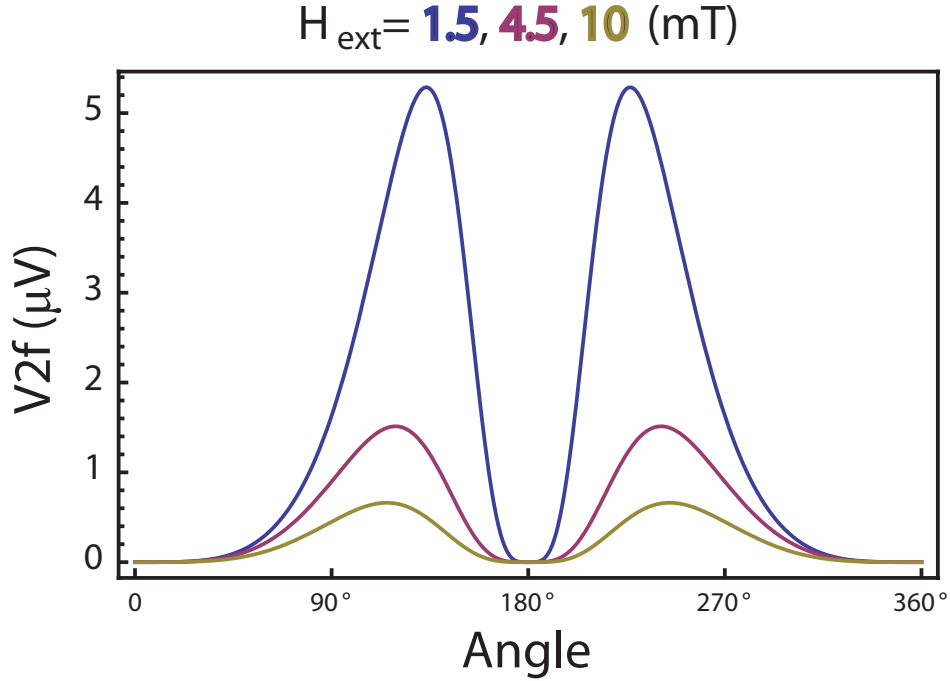


Figure 5.17: Simulation of V_{2f} vs angle measurement with different applied field. $I_{ac}=500\mu A$. blue for 1.5mT, red for 4.5mT, yellow for 10mT.

Although the simulation do not perfectly overlap the data point in our experiment. We can see the same trends between both the data and the simulation, i.e. the peak position shift in V^{2f} , the V^{2f} amplitude change, the GMR shape change with respect to the applied field. There are several points that might need more considerations in the simulations and may improve the analysis of the data and better understand the physical process. First, the anisotropy field might be underestimated, we should have measured a minor loop in the GMR measurement around the free layer magnetization in order to have an idea of the amplitude of the coupling field between layers and the anisotropy field. There might also be multi-domain situation which should be taken into account, but has been simplified and neglected. All these should be done in the future to complete this piece of work.

Chapter 6

Conclusion and Perspectives

In this PhD thesis, I presented a study of spin-dependent transport focusing on the mixed effects of charge, spin, and heat on magnetic nanostructures by using mainly second harmonics voltage response. The experiments were carried out on two aspects. First, we observed the evidence of thermal spin-transfer torque on spin valve by detecting a shift on switching field induced by a heat current. In the second part, we measured the angular dependent second harmonic voltage in order to estimate the amplitude of the transverse spin diffusion length in the free magnetic layer of spin valve.

In the first part, I introduced how I grew nanowires consisting different structures such as spin valve and Co/Cu multilayers by electrodeposition. On these samples, I presented measurement data of GMR, MTGV and V^{2f} . In addition, I analyzed the relations between these measurements, for instance, the V^{2f} peaks always appear around the magnetic field value where the GMR curve experiences a gradual transition. MTGV and V^{2f} show close similarities in certain experimental circumstances. These phenomenons are also discussed and explained accordingly. Taking advantage of V^{2f} measurements with high sensitivity to switching field and high signal to noise ratio, we study the thermal spin-transfer torque effect induced by a heat current generated by asymmetric Joule heating in spin valve nanostructure.

We found two independent evidence on this effect. First is the switching field shift due to heat current. The second is the V^{2f} amplitude change induced by heat current. With a model combining charge, spin, and heat into one onsager matrix, we are able to fit both measurements with same parameters at the same time.

The second part the thesis is mainly the angular dependent measurements of V^{2f} . Due to the fact that V^{2f} is very sensitive to the non-linear configuration of the spin valve, we measurement the V^{2f} signal while we rotate the free layer in the spin valve. To be clear, the sample we use in this part is a lithography made exchanged-bias spin valve nanopillar, rather than electrochemical growth nanowire in the first part. A theoretical model demonstrates that both the amplitude and the peak position of V^{2f} strongly depend on transverse spin diffusion length, which is a key parameter in spintronics and still has controversy of how large it is. By fitting our experimental data with this model, we estimated this characterized parameter is about 6nm.

The study of the interplay between charge, spin and heat in nanostructures is a very interesting topic and yet to be fully understand. V^{2f} measurements presented here can be a simple measurement protocol to “filter” to obtain useful information of spin caloritronics effects in nanostructures. In addition, with a large temperature gradient, the thermal spin-transfer torque effect can possibly be applied to switching the magnetization of magnetic layer. This effect may offer potential applications on magnetic memories assisted by heat current.

Appendix A:

Calculation of second harmonics response induced by an AC current

We start with the Landau-Lifshitz-Gilbert equation including the Slonczewski term for spin-transfer torque,

$$\frac{d\hat{m}}{dt} = -\gamma\hat{m} \times \vec{H}_{all} + \alpha\hat{m} \times \frac{d\hat{m}}{dt} + \gamma h_I \hat{m} \times (\hat{m}_f \times \hat{m}) \quad (1)$$

where $\vec{H}_{all} = \vec{H}_0 + \vec{H}_{ani} + \vec{H}_{demag}$. \vec{H}_0 , \vec{H}_{ani} and \vec{H}_{demag} are applied field, anisotropy field, and demagnetization field, respectively. $h_I = \frac{\hbar I \eta_1}{2e V_m M_s}$ where $\eta_1 I$ indicates the strength of spin-transfer torque. M_s is the saturated magnetization and V_m is the volume of the free magnetic layer in the spin valve. Here \hat{m} and \hat{m}_f are both the unit vector of the free layer and the fixed layer magnetization, i.e. $|\hat{m}| = 1$ and $|\hat{m}_f| = 1$

Now we project the vectors in the frame where \hat{m}_f is fixed. We call it $(\hat{x}, \hat{y}, \hat{z})$. We take \hat{x} normal to the plane. \hat{m}_f is along \hat{y} , i.e. $\hat{m}_f \equiv \hat{y}$, and $\hat{z} = \hat{x} \times \hat{y}$.

As illustrated in Fig. 1, \vec{H}_0 is in the plane (\hat{y}, \hat{z}) . We call θ the angle between \vec{H}_0 and \vec{m}_f . Then in this frame of $(\hat{x}, \hat{y}, \hat{z})$, we have,

$$\vec{H}_0 = \begin{pmatrix} 0 \\ H_0 \cos \theta \\ H_0 \sin \theta \end{pmatrix} \quad (2)$$

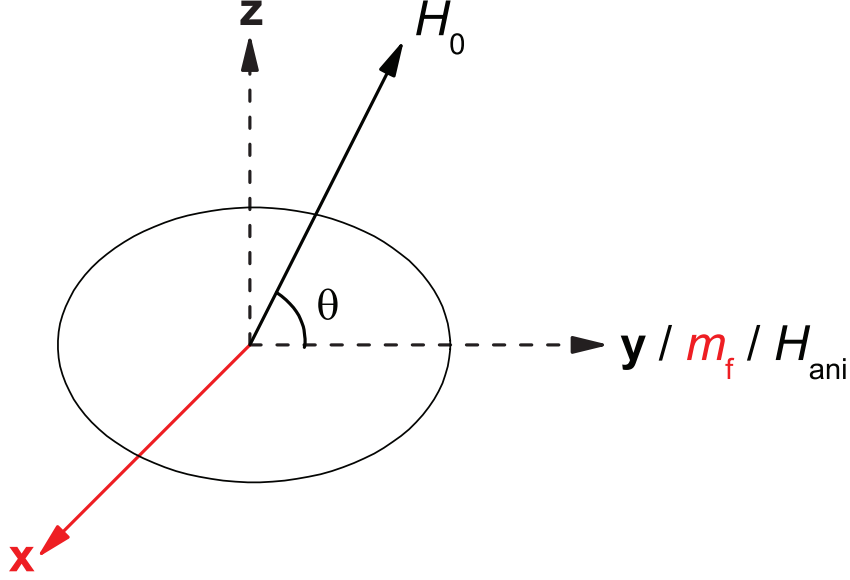


Figure 1: frame of (x,y,z)

$$\vec{H}_{ani} = \begin{pmatrix} 0 \\ H_{ani} \\ 0 \end{pmatrix} \quad (3)$$

For demagnetization effects, we consider the demagnetization factor \tilde{D} to be diagonal for our sample structure.

$$\tilde{D} = \begin{pmatrix} -N_x & 0 & 0 \\ 0 & -N_y & 0 \\ 0 & 0 & -N_z \end{pmatrix} \quad (4)$$

where N_x , N_y and N_z are the demagnetization elements at respective directions. Typically for a thin magnetic layer like our sample, we have $N_x \simeq 0.9$, $N_y \simeq 0.0$ and $N_z \simeq 0.2$.

The demagnetization field is given by,

$$\vec{H}_{demag} = \tilde{D} \hat{m} M_s \quad (5)$$

We search now for the equilibrium of the free layer magnetization \hat{m}_0 in the absence of the applied AC current, i.e. no spin transfer torque. $|\hat{m}_0| = 1$.

From eq 1, taking $\frac{d\hat{m}}{dt}$ to be 0 for the equilibrium, $h_I = 0$ for the absence of the spin-transfer torque, it yields,

$$0 = -\gamma \hat{m} \times \vec{H}_{all} \quad (6)$$

Therefore, \hat{m}_0 and \vec{H}_{all} are along the same direction. Considering $|\hat{m}_0| = 1$, we obtain,

$$\hat{m}_0 = a \vec{H}_{all} = a [\vec{H}_0 + \vec{H}_{ani} + \vec{H}_{demag}] \quad (7)$$

where $a = 1/|\vec{H}_0 + \vec{H}_{ani} + \vec{H}_{demag}|$.

transfer a to the left, and replace \vec{H}_{demag} using eq 5 to obtain,

$$a^{-1} \hat{m}_0 = \vec{H}_0 + \vec{H}_{ani} + \tilde{D} \hat{m}_0 M_s \quad (8)$$

Then we introduce the following notation,

$$\hat{m}_0 = \begin{pmatrix} m_x \\ m_y \\ m_z \end{pmatrix} \quad (9)$$

move $\tilde{D} \hat{m}_0 M_s$ to the left and expand the eq 8 into a vectorial form,

$$\begin{pmatrix} a^{-1} + N_x M_s & 0 & 0 \\ 0 & a^{-1} & 0 \\ 0 & 0 & a^{-1} + N_z M_s \end{pmatrix} \begin{pmatrix} m_x \\ m_y \\ m_z \end{pmatrix} = \begin{pmatrix} 0 \\ H_0 \cos \theta + H_{ani} \\ H_0 \sin \theta \end{pmatrix} \quad (10)$$

By moving the matrix to the right, it becomes,

$$\begin{pmatrix} m_x \\ m_y \\ m_z \end{pmatrix} = \begin{pmatrix} \frac{1}{a^{-1} + N_x M_s} & 0 & 0 \\ 0 & a & 0 \\ 0 & 0 & \frac{1}{a^{-1} + N_z M_s} \end{pmatrix} \begin{pmatrix} 0 \\ H_0 \cos \theta + H_{ani} \\ H_0 \sin \theta \end{pmatrix} \quad (11)$$

Therefore, we have the solution for \hat{m}_0 ,

$$\begin{cases} m_x = 0 \\ m_y = a (H_0 \cos \theta + H_{ani}) \\ m_z = \frac{H_0 \sin \theta}{a^{-1} + N_z M_s} \end{cases} \quad (12)$$

We simplify the problem by considering the magnetic layer very thin, i.e. $N_z = 0$ and $N_x = 1$, which is reasonable for our sample (Fig 2.10(a)) since we have a free layer with tiny aspect ratio of $2.5nm/(250nm \times 400nm)$, and then \hat{m}_0 becomes

$$\hat{m}_0 = \frac{1}{\sqrt{H_0^2 + 2H_0 H_{ani} \cos \theta + H_{ani}^2}} \begin{pmatrix} 0 \\ H_0 \cos \theta + H_{ani} \\ H_0 \sin \theta \end{pmatrix} \quad (13)$$

Now we find that \hat{m}_0 is in fact along the direction of the vectorial sum of \vec{H}_0 and \vec{H}_{ani} , which is very natural to think of. (Fig 2)

We can also rewrite the solution as follow,

$$\hat{m}_0 = \begin{pmatrix} 0 \\ \cos \theta_{12} \\ \sin \theta_{12} \end{pmatrix} \quad (14)$$

where

$$\cos(\theta_{12}) = \frac{H_0 \cos \theta + H_{ani}}{\sqrt{H_0^2 + 2H_0 H_{ani} \cos \theta + H_{ani}^2}} \quad (15)$$

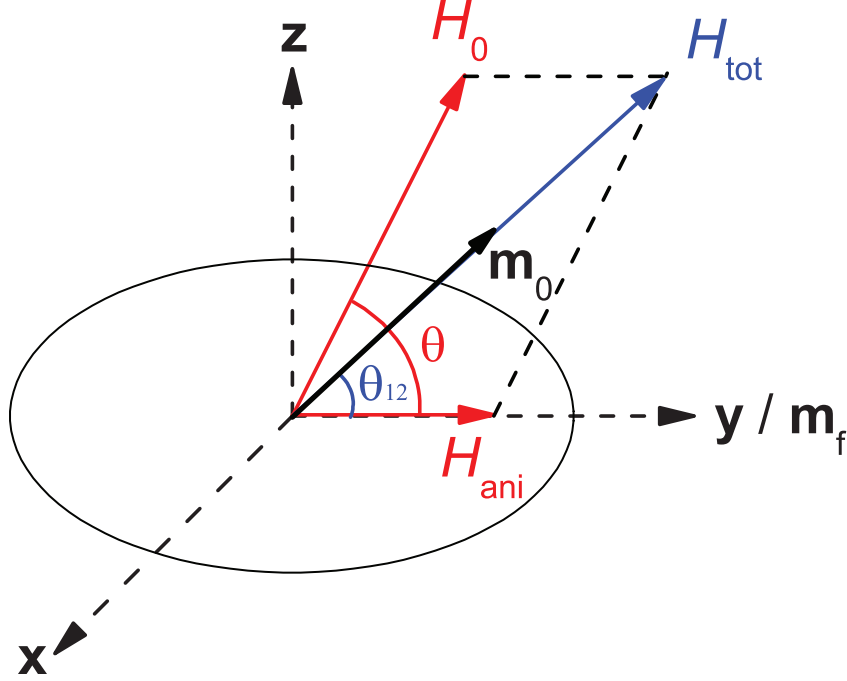


Figure 2: Illustration of the vector \hat{m}_0 and definition of θ_{12}

Above is how we calculate the equilibrium state of the free layer magnetization \hat{m}_0 , and from this point on, we start to calculate the small magnetization perturbation given rise by the AC current induced spin-transfer torque on free layer magnetization.

A new frame of (x', y', z') is defined as follow, $\hat{z}' \equiv \hat{m}_0$, \hat{x}' is perpendicular to the layer, and $\hat{y}' = \hat{z}' \times \hat{x}'$.

We can see in Fig 3 that $\Delta\theta$ is the small deviation from equilibrium, and the asymmetrical angle describes the precession of \hat{m} about \hat{m}_0 . ($\Delta\theta$ is the angle usually called θ . I cannot use θ because θ describes the angle of field with respect to \hat{m}_f). ω is the precession frequency which is the same as the one of the AC spin-transfer torque, hence the AC current frequency.

Due to the fact that the torque induced precession does not change the amplitude

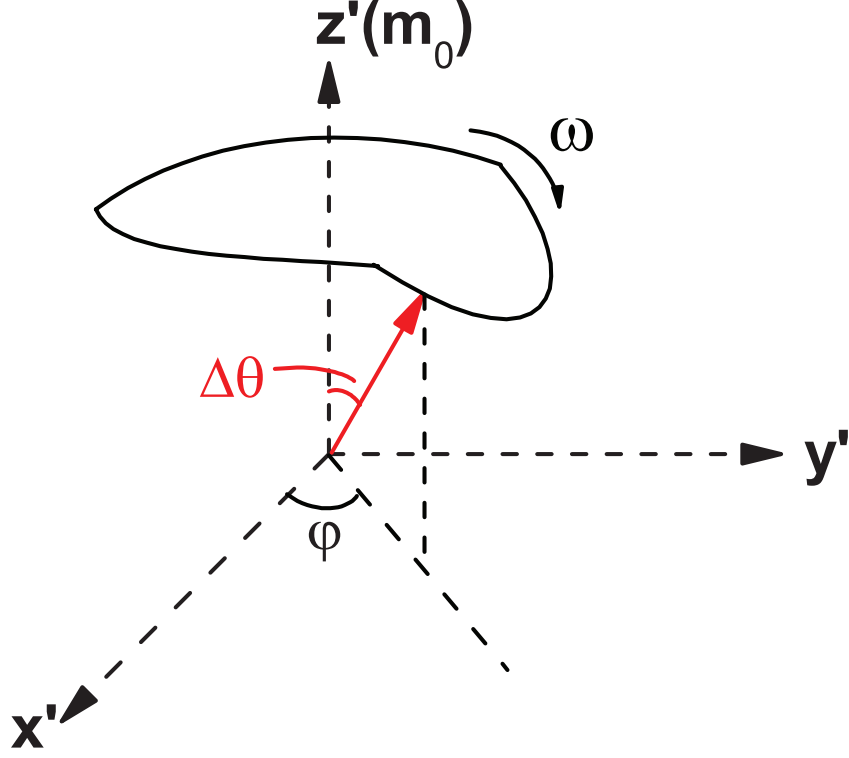


Figure 3: Illustration of frame (x', y', z') , the vector \hat{m} and definition of $\Delta\theta$ and φ

of the magnetization, \hat{m} is also a unit vector. We can write

$$\hat{m} = \begin{pmatrix} \sin \Delta\theta \cos \varphi \\ \sin \Delta\theta \sin \varphi \\ \cos \Delta\theta \end{pmatrix} \quad (16)$$

Since, $\Delta\theta$ is small, \hat{m} becomes

$$\hat{m} = \begin{pmatrix} \Delta\theta \cos \varphi \\ \Delta\theta \sin \varphi \\ 1 \end{pmatrix} \quad (17)$$

Considering \hat{m}_f is in plane, and has an angle of θ_{12} with respect to \hat{m}_0 , we write

$$\hat{m}_f = \begin{pmatrix} 0 \\ \sin \theta_{12} \\ \cos \theta_{12} \end{pmatrix} \quad (18)$$

Then we calculate respectively all the terms in the LLG-Slonczewski equation,

$$\frac{d\hat{m}}{dt} = \begin{pmatrix} \dot{\Delta}\theta \cos \varphi - \Delta\theta \dot{\varphi} \sin \varphi \\ \dot{\Delta}\theta \sin \varphi + \Delta\theta \dot{\varphi} \cos \varphi \\ 0 \end{pmatrix} \quad (19)$$

$$\hat{m} \times \frac{d\hat{m}}{dt} = \begin{vmatrix} \hat{x}' & \Delta\theta \cos \varphi & \dot{\Delta}\theta \cos \varphi - \Delta\theta \dot{\varphi} \sin \varphi \\ \hat{y}' & \Delta\theta \sin \varphi & \dot{\Delta}\theta \sin \varphi + \Delta\theta \dot{\varphi} \cos \varphi \\ \hat{z}' & 1 & 0 \end{vmatrix} = \begin{pmatrix} -\dot{\Delta}\theta \sin \varphi - \Delta\theta \dot{\varphi} \cos \varphi \\ \dot{\Delta}\theta \cos \varphi - \Delta\theta \dot{\varphi} \sin \varphi \\ 0 \end{pmatrix} \quad (20)$$

where we omitted the second order terms.

In the new frame (x', y', z'), we rewrite the \vec{H}_{all}

$$\vec{H}_{all} = \begin{pmatrix} -N_x M_s \Delta\theta \cos \varphi \\ -H_0 \sin(\theta - \theta_{12}) + H_{ani} \sin \theta_{12} \\ H_0 \cos(\theta - \theta_{12}) + H_{ani} \cos \theta_{12} \end{pmatrix} = H_0 \begin{pmatrix} -N_x \frac{M_s}{H_0} \Delta\theta \cos \varphi \\ \sin(\theta_{12} - \theta) + \frac{H_{ani}}{H_0} \sin \theta_{12} \\ \cos(\theta_{12} - \theta) + \frac{H_{ani}}{H_0} \cos \theta_{12} \end{pmatrix} \quad (21)$$

Since $\hat{m}_0 = \begin{pmatrix} 0 \\ 0 \\ 1 \end{pmatrix}$ is the solution of $\hat{m} \times \vec{H}_{all} = 0$, we derive $\sin(\theta_{12} - \theta) + \frac{H_{ani}}{H_0} \sin \theta_{12} = 0$

Therefore,

$$\begin{aligned}
\hat{m} \times \vec{H}_{all} &= H_0 \begin{vmatrix} \hat{x}' & \Delta\theta \cos \varphi & -N_x \frac{M_s}{H_0} \Delta\theta \cos \varphi \\ \hat{y}' & \Delta\theta \sin \varphi & 0 \\ \hat{z}' & 1 & \cos(\theta - \theta_{12}) + \frac{H_{ani}}{H_0} \cos \theta_{12} \end{vmatrix} \\
&= H_0 \begin{pmatrix} \Delta\theta \sin \varphi \left[\cos(\theta - \theta_{12}) + \frac{H_{ani}}{H_0} \cos \theta_{12} \right] \\ -\Delta\theta \cos \varphi \left[\cos(\theta - \theta_{12}) + \frac{H_{ani}}{H_0} \cos \theta_{12} \right] - N_x \frac{M_s}{H_0} \Delta\theta \cos \varphi \\ 0 \end{pmatrix}
\end{aligned} \tag{22}$$

$$\hat{m}_f \times \hat{m} = \begin{vmatrix} \hat{x}' & 0 & \Delta\theta \cos \varphi \\ \hat{y}' & \sin \theta_{12} & \Delta\theta \sin \varphi \\ \hat{z}' & \cos \theta_{12} & 1 \end{vmatrix} = \begin{pmatrix} \sin \theta_{12} - \cos \theta_{12} \Delta\theta \sin \varphi \\ \cos \theta_{12} \Delta\theta \cos \varphi \\ -\sin \theta_{12} \Delta\theta \sin \varphi \end{pmatrix} \tag{23}$$

Then the Slonczewski term becomes

$$\begin{aligned}
\gamma h_I \hat{m} \times (\hat{m}_f \times \hat{m}) &= \gamma h_I \begin{vmatrix} \hat{x}' & \Delta\theta \cos \varphi & \sin \theta_{12} - \cos \theta_{12} \Delta\theta \sin \varphi \\ \hat{y}' & \Delta\theta \sin \varphi & \cos \theta_{12} \Delta\theta \cos \varphi \\ \hat{z}' & 1 & -\sin \theta_{12} \Delta\theta \sin \varphi \end{vmatrix} \\
&= \gamma h_I \begin{pmatrix} -\cos \theta_{12} \Delta\theta \cos \varphi \\ \sin \theta_{12} - \cos \theta_{12} \Delta\theta \sin \varphi \\ -\sin \theta_{12} \Delta\theta \sin \varphi \end{pmatrix} \\
&= \gamma h_I \begin{pmatrix} 0 \\ \sin \theta_{12} \\ 0 \end{pmatrix} - \gamma h_I \Delta\theta \begin{pmatrix} \cos \theta_{12} \cos \varphi \\ \cos \theta_{12} \sin \varphi \\ \sin \theta_{12} \sin \varphi \end{pmatrix} \\
&\simeq \gamma h_I \begin{pmatrix} 0 \\ \sin \theta_{12} \\ 0 \end{pmatrix}
\end{aligned} \tag{24}$$

By substituting the eq 19 20 22 24 into the LLG-Slonczewski equation (eq 1) and putting $\varphi = 0$ for calculating the $\Delta\theta$ in plane, we derive

$$\begin{pmatrix} -\Delta\theta\dot{\varphi} \\ \dot{\Delta\theta} \\ 0 \end{pmatrix} = -\gamma H_0 \begin{pmatrix} \Delta\theta \left[\cos(\theta - \theta_{12}) + \frac{H_{ani}}{H_0} \cos \theta_{12} \right] \\ 0 \\ 0 \end{pmatrix} + \alpha \begin{pmatrix} -\dot{\Delta\theta} \\ -\Delta\theta\dot{\varphi} \\ 0 \end{pmatrix} \\
+ \gamma h_I \begin{pmatrix} 0 \\ \sin \theta_{12} \\ 0 \end{pmatrix} \quad (25)$$

We then solve this equation to obtain $\Delta\theta$,

$$\Delta\theta = \frac{\alpha\gamma h_I \sin \theta_{12}}{(1 + \alpha^2)\dot{\varphi} - \gamma H_0 \left[\cos(\theta - \theta_{12}) + \frac{H_{ani}}{H_0} \cos \theta_{12} \right]} \quad (26)$$

There are a few points that we can simplify this solution. First, $\dot{\varphi} = \omega$ is equal to the frequency of the applied AC current, which is about 400Hz. On the other hand, γH_0 is in the order of magnitude of GHz. Therefore we can ignore the term with $\dot{\varphi}$. In addition, if we look at Fig 2, we realize that $H_0 \left[\cos(\theta - \theta_{12}) + \frac{H_{ani}}{H_0} \cos \theta_{12} \right]$ is actually $|\vec{H}_{tot}|$. Then eq. 29 becomes

$$\Delta\theta = \frac{-\alpha h_I}{H_{tot}} \sin \theta_{12} \quad (27)$$

By using expression of $h_I = \frac{\hbar I \eta_1}{2eV_m M_s}$ and V^{2f} expression (eq. 3.7), we have the angular-dependent V^{2f} expression as follow

$$V^{2f} = I_0 \frac{dR}{d\theta} \Delta\theta = I_0 \frac{dR}{d \cos \theta} \frac{\alpha h_I}{H_{tot}} \sin^2 \theta_{12} = I_0^2 \frac{dR}{d(\cos \theta)} \frac{\alpha \hbar \eta_1}{2eV_m M_s} \frac{1}{H_{tot}} \sin^2 \theta_{12} \quad (28)$$

In conclusion, we have calculated the angular dependent V^{2f} to be

$$V^{2f}(\theta) = I_{AC}^2 \frac{dR(\theta)}{d(\cos \theta)} \frac{\alpha \hbar}{2eV_m M_s} \frac{\eta_1(\theta)}{H_{tot}} \sin^2 \theta \quad (29)$$

where $\eta_1(\theta)$ indicates the angular dependence of spin-transfer torque.

Bibliography

- [1] M. Baibich, J. M Broto, A. Fert, F. N. Guyen Van Dau, F. Petroff, P. Etienne, G. Creuzet, and A. Friedrich, *Phys. Rev. Lett.*, 61, 2472 (1988)
- [2] Binasch G, Grünberg P, Saurenbach F and Zinn W, *Phys. Rev. B*, 39, 4828 (1989)
- [3] Bauer, G. E. W., MacDonald, A. H. and Maekawa, S. (eds) Spin Caloritronics, Special Issue of *Solid State Communications* (Elsevier, 2010)
- [4] J. A. Katine, F.J. Albert, R. A Buhrman, E. B. Myers, and K.C. Ralph, *Phys. Rev. Lett.*, 84, 3149 (2000)
- [5] E. B. Myers, D. C. Ralph, J. A. Katine, R. N. Louie, and R. A. Buhrman. *Science*, 285, 867, 1999
- [6] L. Gravier, S. Serrano-Guisan, F. Reuse and J.-Ph. Ansermet, *Phys. Rev. B*, 73, 052410 (2006)
- [7] Haiming Yu, S. Granville, D. P. Yu, J.-Ph. Ansermet, *Phys. Rev. Lett.*, 104, 146601 (2010)
- [8] Haiming Yu, Julie Dubois, S. Granville, D. P. Yu, J.-Ph. Ansermet, *J. Phys. D: Appl. Phys.*, 42, 175004 (2009)
- [9] Santiago SERRANO GUISAN, EPFL doctoral thesis N° 3504(2006)
- [10] J.-E. Wegrowe, S.E. Gilbert, D. Kelly, B. Doudin, J.-Ph. Ansermet. *IEEE Trans. Magn.* 34, 903 (1998).

- [11] N. Biziere, E. Murè, and J.-Ph. Ansermet. *Phys. Rev. B* 79, 012404 (2009).
- [12] Elena Murè, EPFL doctoral thesis N° 4687(2010)
- [13] C. Scholtenberger, B. M. I. van der Zande, L. G. J. Fokkink, M. Henny, C. Schmid, M. Kruiger, A. Bachtold, R. Huber, H. Birk, and U. Staufer. *J. Phys. Chem. B* 1997, 101, 5497-5505.
- [14] L. Gravier, S. Serrano-Guisan and J.-Ph. Ansermet *J. Appl. Phys.* 97, 10C501 (2005).
- [15] S. Serrano-Guisan, G. di Domenicantonio, M. Abid, J.-P. Abid, M. Hillenkamp, L. Gravier, J.-Ph. Ansermet and Ch. Fèlix, *Nature Materials* 5, 730 (2006)
- [16] A. Brataas, G.E.W. Bauer, P.J. Kelly, *Phys. Reports* 427, 157 (2006).
- [17] S. Granville, H. Yu, J. Dubois, L. Gravier, J.-Ph. Ansermet, *J. Magn. Magn. Mater.* 322, 1464 (2010)
- [18] Juretschke H J *J. Appl. Phys.* 31, 1401 (1960)
- [19] Egan W G and Juretschke H J *J. Appl. Phys.* 14 1477 (1963)
- [20] Moller W M and Juretschke H J *Phys. Rev. B* 2 2651 (1970)
- [21] Brataas A Bauer G E W and Kelly P J *Phys. Rep.* 427 157 (2006)
- [22] Devolder T, Tulapurkar A, Suzuki Y, Chappier C and Crozat P, *J. Appl. Phys.* 98 053904 (2005)
- [23] Haiming Yu, Julie Dubois, S. Granville, D. P. Yu, J.-Ph. Ansermet, *J. Phys. D: Appl. Phys.* 42, 175004 (2009)
- [24] J. Grollier, V. Cross, H. Jaffrès, A. Hamzic, J.M. George, G. Faini, J. Ben Youssef, H. Le Gall, and A. Fert. *Phys. Rev. B* 67, 174402 (2003)

- [25] presentation at One Day International Workshop on Spin Transfer in Nancy by Prof. Cowburn
- [26] Alexey A. Kovalev, Gerrit E. W. Bauer, and Arne Brataas *Phys. Rev. B* 75, 014430 (2007).
- [27] Haiming Yu, S. Granville, D. P. Yu, J.-Ph. Ansermet, *Solid State Commun.* 150, 485 (2010)
- [28] A. Fabian, C. Terrier, S. S. Guisan, X. Hoffer, M. Dubey, L. Gravier, J.-Ph. Ansermet, and J.-E. Wegrowe, *Phys. Rev. Lett.* 91, 257209 (2003).
- [29] M. Hatami, G. E. W. Bauer, Q. Zhang, and P. J. Kelly, *Phys. Rev. Lett.* 99, 066603 (2007).
- [30] J. C. Slonczewski, *J. Magn. Magn. Mater.* 159, L1 (1996)
- [31] L. Gravier, S. Serrano-Guisan, F. Reuse, and J.-Ph. Ansermet, *Phys. Rev. B* 73, 024419 (2006).
- [32] M. Johnson and R. H. Silsbee, *Phys. Rev. Lett.* 55, 1790 (1985).
- [33] M. Johnson and J. Byers, *Phys. Rev. B* 67, 125112 (2003).
- [34] H.-E. Wegrowe, M. C. Ciornei, and H. -J. Drouhin, *J. Phys. Condens. Matter* 19, 165213 (2007).
- [35] A. Slachter, F. L. Bakker, J. Adam, and B. J. van Wees, *Nature Physics* 6, 879-882 (2010)
- [36] T. Valet and A. Fert, *Phys. Rev. B* 48, 7099 (1993)
- [37] J.-Ph. Ansermet, *IEEE Trans. mag* 44, 329-335 (2008)
- [38] J. C. Slonczewski, *J. Magn. Magn. Mater.* 247, 324 (2002).
- [39] S. Zhang, P. M. Levy, and A. Fert, *Phys. Rev. Lett* 88, 236601 (2002).

- [40] J. Dubois and J.-Ph. Ansermet, *Phys. Rev. B* 78, 184430 (2008).
- [41] A. Kovalev, A. Brataas, and G. E. W. Bauer, *Phys. Rev. B* 66, 224424 (2002).
- [42] Chapter 2 Spintronics: Conceptual Building Blocks, J.-Ph. Ansermet E. Beaurepaire et al. (eds.), Magnetism and Synchrotron Radiation, Springer
- [43] A. Shipiro, S. Zhang and P. M. Levy, *Phys. Rev. B* 67, 104430 (2003).
- [44] J. Bass, W. P. Pratt, *J. Phys.: Condens. Matter* 19 (2007) 183201.

Curriculum Vitae

Family Name: Yu

First Name: Haiming

Born the 14 July 1983 in Shenyang (China)

EDUCATION

- **PhD degree in Physics** — July 2011

“Thermal spin transfer torque and transverse spin relaxation in spin valves”

Laboratoire de Physique des Matériaux Nanostructures (LPMN)

Ecole Polytechnique Fédérale de Lausanne (EPFL) Switzerland

Advisor: Prof. Jean-Philippe Ansermet

- **Bachelor in Physics** — July 2006

Peking University - Beijing, China

FOREIGN LANGUAGE

- **English** — TOEFL-ibt Total 104 / IELTS Overall 7.0 / European Language Level C2

- **French** — European Language Level B1 / Capable of everyday communication

PUBLICATION**Evidence for thermal spin transfer torque.**

Haiming Yu, S. Granville, D. P. Yu, J.-Ph. Ansermet, *Phys. Rev. Lett.* 104, 146601 (2010)

Second harmonic detection of spin-dependent transport in magnetic nanostructures.

Haiming Yu, S. Granville, D. P. Yu, J.-Ph. Ansermet, *Chin. Phys. Lett.* 27, 027201 (2010)

Heat and spin transport in magnetic nanowires.

Haiming Yu, S. Granville, D. P. Yu, J.-Ph. Ansermet, *Solid State Commun.* 150, 485 (2010)

Temperature derivative of the resistance of spin-valves.

S. Granville, H. Yu, J. Dubois, L. Gravier, J.-Ph. Ansermet, *J. Magn. Magn. Mater.* 322, 1464 (2010)

Current susceptibility of magnetization in spin valves.

Haiming Yu, Julie Dubois, S. Granville, D. P. Yu, J.-Ph. Ansermet, *J. Phys. D: Appl. Phys.* 42, 175004 (2009)

INTERNATIONAL CONFERENCES

June 2011 Invited talk at University of Hamburg, **Germany**.

June 2011 Recent trends in spintronics, Ordizia **Spain**.

May 2011 Invited talk at University of Regensburg, **Germany**.

May 2011 Invited talk at TU Munich, **Germany**.

December 2010 Invited talk at IBM Almaden, San José, California **USA**.

July 2010 A3-Symposium on Nanomaterials and Nanostructures in Tokyo, **Japan** .

March 2010 APS march meeting in Portland OR, **USA** .

May 2008 E-MRS spring meeting in Strasbourg, **France**.